On the Feasibility of Lifetime Extension Potential for Wind Turbine Drivetrains: Methodology and Implementation

Thesis for the degree of Doctor of Philosophy

Kelly Tartt

Wind and Marine Energy Systems and Structures CDT

Department of Electronic and Electrical Engineering

University of Strathclyde, Glasgow

August 14, 2025

This thesis is the result of the author's original research. It has been composed by the author and has not been previously submitted for examination which has led to the award of a degree.

Signed: Kelly Tartt

Date: December 2024

Abstract

Wind energy capacity is growing rapidly and in addition, there are several wind turbines approaching their end of life. Once wind turbines reach this stage, there are typically three options available: decommissioning, re-powering and lifetime extension. This research investigates lifetime extension, specifically of drivetrains, which has not been extensively studied, as opposed to the supporting structures. Therefore, the aim of this work was to develop a methodology for determining lifetime extension of wind turbine drivetrains. Initially, existing research and industrial guidelines were reviewed to enhance understanding for application in the wind industry. Based upon these findings and a systematic approach, a methodology for wind turbine drivetrain life extension was developed. This proposed method required identifying the most vulnerable components, to which the methodology could be applied. It was realized that vulnerability maps of mechanical drivetrain components already exist, so this work used a data-driven approach to produce a vulnerability map for a power converter. Next, the proposed methodology was tested using data from an onshore wind farm, focusing on the rear generator bearings, which were identified as problematic. SCADA data, particularly temperature readings, were utilised due to their wide availability. Seven years of

Chapter 0. Abstract

SCADA data were analysed using machine learning models to predict remaining useful life (RUL) and failure metrics. Two approaches were implemented: deterministic and probabilistic, using Monte Carlo simulations to improve accuracy. The probabilistic approach employed two methods: discrete confidence interval-based and continuous probability distribution-based, to characterize model errors. Results indicated that while SCADA data can inform predictive maintenance by identifying failure thresholds, its reliability for long-term RUL prediction is limited. This research concludes that combining SCADA data with more detailed condition monitoring methods, such as vibration analysis, is essential for robust drivetrain lifetime extension assessment. Future work will focus on validating these findings through integration and analysis.

Preface/Acknowledgements

Firstly, I would like to say a special thank you to my Supervisors: Dr. Abbas Mehrad Kazemi-Amiri, Professor Amir R. Nejad and Dr. James Carroll. They have provided continuous guidance and been so supportive and understanding throughout the whole PhD process, I couldn't have asked for better Supervisors.

Next, I would like to acknowledge and thank the Engineering and Physical Sciences Research Council (EPSRC) for supporting this work through the EPSRC Centre for Doctoral Training in Wind and Marine Energy Systems and Structures (Grant Number EP/S023801/1).

I would also like to thank all the students and staff on the Wind and Marine Energy Systems and Structures CDT, as well as my fellow PhD students located in the Department of Marine Technology at NTNU, who provided valuable feedback and advice.

Last but not least, I would like to thank my family, my mum, dad and brother, who have been there for the very few highs and many, many lows and who have been my biggest supporters. I don't think I would have got through it without you, so thank you so much.

Contents

List of Figures

List of Figures

List of Tables

Abbreviations

ABS	American Bureau of Shipping
AC	Alternating Current
AIM	Asset Integrity Management
ALARP	As Low As Reasonably Practicable
BV	Bureau Veritas
CapEx	Capital Expenditure
CM	Condition Monitoring
CMMS	Computerized Maintenance Management System
DC	Direct Current
DEL	Damage Equivalent Load
DFIG	Doubly-Fed Induction Generator
DIN	Deutsches Institut für Normung/German Institute for Standardization
DNV	Det Norske Veritas
EESG	Electrically Excited Synchronous Generator
FE	Finite Element
FMEA	Failure Modes and Effects Analysis
FPI	Floating Production Installation
GW	Gigawatt
GWEC	Global Wind Energy Council
IEC	International Electrotechnical Commission
IG	Induction Generator
IGBT	Insulated-Gate Bipolar Transistor

ISO	International Organization for Standardization
kW	Kilowatt
LEI	Lifetime Extension Inspection
LTE	Lifetime Extension
ML	Machine Learning
MW	Megawatt
NDI	Non-Destructive Inspection
OEM	Original Equipment Manufacturer
OpEx	Operating Expenses
PCA	Principal Component Analysis
PDA	Partial Discharge Analysis
PMG	Permanent Magnet Generator
PMSG	Permanent-Magnet Synchronous Generator
RBD	Reliability Block Diagram
RF	Random Forest
RUL	Remaining Useful Life
SCADA	Supervisory Control and Data Acquisition
SHM	Structural Health Monitoring
SPAR	Single Point Anchor Reservoir
SVR	Support Vector Regression
TW	Terawatt
U.K.	United Kingdom
WT	Wind Turbine

Chapter 1

Introduction

1.1 Introduction

“Net zero emissions by 2050" [1], “cut greenhouse gas emissions by at least 55% by 2030" [2], “limit global warming to below 2 degrees Celsius" [3]. These are all targets set by various agreements and countries around the world and one way to assist with achieving these targets, is by increasing the extraction of power from renewable energy sources, including wind.

The first modern wind farm was installed in the 1980s and since then the requirement to move away from using fossil fuels, towards renewable resources to produce electricity, has continued to grow at a remarkable rate. The Global Wind Energy Council (GWEC) states that 117 GW [4] of wind capacity was installed in 2023, bringing the total amount of wind power capacity installed to 1 TW and in order to meet the targets, GWEC explains that they need to triple annual wind installations by 2030. This means that more and more wind turbines are going to be installed, both onshore and offshore.

Along with the large increase in the number of wind turbines being and due to be installed, there are also a number of wind turbines that are due to reach the end of their designed service life, which is typically between twenty and twenty-five (20-25) years. WindEurope [5] states that wind farms totalling 78 GW will have been operational for more than twenty (20) years by 2030. Upon reaching this milestone, there are typically three options that the owner/operator can consider. The first is lifetime extension, which involves assessing the wind turbine to determine if the turbine can continue to operate in an efficient and safe manner, for an extended period, without the need for replacement or modification. The second is re-powering, which comprises of replacing or modifying certain components, to maintain or improve the required power output. The final and third option is decommissioning, which involves dismantling, removing the wind turbine and returning the site back to it's original condition.

The option chosen by the owner/operator is typically dependent on which option is economically beneficial to them, therefore a thorough investigation is carried out to assist with their final decision.

Re-powering is considered to be the preferred option, due to a variety of reasons, including increasing the wind farms output with less turbines. To date, one hundred and seventy (170) wind farms have been re-powered in Europe [5], with numbers expected to increase over the next ten (10) years. Topham and McMillan [6] describes two re-powering options, the first being a partial re-powering or refurbishment and the second being a full re-powering. Partial re-powering involves replacing minor components, whereas, full re-powering involves replacing the existing turbines (excluding the tower) with new larger units.

Even though re-powering is presently the favoured option, according to WindEurope some form of lifetime extension is currently being opted for in the majority of wind farms, due to re-powering legislative frameworks not being in place, [5]. Lifetime extension may allow an extra five (5), ten (10) or X number of years of operation, with little or no modifications.

If neither re-powering nor lifetime extension is an option, decommissioning will be carried out. WindEurope states that 736 MW of wind capacity was decommissioned in Europe in 2023, with approximately 27 GW due to be decommissioned over the next six (6) years. With decommissioning costs estimated at approximately 2 - 3% of the total capital cost [6], this cost can be partially compensated by recycling, where 85-90% of the components can be recycled [7].

A wind turbine can be segregated into three main groups: the tower/supporting structure, the rotor (including blades) and the nacelle. The nacelle houses the drive-train, which is classed as the “heart" or core of the wind turbine because this is where mechanical energy from the rotor, is turned into electrical energy, which is supplied to the grid.

In order to determine if the wind turbine can operate longer than it’s designed service life, all of the main groups need to be assessed because each group is crucial in the operation of the wind turbine. If the assessment at the end of the designed service life (i.e. 20 years), shows that one of the groups is coming to the end of it’s life, then lifetime extension may not be a possibility. On the other hand, if the assessment shows that all groups have life left in them, i.e. can still operate in a safe and efficient manner, then lifetime extension is an option.

To date, a large amount of research has been carried out on the tower/supporting structure and the blades, as detailed in [8], [9], [10] and [11] to name a few but not as much has been done on the nacelle/drivetrain.

The analyses carried out on the tower/supporting structure and drivetrains are fundamentally different, due to the fact the drivetrain contains both mechanical and electrical equipment, such as: the main bearing, gearbox, brake, generator and power converter, whereas the tower/supporting structure is purely structural.

Investigating the drivetrain is crucial because the failure mechanisms and damage rates of the components within the drivetrain, differ significantly from those of structural members. Electro-mechanical components have a much shorter time frame between initiation of the damage and eventual failure, compared to structural members. Additionally, the drivetrain's inherently complex components are subject to uncertainties, associated with both their manufacturing and operation [12]. In reality, the majority of the primary load bearing components located within the drivetrain will not survive the full designed service life of the turbine, i.e. 20 years, they are typically replaced at between twelve and fifteen (12 - 15) years but an assessment can still be carried out at the twenty (20) year mark to determine how much longer they can operate.

Considering all the points discussed above, there appears to be a clear research gap in establishing a comprehensive methodology for determining if lifetime extension is a possibility, for wind turbine drivetrains. Given the drivetrain's critical role in the operation of the wind turbine, developing a systematic approach to determine remaining useful life and in turn the feasibility of lifetime extension potential, would be highly beneficial and valuable.

1.2 Research Questions

1. *Lifetime extension has been implemented on structural components such as the tower, but how can it be applied on the drivetrain? What can be learnt from other industries?*

2. *What approach should be taken to evaluate potential lifetime extension of wind turbine drivetrains, when:*

    a. *Only Supervisory Control and Data Acquisition (SCADA) data is available?*

    b. SCADA and vibration data are available?

1.3 Aim and Scope

Once wind turbines reach the end of their service life, there are typically three options available: decommissioning, re-powering and lifetime extension. The main aim of this thesis is to evaluate the feasibility of lifetime extension potential for the drivetrain, which is not only a critical element but is also typically replaced at the end of the turbine's service life. This has been carried out by learning from oil and gas, as well as marine structures, where the lifetime extension of offshore structures has been practiced over the last twenty (20) years. Based on the amount and type of input data, different approaches have been recommended to assess the possibility of lifetime extension. Mapping of critical components inside the drivetrain has been carried out, to focus on those that are more prone to failure. A state-of-the-art methodology, e.g. data-driven, has then been utilised to evaluate how much longer they can be in service. To

ensure accurate predictions, this methodology has then been enhanced by applying a probabilistic approach, in order to incorporate any model errors and uncertainties.

1.4 Contribution

This work develops a data-driven methodology, in terms of a novel process or procedure that identifies the most suitable well-established machine learning methods, that are best suited to predict the operating temperature of drivetrain components. The merits are the applicability of this procedure to the low resolution (sampling rate-wise) SCADA data, which is more common to be accessible in practice within industry, rather than the more sophisticated methods, that cannot be vastly applied in reality, due to the lack of access to a specific type of monitoring data. More importantly, the developed methodology proposes tracking/monitoring metrics that can detect abnormal components that deviate from their normal operating temperatures. With a priori knowledge obtained of the metrics at the failure time retrieved from a failed component, these proposed metrics can provide an estimate of remaining useful life (RUL) of the problematic components by extrapolation. This is indeed important, as the RUL estimation is a key stage in determination of life extension potential, which is indeed more complicated within mechanical sub-systems of turbines compared to the structural components, due to various reasons, including the higher frequency of load cycles (mechanical, thermal, electrical) leading to a more limited action window. In addition to providing the deterministic representation of those metrics, this work also presents two probabilistic measures of them, to cope with the uncertainties in the temperature

model predictors. Due to the generality of the underlying Monte-Carlo approach, the method can be extended to take account of other uncertainties e.g., from the sensors.

1.5 Layout of Thesis

The chapters are structured in the same sequence the work was carried out. Figure 1.1 shows the connection between each chapter and a brief description of each chapter is as follows:

Chapter 2:

Chapter 2 of this thesis delves into the background of wind turbine drivetrains. It discusses the evolution of wind turbines, along with their design and analysis. It explains the loads/forces/dynamics acting on the turbine, hub and drivetrain, their effects on the equipment/components and how any damage is typically calculated, which may reduce their operational life. It then investigates the different drivetrain topologies and the typical components that make up the drivetrain.

Chapter 3:

Chapter 3 explores existing research related to the selection of critical components, how component failures have been detected by utilising SCADA data, as well as model uncertainty and error assessment methods.

Chapter 4:

Chapter 4 reviews the existing remaining useful life and lifetime extension practices currently used in the wind industry, as well as in other industries, such as: oil and gas, marine vessels, electrical machines and nuclear power plants. It summarizes the methods used within each industry and then determines which key points may be applicable or transferable to the analysis of wind turbines drivetrains.

Chapter 5:

Based upon the literature review conducted in the previous chapter, a methodology for determining lifetime extension is proposed in Chapter 5, along with the theory used.

Chapter 6:

Due to the fact the drivetrain is made up of both mechanical and electrical equipment, Chapter 6 explores the development of a vulnerability map for a power converter. This has been researched in order to determine if it is possible to rank the components, within electrical equipment the same as in mechanical equipment, according to their risk of failure, from high to low.

Chapter 7:

Chapter 7 investigates implementing the method proposed in Chapter 5 on real-life data. SCADA data has been obtained from an onshore wind farm located in the UK. Based upon the type and amount of data collected, a model/process/method has been presented for the assessment stage of the overall process, with the aim of determining

whether useful and reliable results regarding remaining useful life and lifetime extension can be achieved.

Chapter 8:

In Chapter 8, the model/process/method that has been proposed in the previous chapter, is explored for uncertainties and errors, in order to ensure accurate and reliable results.

Chapter 9:

The final chapter, Chapter 9 summarizes all the findings, continues any discussions, answers the research questions and draws conclusions from all the work completed within this thesis. Future work is also discussed.

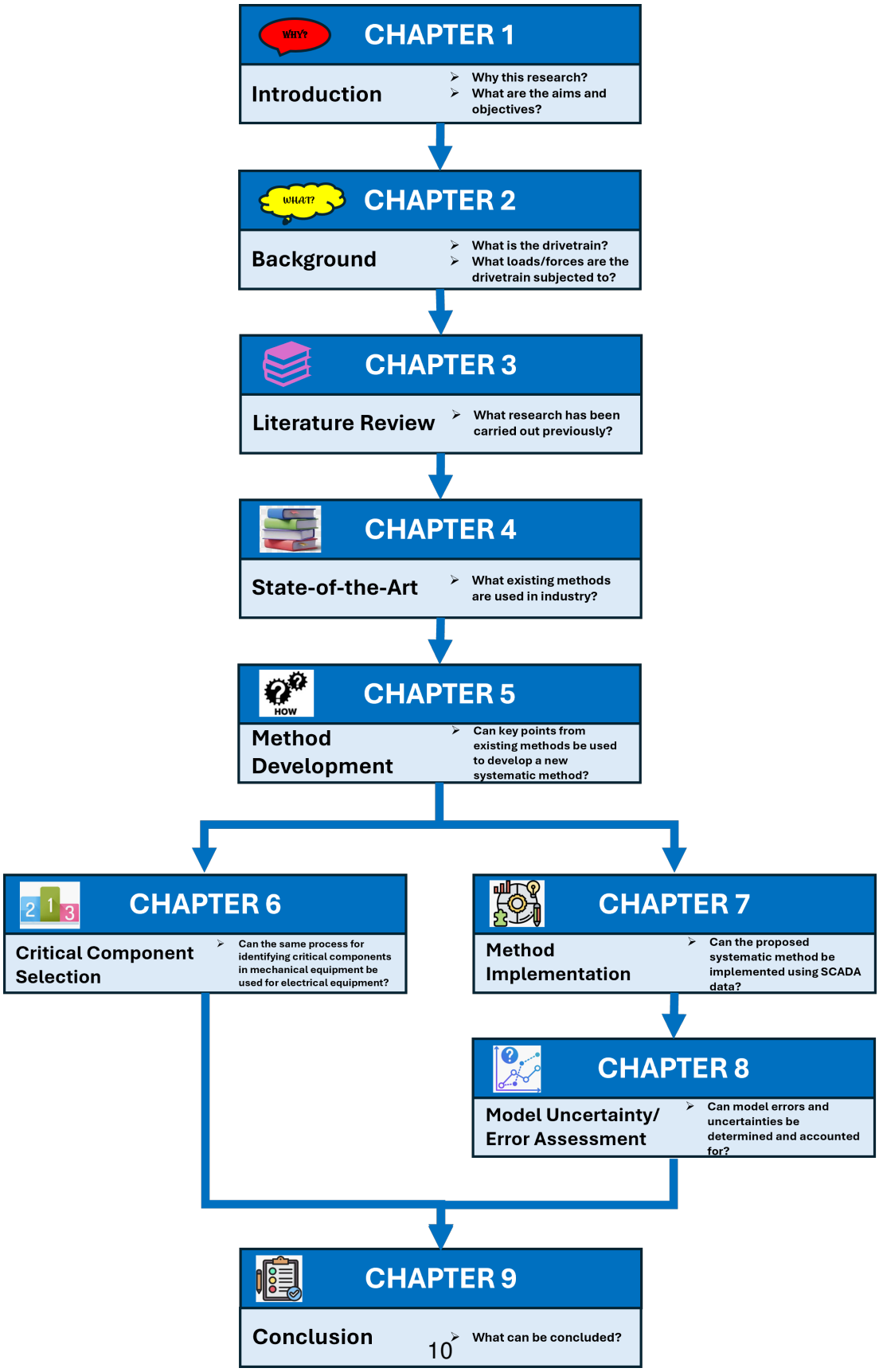

Figure 1.1: Chart showing the Chapters making up the Thesis and the Connections between them

1.6 List of Papers

The following papers have been published over the course of the PhD:

Paper 1:

On Lifetime Extension of Wind Turbine Drivetrains.

Authors: Kelly Tartt, Amir R. Nejad, Abbas Kazemi-Amiri, Alasdair McDonald

Published in *ASME 2021 40th International Conference on Ocean, Offshore and Arctic Engineering*, 2021, DOI: 10.1115/OMAE2021-62516.

Paper 2:

Development of a Vulnerability Map of Wind Turbine Power Converters.

Authors: Kelly Tartt, Abbas Kazemi-Amiri, Amir R. Nejad, Alasdair McDonald

Published in *Journal of Physics: Conference Series (Torque 2022)*, 2022, DOI: 10.1088/1742-6596/2265/3/032052.

Paper 3:

Life Extension of Wind Turbine Drivetrains by means of SCADA Data: Case Study of Generator Bearings in an Onshore Wind Farm.

Authors: Kelly Tartt, Abbas Kazemi-Amiri, Amir R. Nejad, James Carroll, Alasdair McDonald

Published in *Results in Engineering*, 2024, DOI: 10.1016/j.rineng.2024.102921.

The following paper has been approved and will be published shortly:

Paper 4:

On Confidence Interval-Based Anomaly Detection Approach for Temperature Predictions of Wind Turbine Drivetrains to Assist in Lifetime Extension Assessment.

Authors: Kelly Tartt, Abbas Kazemi-Amiri, Amir R. Nejad, James Carroll

Approved by *Engineering Research - Forschung im Ingenieurwesen*.

The following papers have been published in addition to the above, although not directly related to the PhD research:

Paper 5:

Structural Optimisation of Offshore Direct-Drive Wind Turbine Generators Including Static and Dynamic Analyses.

Authors: Kelly Tartt, Abbas Kazemi-Amiri, Alasdair McDonald, Pablo Jaen-Sola

Published in *Journal of Physics: Conference Series (DeepWind 2021)*, 2021, DOI: 10.1088/1742-6596/2018/1/012040.

Paper 6:

Identifying Path Ahead for Tackling Future Challenges in Direct-drive Wind Turbine Generator's Electro-Mechanical Design and Manufacturing.

Authors: Abbas Kazemi-Amiri, Kelly Tartt, Alasdair McDonald

Published in *Forsch Ingenieurwes 89, 52*, 2025, DOI: 10.1007/s10010-025-00792-4.

1.7 References

[1] International Energy Agency. Net zero roadmap a global pathway to keep the 1.5 ℃ goal in reach. https://iea.blob.core.windows.net/assets/9a698da4-4002-4e53-8ef3-631d8971bf84/NetZeroRoadmap_AGlobalPathwaytoKeepthe1.5CGoalinReach-2023Update.pdf, 2023.

[2] International Energy Agency. European climate law. https://eur-lex.europa.eu/eli/reg/2021/1119/oj, 2021.

[3] Paris Agreement. Paris agreement. In *Report of the Conference of the Parties to the United Nations Framework Convention on Climate Change (21st Session, 2015: Paris). Retrived December*, volume 4, page 2017. HeinOnline, 2015.

[4] Global Wind Energy Council. Gwec - global wind report 2024. Technical report, Global Wind Energy Council, 2024.

[5] Wind Europe. Repowering europe's wind farms is a win-win-win. https://windeurope.org/newsroom/press-releases/repowering-europes-wind-farms-is-a-win-win-win/#:~:text=170%20wind%20farms%20have%20so,reap%20the%20benefits%20of%20repowering., 2022.

[6] Eva Topham and David McMillan. Sustainable decommissioning of an offshore wind farm. *Renewable energy*, 102:470–480, 2017.

[7] WindEurope. What happens when wind turbines get old? new industry guidance document for dismantling and decommissioning. https://windeurope.org/newsroom/press-releases/what-happens-when-wind-turbines-get-old-new-industry-guidance-document-for-dismantling-and-decommissioning/, 2020.

[8] Tim Rubert, P Niewczas, and D McMillan. Life extension for wind turbine structures and foundations. In *International Conference on Offshore Renewable Energy 2016*, 2016.

[9] Marcel Schedat, Torsten Faber, and Abiman Sivanesan. Structural health monitoring concept to predict the remaining lifetime of the wind turbine structure. In *2016 International Conference on the Domestic Use of Energy (DUE)*, pages 1–5. IEEE, 2016.

[10] Lisa Ziegler, Ursula Smolka, Nicolai Cosack, and Michael Muskulus. Brief communication: Structural monitoring for lifetime extension of offshore wind monopiles: can strain measurements at one level tell us everything? *Wind Energy Science*, 2(2):469–476, 2017.

[11] Elize Petrovska, Jean-Baptiste Le Dreff, Selda Oterkus, Philipp Thies, and Edward McCarthy. Application of structural monitoring data for fatigue life predictions of monopile-supported offshore wind turbines. In *ASME 2020 39th Interna-*

tional Conference on Ocean, Offshore and Arctic Engineering. American Society of Mechanical Engineers Digital Collection, 2020.

[12] Yi Guo, Roger Bergua, Jeroen van Dam, Jordi Jove, and Jon Campbell. Improving wind turbine drivetrain reliability using a combined experimental, computational, and analytical approach. In *International Design Engineering Technical Conferences and Computers and Information in Engineering Conference*, volume 46407, page V007T05A004. American Society of Mechanical Engineers, 2014.

Chapter 2

Background of Wind Turbine Drivetrains

2.1 Introduction

A wind turbine can be defined as a machine or device that changes kinetic energy from the wind into electrical energy or electricity [1].

They typically consist of three main sub-systems: the tower/supporting structure, rotor including blades and nacelle. The tower is the structural component that supports the turbine and can be designed and manufactured in many forms, such as monopiles and three or four legged jacket types, to name just a few. The blades are aerofoils that are located at the top of the tower and which rotate when the wind blows, converting the kinetic energy from the wind into mechanical energy. Finally, there is the nacelle, in which the blades are attached to the front of via a rotor and which houses the drivetrain, also known as the “heart" of the turbine [2], as this is where the mechanical

energy is converted into electrical energy.

In general, modern wind turbines (Figure 2.1) are:

1. Three-bladed.
2. Horizontal axis.
3. Variable Speed.
4. Pitch Regulated.
5. Located upwind.

Figure 2.1: Typical Wind Turbine. Courtesy of Wikipedia.

Wind turbines can also be either:

1. Land-based.
2. Offshore based.
    (a) Fixed-bottom.
    (b) Floating.
        i. Semi-submersible.
        ii. Spar.
        iii. Tension Leg Platform.

2.2 Evolution of Wind Turbines

Over the last century the wind energy sector has exploded. To date the global wind power capacity has reached 1 TW, [3]. Figure 2.2 shows the exponential increase in both onshore and offshore wind capacity over just the last 10 years [4].

The graph shows that although the biggest wind sector at the moment is still onshore wind, that offshore is starting to increase. This is mainly due to the fact that the wind turbines installed offshore can be much larger, as there is a lot more space and noise is not a problem offshore. The downsides though, are that the CapEx and OpEx costs are much more expensive. These are summarised in [5] and show that for a 3.3 MW land based turbine the CapEx and OpEx costs are $1,968/kW and $43/kW/yr respectively, whereas for a 12 MW fixed bottom offshore turbine, the CapEx and OpEx costs are $5,411/kW and $135/kW/yr respectively, so more than double, with

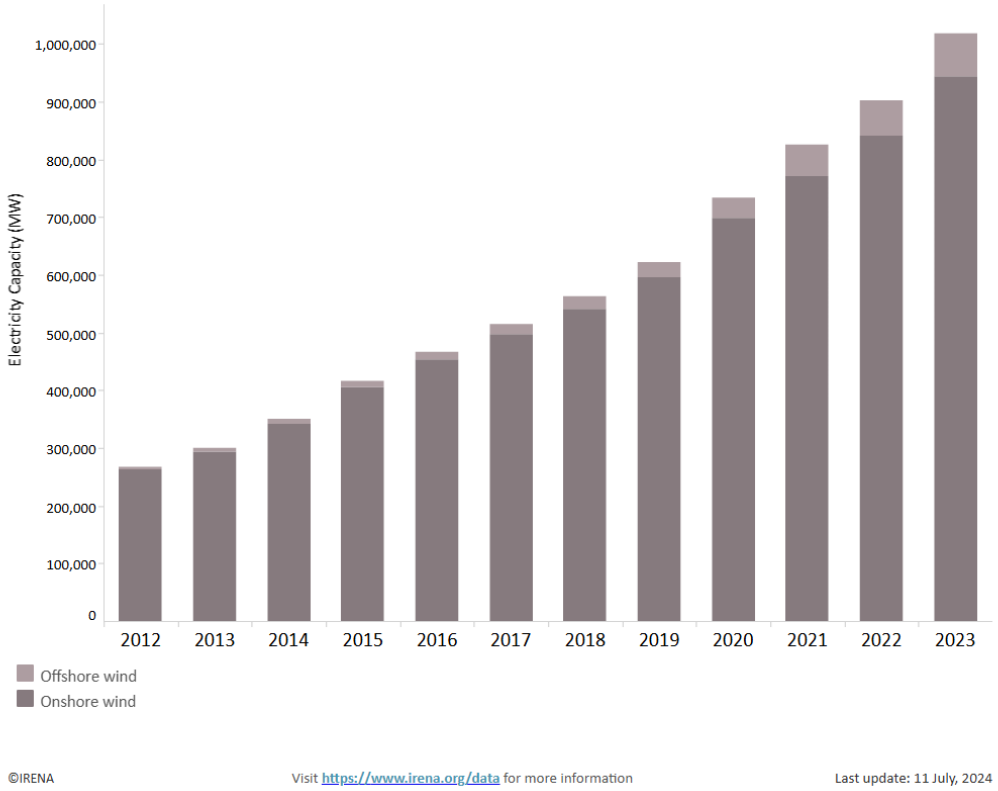

Figure 2.2: Graph Showing Growth of the Wind Industry. Courtesy of IRENA.

the CapEx costs for a 12 MW floating offshore turbine being even higher, $7,349/kW and $108/kW/yr for CapEx and OpEx respectively. This is mainly due to the fact accessibility is an issue and the turbines are located in a much harsher environment, but if the targets that are being set by multiple governments and institutions are to be met, then many more offshore wind turbines need to be installed over the coming decades.

Figure 2.3 shows how the power and size of the wind turbines have evolved over the years.

It is important to note that not only do the structural components, such as the tower and blades increase, the mechanical and electrical components also have to evolve to support the increased power output and size.

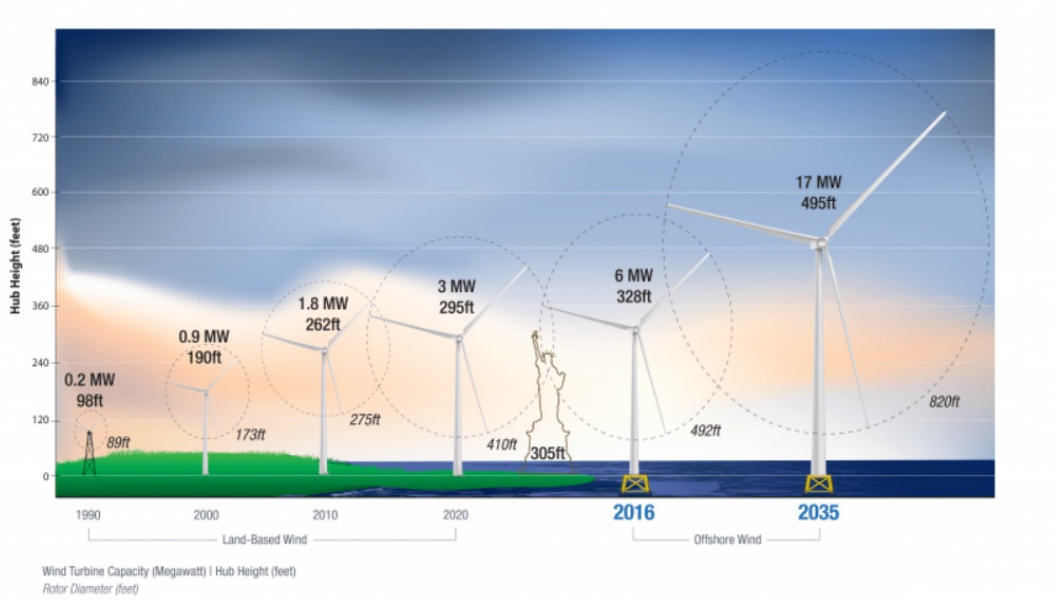

Figure 2.3: Evolution of Wind Turbines. Courtesy of Department of Energy.

2.3 Design and Analysis of Wind Turbines

As discussed, wind turbines are large structures situated outdoors in harsh environments, therefore they are subjected to environmental loads, as well as other loads (which are discussed more in Section 2.3.3) and because they are dynamic systems, they respond to all the applied varying loads, all of which they need to survive for the duration of their designed life, which is typically between 20-25 years.

2.3.1 Design Standards

During the design of wind turbines, technical standards are consulted. Technical standards are defined as documented rules or guidelines for carrying out a task or process and they are important in ensuring that a process or item meets a set specification, as well as standardising the methods used, which ensures a consistent approach [6].

For wind turbines, the International Electrotechnical Commission (IEC) 61400-1 (land-based), 61400-3-1 (offshore fixed) and 61400-3-2 (offshore floating) standards explain how to determine the loads, both fatigue and extreme, in which the wind turbines need to survive. Extreme loads can be defined as loads that may rarely occur but if or when they do could cause catastrophic damage, whilst fatigue loads are defined as loads which occur almost continuously and are constantly varied, causing "wear and tear" on the system [7].

The above mentioned standards contain a large number of design load cases, which are divided into a number of scenarios [8], including:

1. Power production.
2. Power production with fault.
3. Start up.
4. Emergency shut down.
5. Parked.
6. Parked with fault conditions.
7. Transporting, assembling, maintenance and repair.

All of these scenarios need to be taken into account when designing the turbines, as they are all likely to occur during the wind turbine's life.

In addition to the standards described above, there are a number of standards that are used for specific components, such as IS0 6336 for gears, ISO 281 for bearings and DIN 743 for shafts.

2.3.2 Global Modelling

To assist with the design and analysis of wind turbines, typically a global model is developed. FAST and HAWC2 are just a few examples of aero-hydro-servo-elastic dynamic software that can be used to construct the global model. All the various types and sources of loads, discussed in the next section, are applied to the model and the response including forces, moments and motions obtained [9].

2.3.3 Description of the Loads Acting on a Wind Turbine

This section begins with a brief high-level summary of the wind turbine process, before delving deeper into all the various loads that the turbines are subjected too. When the flow of wind hits the turbine blades it exerts a force, due to the shape of the blades a lift and drag force is produced, as per Figure 2.4. The lift force is due to the pressure difference above and below the blade and acts perpendicularly to the direction of wind flow, whereas the drag force acts in parallel to the direction of wind flow. The resultant or total force from both these forces (lift and drag), produces a turning force or torque and a thrust force. The turning force or torque, which is a tangential force, rotates the blades and the thrust force, which is a perpendicular force, bends the blades and tower, [10]. This is due to the fact that wind turbines are flexible, not rigid, so the components that make up the turbine, including the tower and blades bend when they are subjected to loads induced by the wind. As the blades are attached to the rotor hub, which is in turn attached to the main shaft, which is located in the nacelle, the loads experienced by the hub are transferred to the main shaft through to the drivetrain.

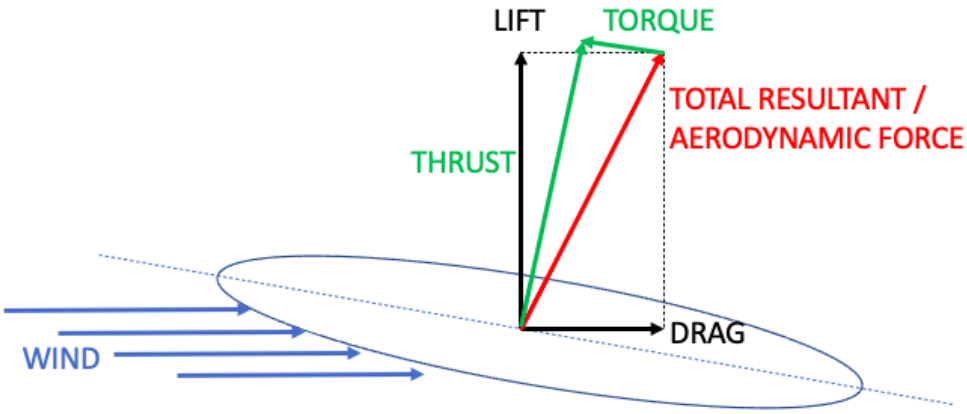

Figure 2.4: Forces Acting on Wind Turbine Blades

2.3.3.1 Loads/Forces/Dynamics Acting on Wind Turbine

Whether the wind turbines are installed onshore or offshore, they are subjected to a number of varying loads and due to the fact that wind turbines are dynamic systems, they are constantly responding to the continuously changing load conditions [8], all of which they should be designed to withstand, as discussed in Section 2.3. The sources of these applied loads include:

1. Environmental i.e. Aerodynamics, Hydrodynamics (if offshore-based).
2. Operational.
3. Inertial.
4. Gravitational.

These loads can be classed as either external or internal loads, as well as extreme/ultimate or fatigue loads, [7]. The effects of these applied loads are ultimate limit states and/or fatigue and are discussed in more detail in Section 2.3.5. Figure 2.5

shows the type of loads that fall under these categories, including: steady-state, transient, cyclic and stochastic load types.

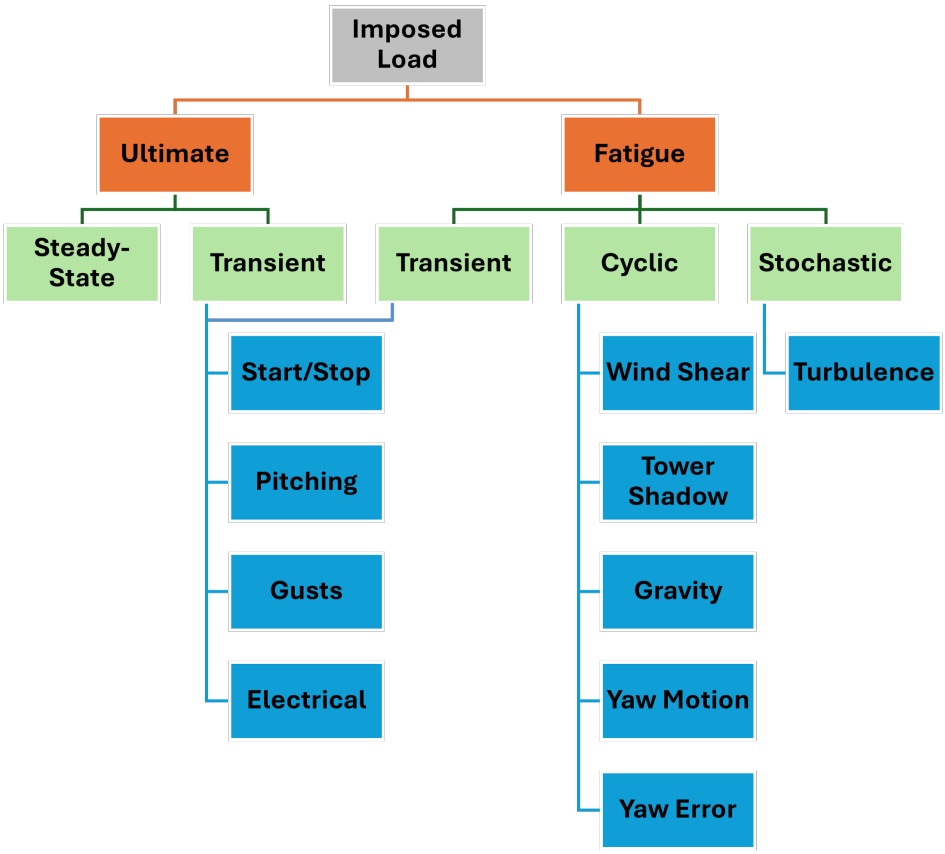

Figure 2.5: Different Types of Loads ([10])

One of the main sources of applied loads for wind turbines is from environmental conditions, which includes aerodynamics. Aerodynamics can be defined as the study of moving air and it's interaction with solid bodies, either stationary or moving, that are located within the air flow. Therefore, in the case of wind turbines, the moving air is the wind and the solid body is the wind turbine, specifically the blades and tower.

Wind can be complex and is made up of different components that vary in size and frequency [13], so the loads and forces acting on the wind turbine vary accordingly but

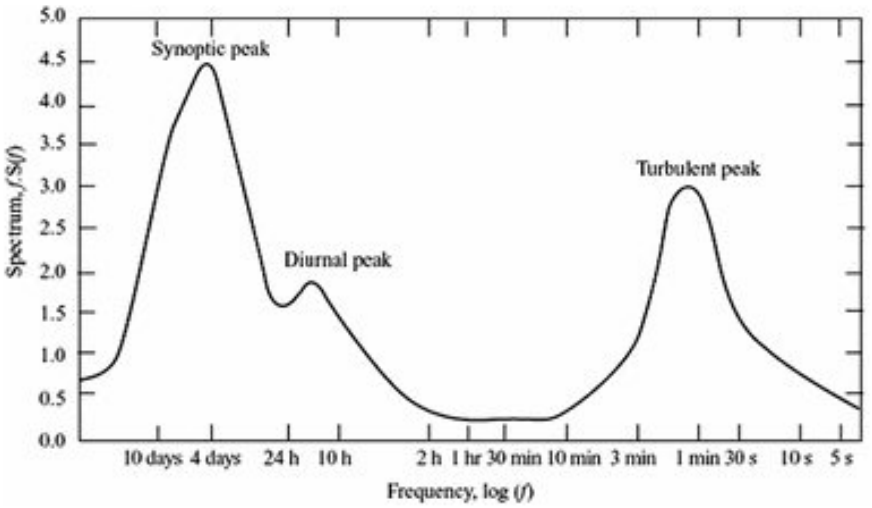

Figure 2.6: Van der Hoven Spectrum [11], [12]

all the aspects have to be taken into account when designing or calculating the loads acting on a turbine. Figure 2.6 displays the Van der Hoven graph, which shows the different components.

Phenomena that either effect and/or contribute to aerodynamic loading include:

1. Mean wind.
2. Wind Shear.
3. Tower Shadow.
4. Turbulence.
5. Yaw Error.
6. Tilt.

Mean wind is classed as a steady-state load. These are loads that stay pretty consistent over long periods of time [8].

Wind shear is defined as the speed of the wind increasing with height, due to the effects of obstacles on the ground affecting the flow of the wind (Figure 2.7). Therefore, the wind speeds that each blade sees varies as it rotates, this can be referred to as 1P loading, where P is the rotational speed. Other causes of 1P loading can include: imbalance of masses, misalignment of the main shaft to the rotor, gyroscopic forces etc. ([10]).

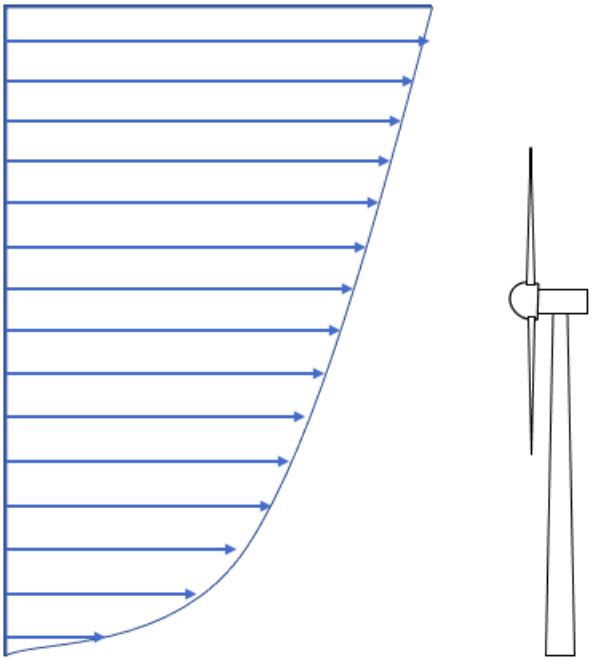

Figure 2.7: Wind Shear Effect

Tower shadow can be defined as the phenomena where the flow of wind is disrupted/blocked by the tower structure (Figure 2.8), i.e. the wind is forced to go around, this causes an effect on the flow i.e. it slows it down, which in turn causes thrust variations when each blade passes through the disrupted flow, [14]. This is referred to as 3P loading because each blade i.e. three, experiences this during one full rotation.

Turbulence can be defined as short bursts or gusts, typically of less than 10 min-

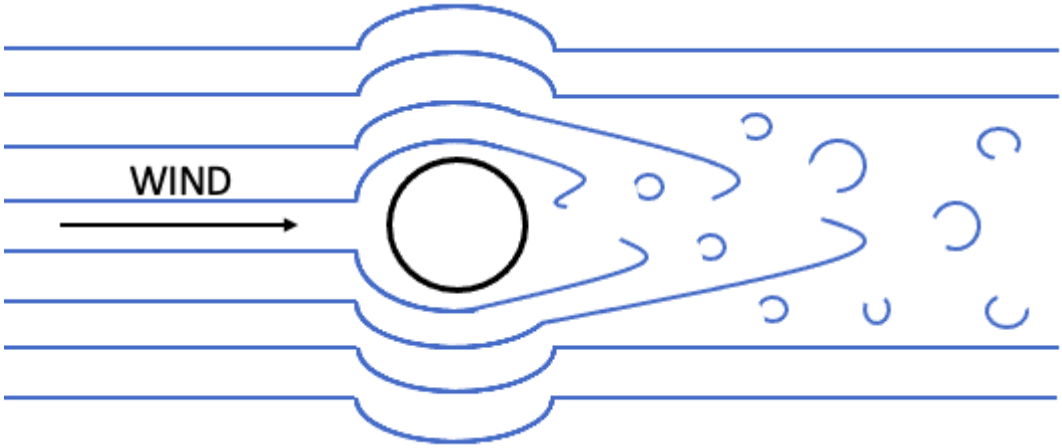

Figure 2.8: Tower Shadow Effect

utes, of varied wind speeds. For large turbines, as the blades sweep in and out of the gust, ‘clumping’ of loading at multiples of blade passing frequency occurs, whereas for smaller turbines all the blades “experience changes in the wind speed as they occur, spread across the whole turbulence spectrum" [10].

Yaw error and tilt are similar in the fact that the cyclic loading varies the steady in-plane wind, which in turn changes both the resultant wind speed and lift coefficient [10].

The wind speed variation over the blades for wind shear, tower shadow, yaw error and tilt are classed as deterministic/cyclic, whereas turbulence is classed as stochastic. Cyclic loads are repetitive, in that they repeat as the rotor or cycle rotates, whereas stochastic loads change randomly and there is no pattern [8].

Offshore wind turbines have additional loading specifically on the tower due to the waves i.e. hydrodynamic loading.

Inertia is another source of loading on the wind turbine. Inertial loads are caused

when starting or stopping the wind turbine and they are classed as transient loads. Transient loads occur for very short time periods. Additional transient loads also include gusts and pitch motion [8].

Another source of loads that the turbine is subjected to is gravity. Gravitational loads due to the weight of the blades produce an “in plane root bending moment" [10], which naturally increases with blade/turbine size. This is a cyclic load, as it repeats as the rotor spins.

Another type of cyclic load is resonance load, this occurs when the unbalanced rotor blades “rotational frequency matches with the structural components" natural frequency [8].

2.3.3.2 Loads/Forces/Dynamics Acting on the Hub

As discussed, the blades are attached to the rotor hub. Therefore, the hub is subjected to the aerodynamic, inertial and gravitational loads as discussed above. The dominant loads on the hub come from the loading of the blades, i.e. thrust force, which acts downwards, the weight of the rotor, which acts in a vertical direction and blade root moments from the in- and out-of- plane blade loading, [13]. Figure 2.9 and Figure 2.10 are taken from [13] and shows the power spectra for both the forces and out-of-plane loading on the hub. The graphs show obvious peaks at 3ω, which is the number of blades multiplied by the rotational speed and it’s multiples. This is due to the fact that in both the deterministic and stochastic aerodynamic loads, which contribute to the hub moment, the hub experiences all the blades passing through the same wind phenomena at a rotational speed, hence the obvious peaks in the graphs at 3ω, 6ω,

9ω etc.

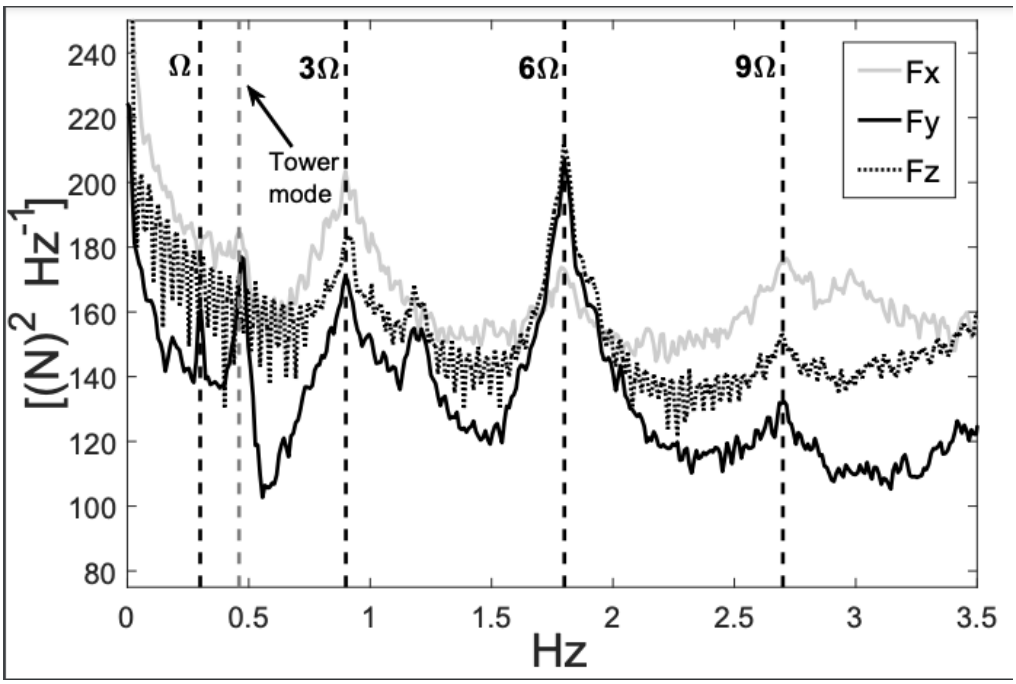

Figure 2.9: Power Spectra of Forces on Hub [13]

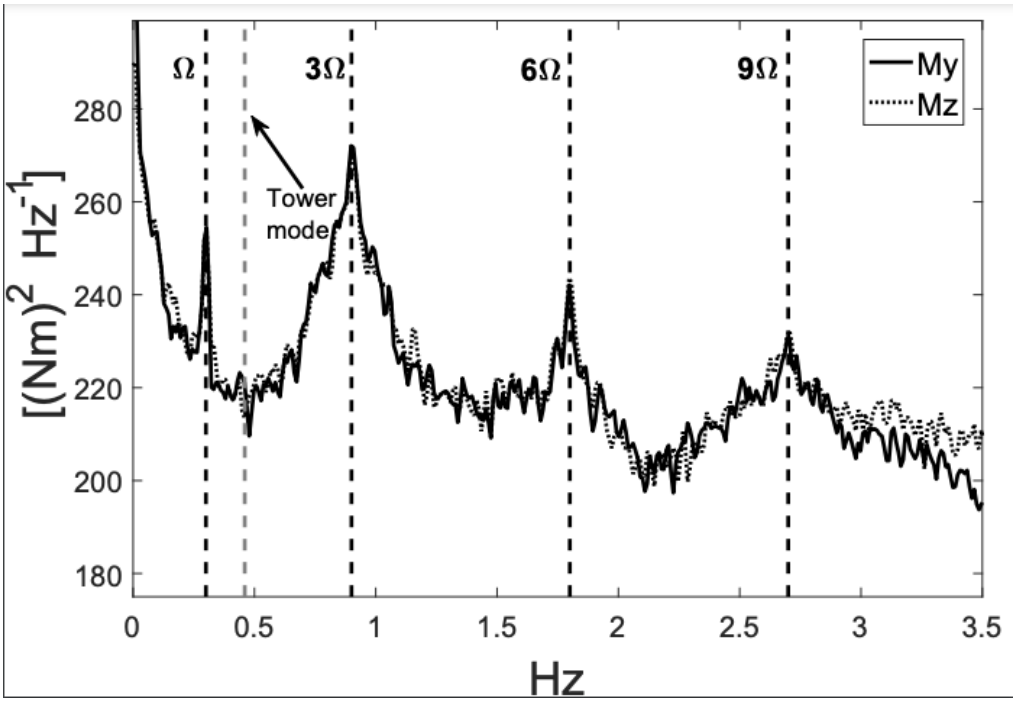

Figure 2.10: Power Spectra of Out-of-Plane on Hub [13]

2.3.3.3 Loads/Forces/Dynamics Acting on the Drivetrain

Loads on the drivetrain can come from both external and internal sources. The external sources include both aerodynamic and grid loads, whereas the internal sources include gear meshing caused by the interaction of mating gears and bearing roller contact [15].

The flow of the loading from the wind through the rotor to the drivetrain is shown in Figure 2.11.

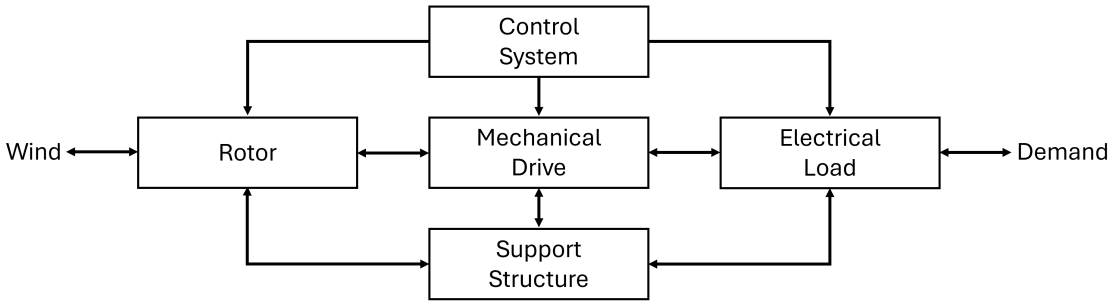

Figure 2.11: Flow of Loads throughout the Wind Turbine ([10])

With the dynamics throughout the wind turbine, including the drivetrain, shown in Figure 2.12.

The torque and non-torque loads from the hub are transferred to the main shaft. The non-torque loads are caused by gravitational loads, wind shear and tower shadow, [16].

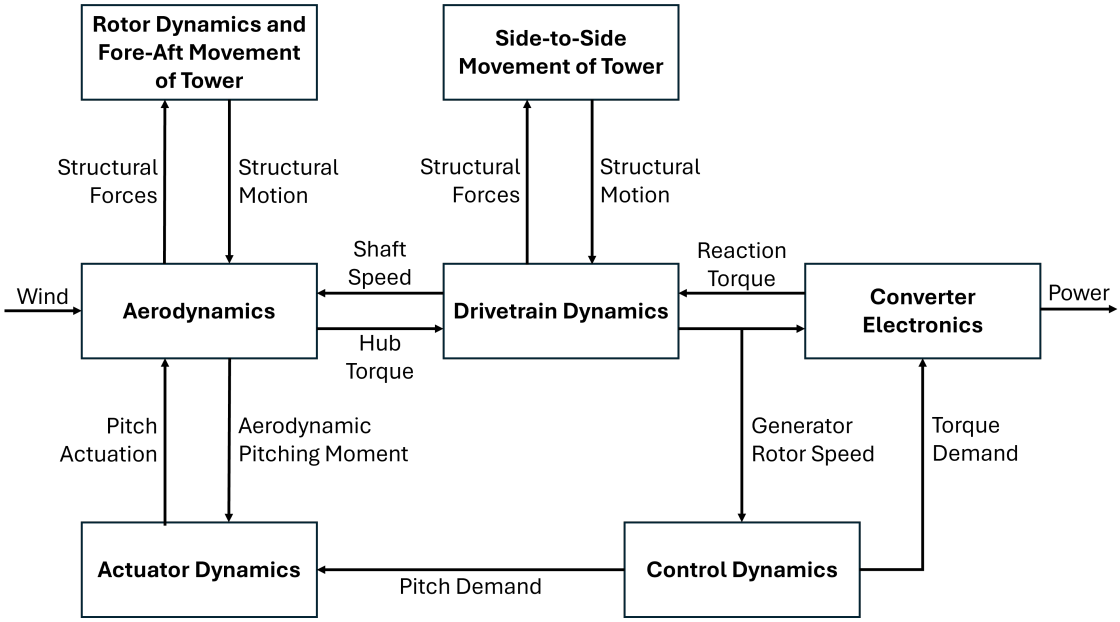

Figure 2.12: Dynamics on Wind Turbine ([10])

2.3.4 Local Modelling

Typically after developing a global model, a decoupled analysis or local modelling/simulation is constructed, particularly for the drivetrain, in order to get more accurate response results. The following software tools may be used, this list is not exhaustive but just highlights the most common:

1. Multi-body software packages.

2. High fidelity finite element analysis models.

3. Dynamic analytical models.

From both the global and the decoupled/local models/simulations, useful information with regards to specific forces on particular components can be extracted. Determining the magnitude of these forces is important because as mentioned earlier, all

wind turbines are subjected to loading, which in turn causes forces and stress on the components, which needs to be calculated so that the amount of damage particularly fatigue, on each component can be determined. Calculating the fatigue damage is explained more in Section 2.3.5.

2.3.5 Effects of Loading - Fatigue Damage

As mentioned previously, all the various loads acting on the wind turbine have an effect, with the most common effect being fatigue, which causes up to 90% of mechanical failures, [17]. Fatigue impacts both the structural and mechanical components.

Continuous cyclic loading causes stress on the system, which in turn causes fatigue. Stress can be defined as an “external force acting over a cross-sectional area of an object" and fatigue can be defined as the reduction of strength of the object/system, which can lead to damage and/or failure.

2.3.5.1 Calculating Structural Fatigue

S-N curves can be used to determine fatigue, where S refers to the stress and N refers to the number of cycles. A typical S-N curve is shown in Figure 2.13, where both the y and x axis are the log values for S and N, respectively. From the S-N curve, the number of cycles to failure for a specific applied stress can be determined.

The S-N curve can be used for a consistent applied stress but in real life for wind turbines the loading is varied, hence the stress acting on the components also varies, therefore a method called rainflow counting can be used. Rainflow counting uses a load vs. time graph, which has been rotated clockwise by 90 degrees, to determine

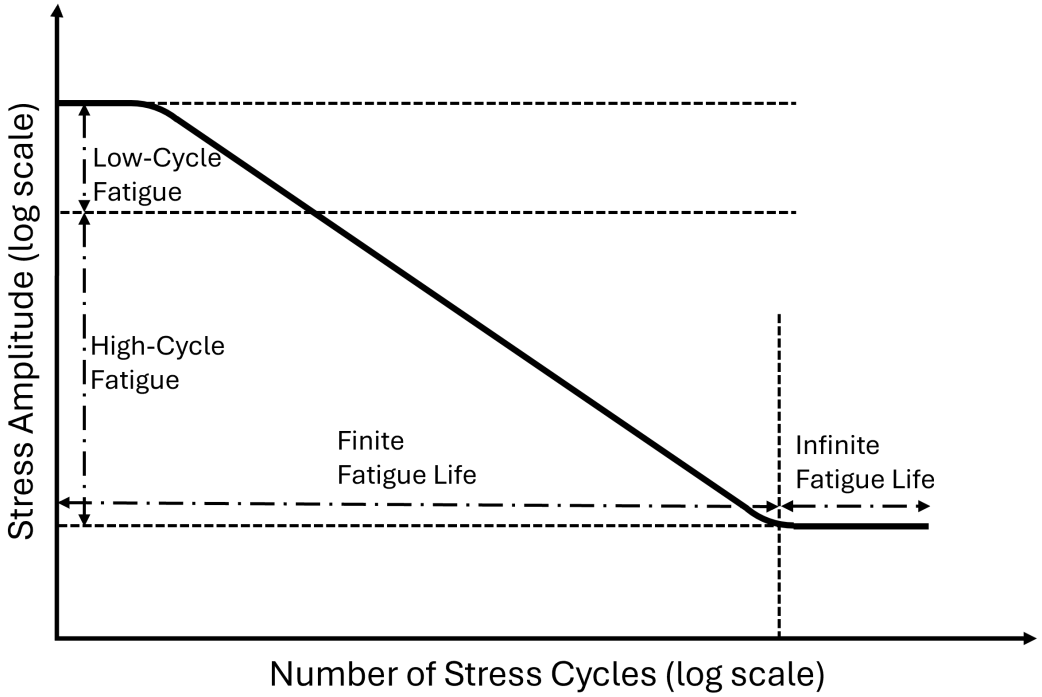

Figure 2.13: Typical S-N Curve (Figure adapted from [18])

the number of cycles for each stress range. The stress cycles need to be treated individually, so the time series is split into single stress cycles. Upon completion of the counting method, the results are put into bins, to show the stress ranges in histogram form. An example of rainflow counting is shown in Figure 2.14.

Whether the S-N curve or rainflow counting method is utilised to determine the number of cycles, the Miner's Rule can then be used to calculate the fatigue damage/life. Following the rainflow counting method, the total damage is determined by adding up the damage done by each individual stress cycle. Miner's Rule states that when fatigue damage, D, equals to 1, then failure will occur. Equation 2.1 can be used to calculate fatigue damage:

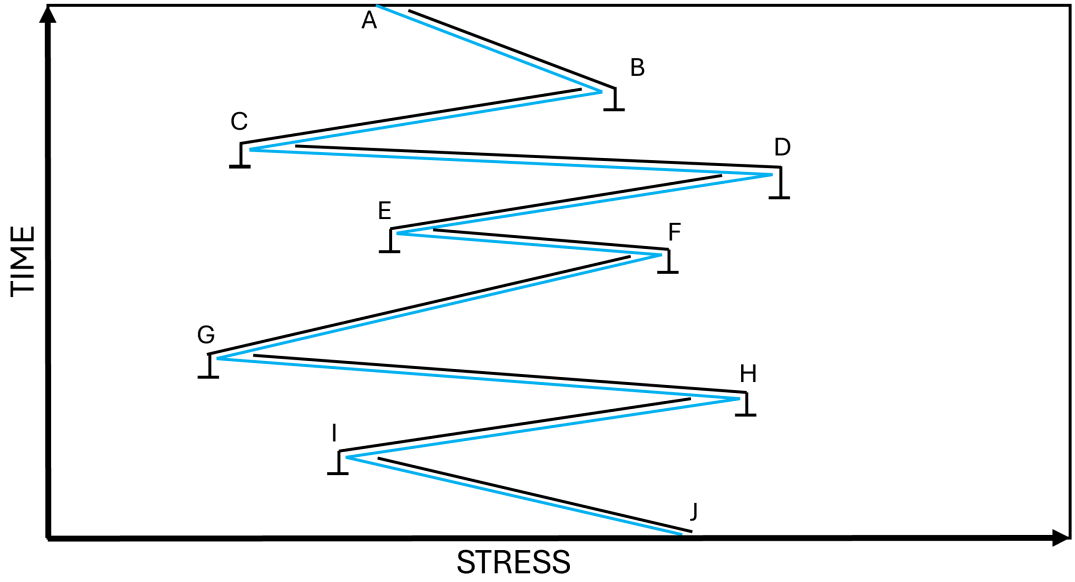

Figure 2.14: Rainflow Counting Method [19])

$$\sum_{i=1}^{k} n_i/N_i = D \tag{2.1}$$

Where D is the fatigue damage, k is the number of stress ranges, n_i is the number of cycles at each stress range, i and N_i is the number of fatigue life cycles at each stress range, i.

2.3.5.2 Calculating Mechanical Fatigue

The Miner's Rule described above can also be used to determine the damage for mechanical components but the stresses are calculated differently.

2.3.5.3 Bearing Fatigue

The fatigue life of bearings, including the main bearings, are calculated using the axial and radial loads that are exerted on the bearing, along with the rotational speed. The hub loads that have been taken from the aeroelastic model are used on a beam model, in order to calculate the axial and radial loads exerted on the bearings at each operating point and across all time-steps, [20]. The hub's loads are required because the hub is attached to the main shaft, which is where the bearings are located, so the hub loads are transferred to the main shaft, which in turn are transferred to the bearings. These axial and radial loads at each operating point are then used to determine the dynamic equivalent radial load at each time step, which is then averaged at each operating point. Miner's rule is then used to calculate the one equivalent load for the whole loading history, as a load value is required, P_r, that accurately represents the loading that the bearing sees over it's lifetime. This value can then be used in Equation 2.2 to calculate the basic life rating for roller bearings.

$$L_{10} = (C_r/P_r)^{(10/3)} \tag{2.2}$$

Where L_{10} is the life rating or the number of revolutions that 90% of bearings are expected to not experience any fatigue damage [13], C_r is the dynamic load rating (from manufacturer) and P_r is the dynamic equivalent radial load of the bearing.

Damage equivalent loads (DEL) can be defined as one single load that will create the same fatigue damage as all the loads over a time period. Damage equivalent loads use the Palmgren-Miner linear cumulative damage theory [21]. This theory assumes

that there is a linear relationship between fatigue damage and the number of cycles, up until a certain ”prescribed life exhausted of material" and that only cycle load range, not the cycles mean value, promotes fatigue damage, [8].

2.3.5.4 Gear Fatigue

Fatigue damage on gears can occur in the form of pitting and/or root bending damage. The fatigue damage for gears is calculated in a similar method to the bearings. From the models/simulations, the “time-varying gear transmitted loads" [9] are used to calculate the bending stresses and tooth contact. The stress cycle counting method is then used to determine bins. Fatigue damage for each wind speed over a short term of 1 hour, is calculated using the “Palmgren-Miner linear accumulative damage hypothesis" using Equation 2.3, where k and m are S-N curve parameters, u is wind speed, $D(u)$ is the 1-hour fatigue damage at wind speed u, [9].

$$D(u) = 1/k \sum_i n_i(u).s_i^m \tag{2.3}$$

The long-term damage is then calculated using Equation 2.4, where $cut-in$ and $cut-out$ are wind speeds in m/s, T is the design life, e.g. 20 years and $f(u)$ is the probability density function of the mean wind speed, [9].

$$D^{LT} = \int_{cut-in}^{cut-out} T.D(u).f(u).du \tag{2.4}$$

2.4 Types of Drivetrains

A wind turbine's drivetrain can be either geared or direct-drive (gearless), as shown in Figure 2.15. [22] and [23] state that fourteen (14) years ago, 83% of wind turbines were geared, while 17% were direct-drive.

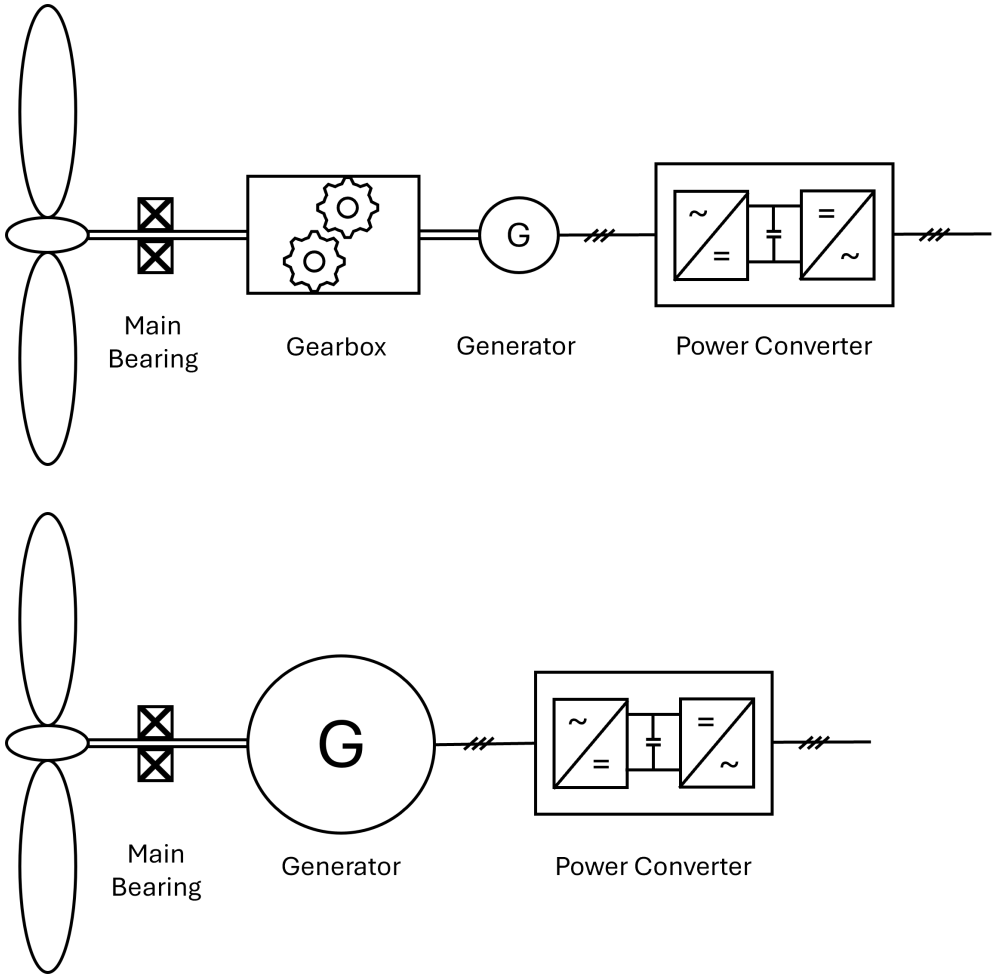

Figure 2.15: Different Types of Drivetrains - Geared (top) and Direct-drive (bottom) [24]

Typically modern wind turbines contain a gearbox to increase the rotational speed and reduce the torque of the main shaft to the generator but recently direct-drive or gearless turbines are becoming more popular. This is mainly due to the fact that not

only is the gearbox one of the main components in the drivetrain that fails but also once it fails it causes the most downtime for the wind turbine and is extremely costly [25]. Therefore, by eliminating the gearbox, the number of moving parts within the drivetrain is reduced, which in turn will reduce maintenance costs and increase the reliability.

Geared drivetrains can be classed as either medium speed or high speed systems, depending upon the gearbox installed and come in a number of different topologies, as shown in Figure 2.16. More specific information on the gearbox can be found in the next section.

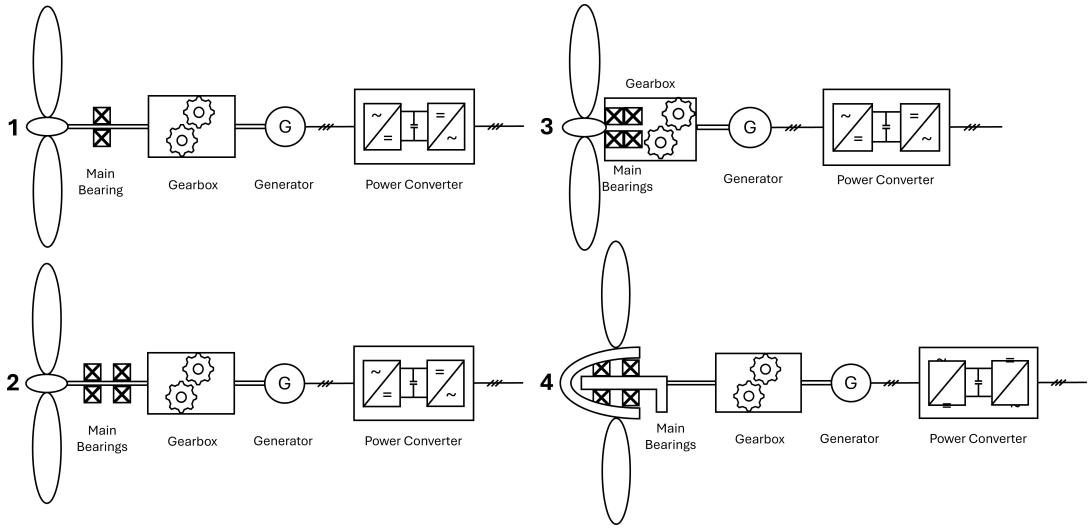

Figure 2.16: Different Types of Geared Drivetrains - 1 (Single main bearing), 2 (Double main bearing), 3 (Gearbox-integrated main bearing) and 4 ("Floating drivetrain" design) [13]

Although there are many benefits to eliminating the gearbox, there can also be some issues, such as the size and weight of the generator having to increase. Direct-drive generators are called low-speed generators because they are directly connected to the rotor hub via the main shaft, which is rotating at a low speed. Therefore, in order

for the generator to produce the required power output the torque needs to increase, which can be seen in Equation 2.5, where P corresponds to the power output, T is the required torque and ω is the rotational speed.

$$P(\uparrow) = T(\uparrow)\omega(\downarrow) \tag{2.5}$$

Torque can be calculated from Equation 2.6, where R is the radius, σ is the shear stress and l is the axial length of the machine.

$$T(\uparrow) = 2\pi R^2(\uparrow)\sigma l(\uparrow) \tag{2.6}$$

So in order to meet the required torque, the dimensions of the generator such as radius, and/or length, needs to increase, thus increasing the size and weight of the generator.

There are also a number of different topologies for direct-drive drivetrains as shown in Figure 2.17. All topologies show the main shaft connected directly to the generator, with the main difference being the number of main bearings on the shaft - single, double or triple.

The components most likely to fail in a direct-drive drivetrain include: the electrical sub-assemblies and the generator, [26] and [27], compared to the: electrical sub-assemblies, gearbox and generator, in the geared drivetrains.

Tables A.1 - A.7, show the various drivetrain layouts of turbines from Siemens Gamesa, Vestas, GE and Goldwind. They show that for Siemens Gamesa, GE and Vestas the majority of the models are geared drivetrains, for example 63% for Siemens

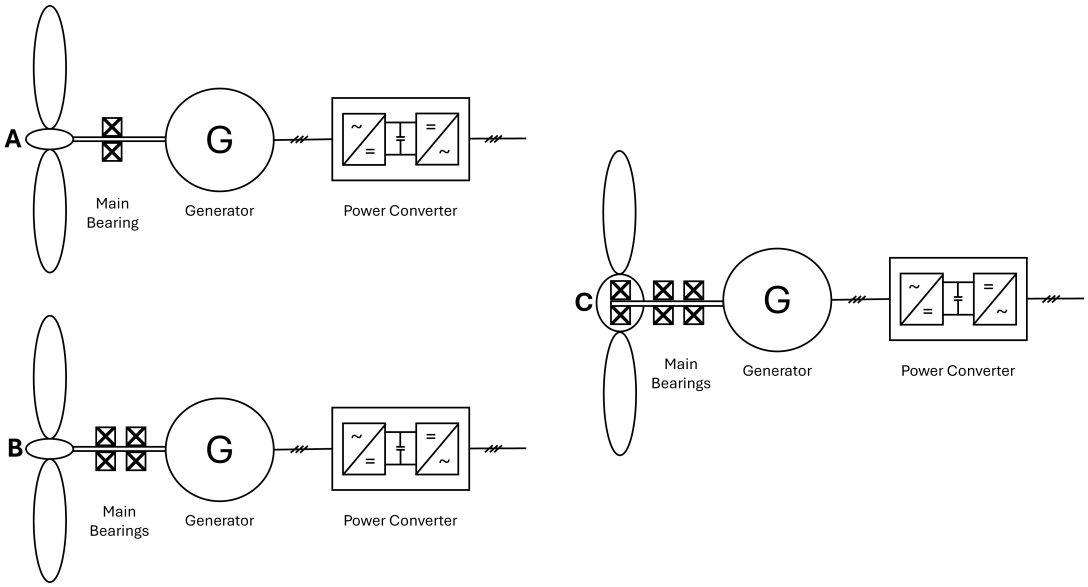

Figure 2.17: Different Types of Direct-Drive Drivetrains - 1 (Single main bearing), 2 (Double main bearing) and 3 (Triple main bearing) [13]

Gamesa and approximately 90% for GE but this is the opposite case in Goldwind, with the majority of their models being direct-drive.

Articles recently published by the Global Wind Energy Council (GWEC) [28] and Blackridge [29] both state that Vestas and Siemens Gamesa were the top two turbine manufacturers in Europe, in 2023.

2.5 Drivetrain Components

Both types of drivetrains contain a main shaft, main bearing, brake, generator and power converter, with a gearbox included in the geared drivetrains.

2.5.1 Main Shaft

The main shaft connects the rotor hub, in which the blades are attached, to the gearbox or generator depending upon the drivetrain type (geared or direct-drive), so it carries both torque and non-torque loads from the hub. It rotates at a low speed, typically 15 rpm but is subjected to large dynamic and stochastic loads i.e. torque [30], thrust and bending moments.

2.5.2 Main Bearing

The next component in the drivetrain is the main bearing (Figure 2.18). Within a geared drivetrain, there can be either single or double main bearings depending on the suspension (3 or 4 point) and single, double or triple main bearings in direct-drive drivetrains. Their main purpose in the drivetrain is to support “the rotor while reacting non-torque loads either independently, preventing them being transmitted further down the drivetrain, or in combination with the gearbox and mounts" [13]. They do this by being placed on the main shaft, that connects the rotor hub to either the gearbox or generator because this shaft is subjected to large torque and non-torque loads, such as bending moments. With regards to the direct-drive drivetrains, the role of the main bearing can also be to both support the rotor of the generator and keep the

recommended air gap [24].

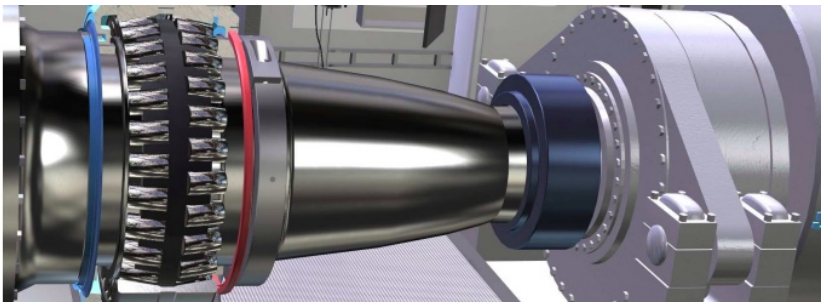

Figure 2.18: Main Bearing. Courtesy of SKF.

The main types of bearings are: spherical roller bearings, tapered roller bearings, cylindrical roller bearings and toroidal roller bearings. Spherical roller bearings are the most common for 3-point suspension, as they react to both axial and radial loads but they don't react to moments, so there is a trend moving towards using tapered roller bearings, as these do react to moments.

The main causes of failure include: fatigue, micro-pitting, spalling, smearing, abrasive wear and debris damage and fretting [13].

The design life is twenty (20) years but it is a common fact that the main bearing does not reach this target [31], it is lucky if it reaches ten (10) years, [32] and [33]. It has been reported that single main bearing failure rates can reach up to 30% [32] over the typical twenty (20) year life of the turbine. Typically, upon failure they require complete removal and replacement [13].

Hertzian elastic contact theory, multibody models and finite-element models are all the modelling tools that can be used for modelling the main bearings [13].

2.5.3 Gearbox

The next component within a geared drivetrain is a gearbox (Figure 2.19).

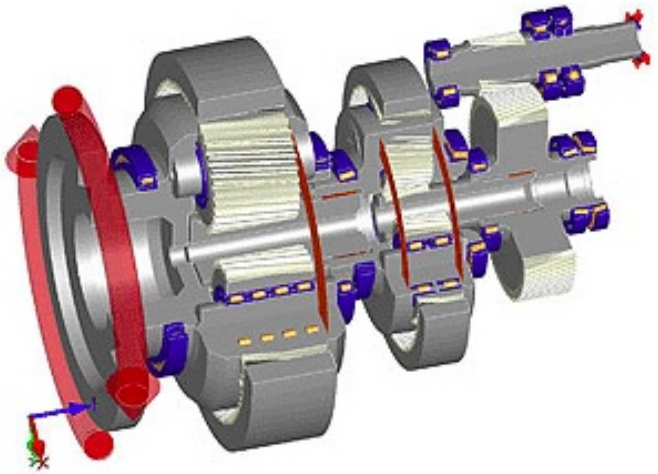

Figure 2.19: Gearbox. Courtesy of Romax/NKE.

The main purpose of the gearbox is to connect the low-speed shaft/main shaft to the high-speed shaft, to increase the speed and reduce the torque from the rotor to the generator. The gearbox is made up of a variety of gears, bearings and shafts.

Gearboxes typically consist of three gear stages and there are different gearbox layouts, [34], the most common are: one planetary and two parallel gear stages, two planetary and one parallel gear stages and even just two planetary gear stages (Figure 2.20). A planetary gear stage consists of a sun at the centre, which is where the shaft is connected, with 'planets' connected to/in between the sun and the planet carrier. Planetary gears are used as they are believed to be able to withstand harsh loading [35].

Along with the main bearing, the gearbox is also a component that does not meet it's twenty (20) year design life [31]. Gearboxes are one of the pieces of equipment

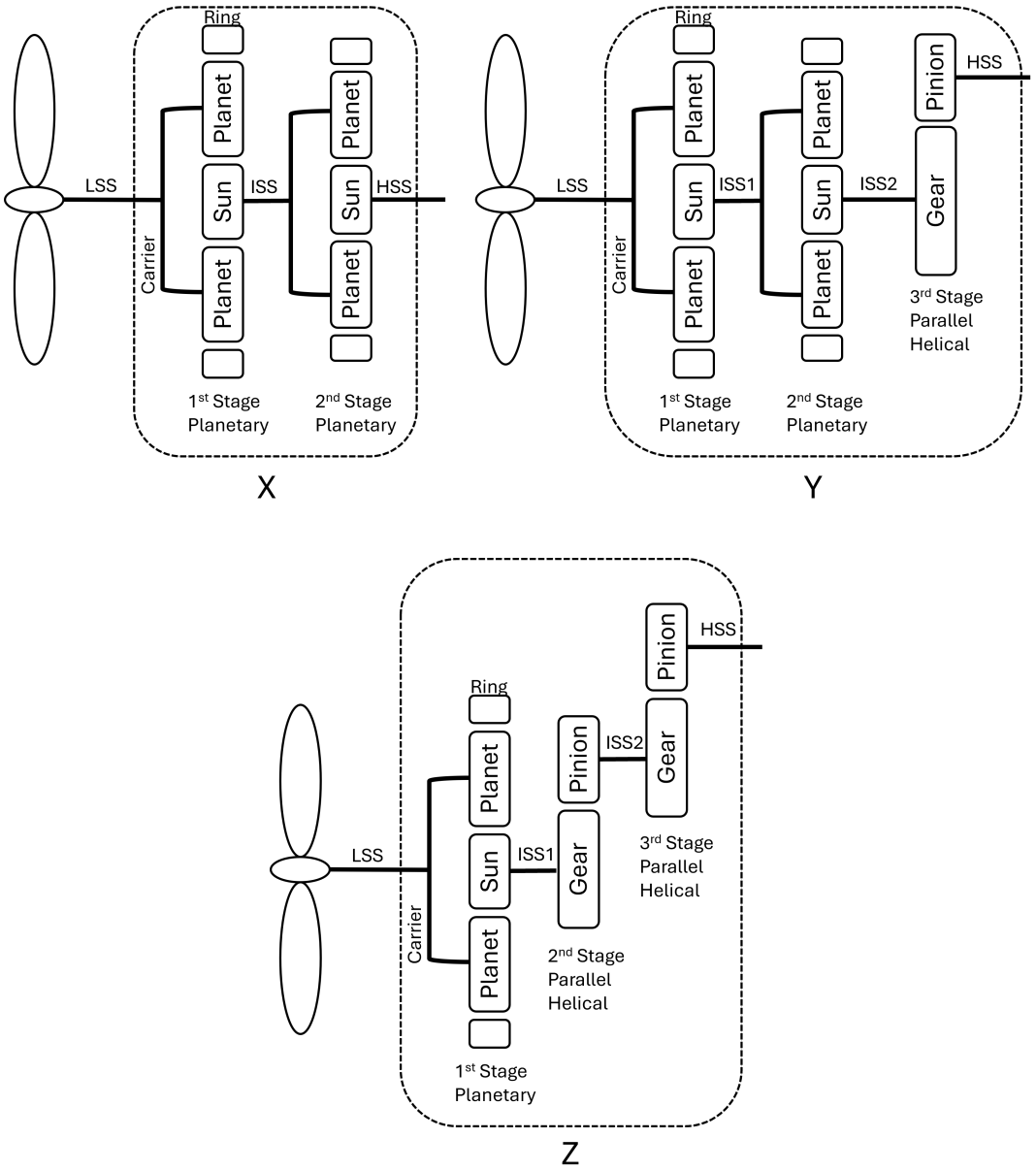

Figure 2.20: Different Gearbox Layouts - X (Two planetary gear stages), Y (Two planetary and one parallel gear stages) and Z (One planetary and two parallel gear stages) [34]

in the drivetrain with high failure rates [36] and [37], with the bearings on the high speed and intermediate shafts having the highest probability of fatigue damage [38]. If they fail then the downtime and cost are both high, due to the fact that in order to

carry out any repairs, then they need to be removed and sent back to the workshop for dismantling.

A similar process to the one used for the main bearings (Section 2.3.5.3) is used to calculate the fatigue damage of the gearbox.

2.5.4 Generator

The generator converts mechanical energy to electrical energy. There are a number of different types, including:

1. Induction Generators (IG).
2. Doubly-Fed Induction Generators (DFIG).
3. Permanent-Magnet Synchronous Generators (PMSG).
4. Electrically Excited Synchronous Generators (EESG).
5. Superconducting Generators.

Induction or asynchronous generators (IG) are the simplest type of generators. They have a fixed stator winding and either a rotating squirrel cage or wound rotor. They start up once connected to a live AC system, the three phase current flowing in the stator produces a magnetic field, which induces a current in the rotor. This current also produces a magnetic field, which interacts with the magnetic field in the stator producing a torque, [39] The speed of the generator varies with the torque, resulting in less “wear and tear" on the gearbox, [40].

Doubly-Fed Induction Generators (DFIG) have a wound rotor that is connected to slip rings, in order to take current in and out. “The rotor winding is fed through a variable frequency power converter. The power converter decouples the network electrical frequency from the rotor mechanical frequency enabling the variable-speed operation of the wind turbine", [39]. DFIG have been a popular choice of generator for 3–6 MW medium-sized turbines [24].

Figure 2.21: Synchronous Generator. Courtesy of ABB.

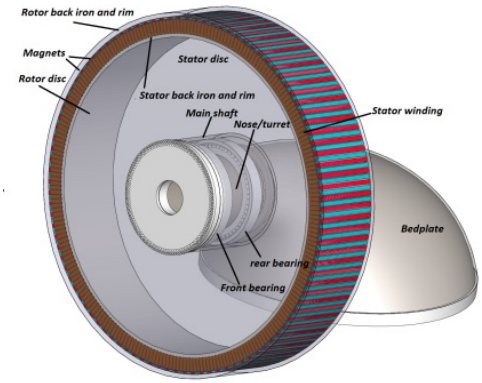

Figure 2.22: Direct Drive Generator. Courtesy of NREL.

The main difference between an asynchronous generator and synchronous generator is that an asynchronous generator takes reactive power from the grid for excitation, whereas in synchronous generators the voltage generated is directly related to the speed of the rotor [41]. The rotor can consist of either permanent magnets or be field wound (electrically excited). Direct-drive (DD) drivetrains (Figure 2.22) typically use permanent magnet synchronous machines, as they do not require an external power source for magnetization, so this decreases the heat produced by the system and increases the efficiency and energy yield. Permanent magnet synchronous generators (PMSG) (Figure 2.21) are becoming more popular than DFIGs [24], although

the cost associated with PMSGs are higher than DFIGs, due to the use of rare earth materials (e.g. NdFeB magnets) and manufacturing complexity.

2.5.5 Power Converter

The power converters (Figure 2.23) are electrical sub-assemblies. They take the output from the generator and convert the signal to match the grid requirements.

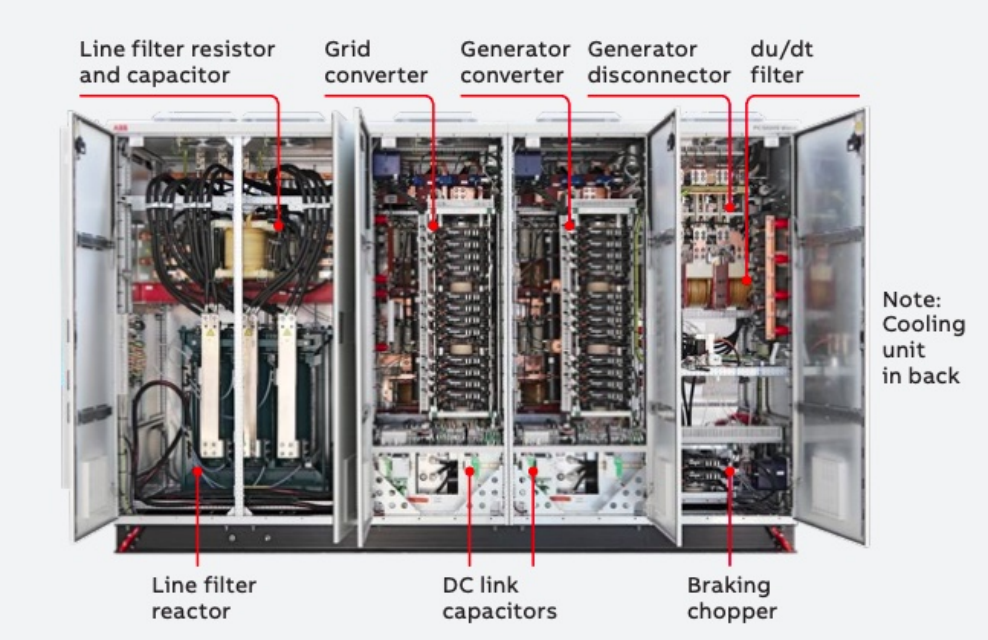

Figure 2.23: Power Converter. Courtesy of ABB.

Their first step is to convert the AC signal from the generator to a DC signal, this DC signal is then passed through a DC link, before being converted back to an AC signal matching the grid signal. Depending on the generator type, power converters can be either partially rated or fully rated (Figure 2.24). They consist of a number of switches and capacitors.

Power converters have one of the highest failure rates [43], out of all the other

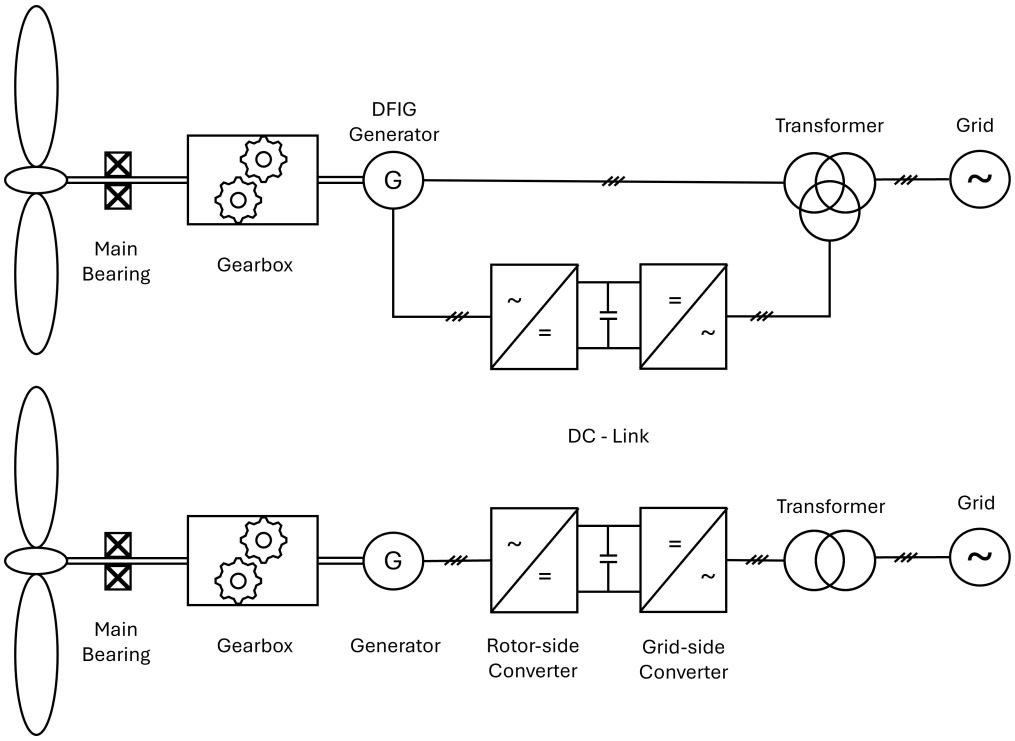

Figure 2.24: Types of Power Converter (Partially rated (top) and fully rated (bottom)) [42]

pieces of equipment within the drivetrain. Unlike the mechanical components within the drivetrain, power converters are fully electrical, so thermal expansion and contraction of the different layers in semiconductors can be a fatigue issue. Research has shown that the main cause of failure is the environment [43] and that failure can happen at anytime without warning. Phase modules are found to be the components with the highest failure rates [43].

2.6 Summary

A wind turbine's drivetrain is made up of a number of pieces of equipment, which are in turn made up of a number of components. Due to the dynamic nature of the complete system (drivetrain), each component undergoes various loads and forces throughout it's lifetime, which gradually reduces it's remaining useful life. Considering the interconnections between equipment within the drivetrain, if any piece of equipment or component within a piece of equipment fails, the entire drivetrain can be affected, which in turn affects the wind turbine. So in the case of evaluating lifetime extension, it is important to not only investigate all the components, it is also beneficial to determine or rank the 'weakest links' or components most likely to fail.

2.7 References

[1] Acciona. Wind turbines. https://www.acciona.com/renewable-energy/wind-energy/wind-turbines/?_adin=01742670631.

[2] Amir R Nejad and Torgeir Moan. On model-based system approach for health monitoring of drivetrains in floating wind turbines. *Procedia engineering*, 199: 2202–2207, 2017.

[3] Global Wind Energy Council. Gwec - global wind report 2024. Technical report, Global Wind Energy Council, 2024.

[4] IRENA. Wind energy. https://www.irena.org/Energy-Transition/Technology/Wind-energy, .

[5] Tyler Stehly, Patrick Duffy, and Daniel Mulas Hernando. Cost of wind energy review: 2024 edition. Technical report, National Renewable Energy Lab.(NREL), Golden, CO (United States), 2024.

[6] IRENA. What are standards? https://www.irena.org/inspire/Standards/What-are-Standards, .

[7] Bill Leithead. Wind, waves and tides in offshore renewable energy. Notes as part of the WAMESS CDT Course.

[8] Romans Kazacoks and P Jamieson. *A Generic Evaluation of Loads in Horizontal Axis wind Turbines*. PhD thesis, University of Strathclyde, 2017.

[9] Shuaishuai Wang, Amir R Nejad, and Torgeir Moan. On design, modelling, and analysis of a 10-mw medium-speed drivetrain for offshore wind turbines. *Wind Energy*, 23(4):1099–1117, 2020.

[10] Dr. Julian Feuchtwang. Wind, waves and tides in offshore renewable energy. Notes as part of the WAMESS CDT Course.

[11] Isaac Van der Hoven. Power spectrum of horizontal wind speed in the frequency range from 0.0007 to 900 cycles per hour. *Journal of Atmospheric Sciences*, 14 (2):160–164, 1957.

[12] Jie Wan, Jinfu Liu, Guorui Ren, Yufeng Guo, Wenbo Hao, Jilai Yu, and Daren Yu. A universal power-law model for wind speed uncertainty. *Cluster Computing*, 22 (4):10347–10359, 2019.

[13] Edward Hart, Benjamin Clarke, Gary Nicholas, Abbas Kazemi Amiri, James Stirling, James Carroll, Rob Dwyer-Joyce, Alasdair McDonald, and Hui Long. A review of wind turbine main bearings: design, operation, modelling, damage mechanisms and fault detection. *Wind Energy Science*, 5(1):105–124, 2020.

[14] Professor Erin Bachynski-Polić. Tmr4505 - marine structures, specialization course. Notes as part of the Course.

[15] Shuaishuai Wang. *Design and dynamic analysis of a 10-MW medium-speed drivetrain in offshore wind turbines*. PhD thesis, Norwegian University of Science and Technology, 2021.

[16] Zhanwei Li, Binrong Wen, Zhike Peng, Xingjian Dong, and Yegao Qu. Dynamic

modeling and analysis of wind turbine drivetrain considering the effects of non-torque loads. *Applied Mathematical Modelling*, 83:146–168, 2020.

[17] https://slideplayer.com/slide/12640546/.

[18] Morteza Ahmadivala. *Towards optimal maintenance planning of existing structures based on time-dependent reliability analysis*. PhD thesis, Université Clermont Auvergne [2017-2020], 2020.

[19] NESC Academy. Shock and vibration: 39. rainflow cycle counting for random vibration fatigue analysis. https://nescacademy.nasa.gov/video/30d9042b470d4f61aaac0037b27689951d.

[20] Dr. James Carroll. Nacelle mechanical and electrical technologies in offshore renewable energy. Notes as part of the WAMESS CDT Course.

[21] Milton A Miner. Cumulative damage in fatigue. 1945.

[22] Adam Ragheb and Magdi Ragheb. Wind turbine gearbox technologies. In *2010 1st international nuclear & renewable energy conference (INREC)*, pages 1–8. IEEE, 2010.

[23] Geerten van de Kaa, Martijn van Ek, Linda M Kamp, and Jafar Rezaei. Wind turbine technology battles: Gearbox versus direct drive-opening up the black box of technology characteristics. *Technological Forecasting and Social Change*, 153: 119933, 2020.

[24] Amir R Nejad, Jonathan Keller, Yi Guo, Shawn Sheng, Henk Polinder, Simon Watson, Jianning Dong, Zian Qin, Amir Ebrahimi, Ralf Schelenz, et al. Wind

turbine drivetrains: state-of-the-art technologies and future development trends. *Wind Energy Science Discussions*, pages 1–35, 2021.

[25] Shuangwen Sheng. Wind turbine gearbox reliability database, condition monitoring, and operation and maintenance research update. Technical report, National Renewable Energy Lab.(NREL), Golden, CO (United States), 2016.

[26] PJ Tavner, Fabio Spinato, GJW Van Bussel, and Efstathios Koutoulakos. Reliability of different wind turbine concepts with relevance to offshore application. In *European Wind Energy Conference*, page 9, 2008.

[27] Wenxian Yang. Condition monitoring the drive train of a direct drive permanent magnet wind turbine using generator electrical signals. *Journal of Solar Energy Engineering*, 136(2), 2014.

[28] GWEC. Wind turbine manufacturers see record year driven by growth in home markets. `https://gwec.net/wind-turbine-manufacturers-see-record-year-driven-by-growth-in-home-markets/`.

[29] Blackridge. Global top 15 wind turbine manufacturers [2024]. `https://www.blackridgeresearch.com/blog/top-wind-turbine-manufacturers-makers-companies-suppliers`.

[30] Zhanqi Zhang, Zhongjun Yin, Tian Han, and Andy CC Tan. Fracture analysis of wind turbine main shaft. *Engineering Failure Analysis*, 34:129–139, 2013.

[31] Jonathan Keller, Shawn Sheng, Yi Guo, Benjamin Gould, and Aaron Greco. Wind turbine drivetrain reliability and wind plant operations and maintenance research

and development opportunities. Technical report, National Renewable Energy Lab.(NREL), Golden, CO (United States), 2021.

[32] Edward Hart, Alan Turnbull, Julian Feuchtwang, David McMillan, Evgenia Golysheva, and Robin Elliott. Wind turbine main-bearing loading and wind field characteristics. *Wind Energy*, 22(11):1534–1547, 2019.

[33] D Brake. Wtg srb main bearing failures. In *UVIG wind turbine/plant operations & maintenance users group meeting*, 2013.

[34] Haider Al-Hamadani, Taylan An, Matthew King, and Hui Long. System dynamic modelling of three different wind turbine gearbox designs under transient loading conditions. *International Journal of Precision Engineering and Manufacturing*, 18 (11):1659–1668, 2017.

[35] WindPower Engineering and Development. Why wind-turbine gearboxes fail to hit the 20-year mark. `https://www.windpowerengineering.com/wind-turbine-gearboxes-fail-hit-20-year-mark/`, February 2018.

[36] James Carroll, Alasdair McDonald, and David McMillan. Failure rate, repair time and unscheduled o&m cost analysis of offshore wind turbines. *Wind Energy*, 19 (6):1107–1119, 2016.

[37] James Carroll, Sofia Koukoura, Alasdair McDonald, Anastasis Charalambous, Stephan Weiss, and Stephen McArthur. Wind turbine gearbox failure and remaining useful life prediction using machine learning techniques. *Wind Energy*, 22(3):360–375, 2019.

[38] Amir Rasekhi Nejad, Yi Guo, Zhen Gao, and Torgeir Moan. Development of a 5 mw reference gearbox for offshore wind turbines. *Wind Energy*, 19(6):1089–1106, 2016.

[39] Dr. David Campos-Gaona. Nacelle mechanical and electrical technologies in offshore renewable energy. Notes as part of the WAMESS CDT Course.

[40] Alternative-Energy-Tutorials. Induction generator as a wind power generator. `https://www.alternative-energy-tutorials.com/wind-energy/induction-generator.html`.

[41] Electrical Easy. Synchronous generator vs. induction generator. `https://www.electricaleasy.com/2014/12/synchronous-vs-induction-generator.html`.

[42] Michael S Okundamiya and Emmanuel A Ogujor. Power electronics technology: enabling large-scale injection of wind energy into the grid. *Advances in Energy Research*, 27:123–148, 2017.

[43] Katharina Fischer, Karoline Pelka, Sebastian Puls, Max-Hermann Poech, Axel Mertens, Arne Bartschat, Bernd Tegtmeier, Christian Broer, and Jan Wenske. Exploring the causes of power-converter failure in wind turbines based on comprehensive field-data and damage analysis. *Energies*, 12(4):593, 2019.

Chapter 3

Literature Review

A literature review has been conducted, covering the main topics including: current approaches to lifetime extension, ways of selecting critical components, utilising SCADA data for predicting component failures and model uncertainty and errors.

Current approaches to lifetime extension are covered in Chapter 4.

3.1 Selection of Critical Components

A vulnerability map for the components within a 750 kW wind turbine gearbox was established by Nejad et al. [1]. This vulnerability map (Figure 3.1) was used to determine a suitable inspection and maintenance plan. It used fatigue damage of the components, i.e. bearings and gears, to establish the map, ranking the components between the lowest and highest.

Wang et al. [2] also developed a vulnerability map for the components of a wind turbine gearbox, as well as for the main bearings, all within the same map, but the

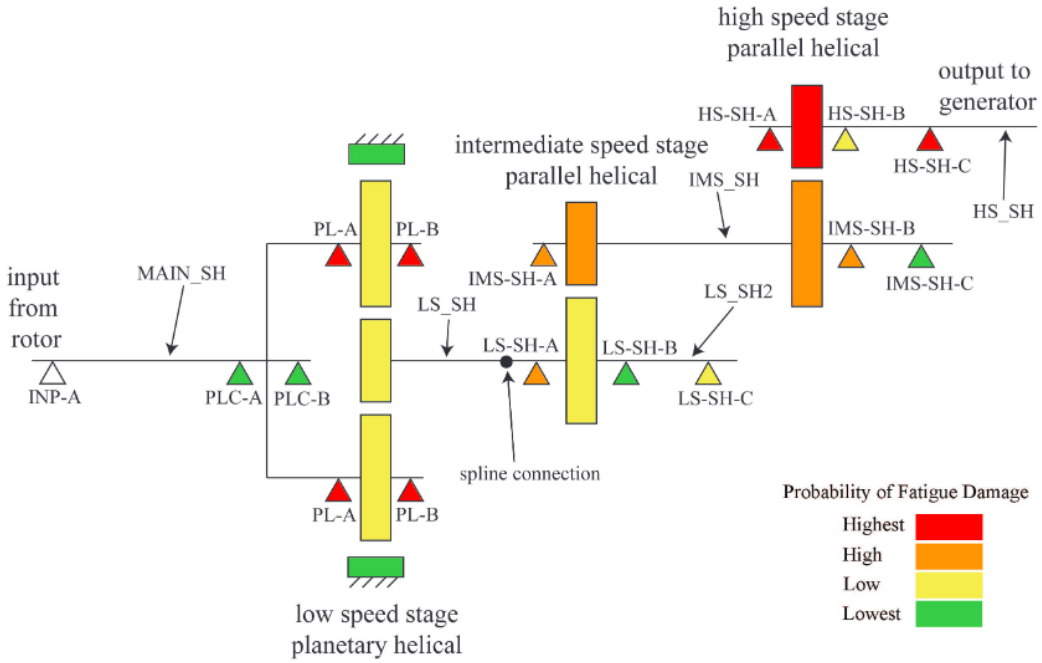

Figure 3.1: Vulnerability Map of 750 kW Gearbox [1]

size of this turbine was a 10 MW medium speed offshore turbine. The fatigue damage was calculated using four methods, which were the “stress or equivalent load duration distribution, the Palmgren-Miner linear accumulative damage hypothesis, and long-term environmental condition distributions". Again, the components were ranked from lowest to highest with regards to fatigue damage.

According to Zhu and Li [3], the gearbox, generator and blades have the highest failure rates. They mention how the main root causes of failure include: design and operational issues, environmental conditions and maintenance practices. They list the typical failure modes as: faults, overheating, overspeed, seizure of the bearings and jammed bearings. The associated causes include: environmental conditions, fatigue, mechanical failure, misalignment, overload, loss of control and zero excitation.

Applying the failure, modes, effects and criticality analysis (FMECA) to a number

of wind turbines in different climates and identifying any gaps, was a method used by Ozturk et al. [4]. They found that the typical generator failures were wear on the bearings and miscellaneous items. Typical electric system failures were wear on the switches, miscellaneous items, cables/connections, fuses and converter. There were higher failure rates and downtime per failure for direct-drive turbines, as opposed to geared-drive. In both turbine types, the generators showed the highest downtime criticality.

The faults of a number of components within the drivetrain were highlighted by Qiao and Lu [5]. Faults in the hydraulic system can include: oil leakage and sliding valve blockage. The mechanical brake is made up of a disc, calipers and hydraulic mechanism. Failures can include: cracking in the disc and over-wearing of both the disc and calipers, which are typically caused by overheating. Faults in the generator can be split into either electrical or mechanical faults. Where electrical faults can include: “stator or rotor insulation damage or open circuit and electrical imbalance" and the mechanical faults can include: "broken rotor bar, bearing failure, bent shaft, air gap eccentricity, and rotor mass imbalance". They also state that the most common faults occur with the electronic subsystem and that power converters have a high failure rate.

A comparison was carried out by Carroll et al. [6], between the reliability of doubly fed induction generator (DFIG) and permanent magnet generator (PMG) drivetrains within wind turbines, with regards to generators and converters. Their results show that DFIG drivetrains have more generator failures but PMG drivetrains have more converter failures. The largest contributor to generator failure in DFIG drivetrains is with the slip ring/brush, followed by the bearing, cooling system, insulation, encoder

and alignment. Whereas the largest contributor to generator failure in PMG drivetrains is with the lubrication system, followed by the cooling system and alignment. The largest contributor to partial rated converter failure, which is located in the DFIG drivetrains, is the control modules, followed by connection issues, cooling system and protection. The largest contributor to fully rated converter failure is the cooling system, then the control module, connection issues, protection issues and converter replacement.

In a separate paper, Carroll et al. [7] investigated the failure rates of offshore wind turbines. With regards to generator failure modes, the highest number of failures were with the slip ring, followed by the generator bearing, grease pipes, rotor issues and fan. They also mention that the generator has a higher failure rate onshore.

Electrical winding failures within generators in wind turbines was discussed by Alewine and Chen [8]. They determined that out of all the 1200 turbines reviewed, “fewer than half of the failures were electrical in nature and most of those were due to mechanical failures of the insulation support structure". They discussed typical electrical failures including: rotor banding, conductive wedges, cooling system failures, rotor lead failures, under-designed materials and systems, surges, contamination issues and lubrication.

Due to their frequent failures, the investigation of power converter failures within the wind turbine are an important area to research. Along with their high frequency of failure, they are also one of the main causes of fire. Fischer et al. [9] explain that failures can include electrical overstress. Some of the causes of failures include: lightning strikes, thermal cycling, condensation build up after standstill and salt ingress.

Another paper written by Fischer et al. [10] looked at the root cause of power converter failures using a field experience based analysis. They mention some common causes of failure, which may include: temperature, humidity, vibration, cleanliness, electrical, components and test and qualification. The analysis method they used to identify the failure modes and causes, were the failure-data analysis, the operating conditions of the field and “postoperational analysis of converter hardware/modules". They concluded that the thermal cycling, which occurs in the generator-side converter was not a predominant factor in causing failure because failures occurred in both the grid-side and generator-side converters. In addition, bond-wire damage and solder cracking, which are both classed as fatigue-related effects were also not a predominant cause of failure. Whereas, inadequate protection of the converter's components from the environment were present within the converters. Corrosion and salt traces may have caused conductive paths, which were unwanted. Insects were also found within the device, which may have reduced the insulation-relevant air gaps thus causing flashover. After standing still for long periods of time the condensation build up could cause overheating, due to inadequate heat dissipation. Finally, electrical overstress caused by lightning strikes was found in the samples, supporting what was discussed in [9].

Analysing worldwide operating field data provided by project partners, was another method used by Fischer et al. [11], to look at power converter failures. They reviewed the differences between different generator-converter combinations, different manufacturers and turbine generations. Their conclusions were similar to the conclusions of their other papers, with regards to thermal cycling not inducing fatigue and that envi-

ronmental factors played a part in the failures. They reviewed all the components within the power converter system and concluded that the “phase-module" components had the highest number of failures. Induction generators with full scale converters had the lowest phase-module reliability. Reliability of the phase-modules were pretty consistent across all ages of fleets, young and old. Results also suggest that humidity and/or condensation play a part in the high failure rate of phase-modules. Failure is also highest when the turbine was operating very close and above rated power.

A large consortium, consisting of three research organisations and sixteen companies has been established, lead by the Fraunhofer Innovation Cluster on Power Electronics for Renewables, to determine the main causes of power converter failures in wind turbines. This confirms how important it is to identify these causes of failure, to try and reduce the amount of failures that occur, as these failures can have huge economic impacts on the wind turbine industry. Their results from Fischer et al. [12] confirmed the results and conclusions described in [9] and [10], where one of the major causes of failure appear to be related to the environmental conditions, as opposed to fatigue caused by thermal cycling. Other factors contributing to failure were: contamination, overheating, design issues, quality issues and human error. The method of analysis they used included: field measurements, evaluation of both failure and operating data, specifically for power converters and “post-mortem investigation".

An alternative method to determine the remaining useful life of converters was used by Alsaadi [13] when conducting a comparison between a three level neutral point clamped (3L-NPC) converter and two level voltage source converter (2L-VSC). They used wind speed samples, SIMULINK models, thermal cycles and Weibull dis-

tribution in order to determine the expected remaining useful life. This research by Alsaadi which was presented at the Wind Energy Science Conference (WESC) 2021, concluded that the 3L-NPC has the higher reliability.

3.2 Utilising SCADA Data for Detecting Component Failure

Typical indicators of component failure include: elevated temperature and increased vibration. Temperature data is readily available through SCADA systems, while vibration data is typically obtained from condition monitoring systems.

A vast amount of research has been conducted, investigating the use of vibration data to predict component failures in a wind turbine drivetrain, due to the fact changes in vibration provide more accurate and reliable information. Turnbull et al. [14, 15], Gómez et al. [16], Joshuva and Sugumaran [17], Igba et al. [18], Hussain and Gabbar [19], Teng et al. [20], Zhang et al. [21] have all carried out research, to name a few.

The dataset which will be used for this work is from SCADA data, therefore changes in temperatures will be investigated. Utilizing temperature data for fault detection or remaining useful life estimation of drivetrain components or the entire system would be highly beneficial, as temperature data is typically readily available in SCADA systems. Considering this, extensive research has been conducted to explore various methods.

Carroll et al. [22] found that simple trending using temperature rarely highlighted potential failures. Yang et al. [23] also mentions that because SCADA data varies “over wide ranges under varying operational conditions", then without “an appropriate data analysis tool" it is difficult to detect faults from raw SCADA data. A condition monitoring

technique based upon certain SCADA data correlations was proposed, in which it was concluded by Yang et al. [23] worked well in detecting faults within the drivetrain.

The suitability of using SCADA-based condition monitoring, in order to diagnose faults within a wind turbine, by analysing temperature data, was investigated by Murgia et al. [24]. They used normal-behaviour modelling and identification of a threshold value and concluded that drivetrain faults could be identified months in advance, as long as “qualifying points are addressed".

In another example, a normal behaviour model based upon an artificial neural network (ANN), using SCADA data has been proposed and tested on twelve wind turbines by Encalada-Dávila et al. [25] and it showed that main bearing faults could be detected several months in advance. A “state prediction approach" was used by Herp et al. [26], which was based on “bearing temperature residuals" along with Gaussian processes. This method was able to predict a failure approximately one month before failure. In addition, Dai et al. [27] looked at four different assessment criteria for assessing the performance of an ageing asset. One of the assessment criteria used the main bearing temperature data, it looked for changes and processed this data using Kernel Density Estimation.

The most commonly used data-driven models include: support vector machines, neural networks, probabilistic models and decision trees according to Pandit et al. [28]. They explain that condition monitoring based on SCADA data “targets secondary effects of the fault". They discuss that the model’s accuracy can be increased with feature selection and extraction but that it is a fine line to avoid over-fitting.

With regards to gearbox failures, a gearbox planetary stage failure was detected by

monitoring gearbox oil temperature, power output and rotational speed in Feng et al. [29]. Whereas based on the first law of thermodynamics, a relationship between temperature, efficiency, and either the power output or rotational speed was established by Feng et al. [30]. A new algorithm was then developed to detect gearbox failures based on both oil and bearing temperature measurements. It was concluded that the simple algorithms worked well in providing early warnings of gearbox failures. A Multivariate State Estimation Technique (MSET) was used by Yongjie et al. [31], along with the Moving Window Calculation (MWC). Where the MSET was used to estimate the gearbox temperature and the MWC used to get the dynamic trend of the average value of the differences between the estimated and real values. This paper concluded that the method was effective in detecting any anomalies. Moreover, thermal modelling, as well as thermal modelling combined with machine learning was investigated by Corley et al. [32] and Corley et al. [33] respectively, where it was found that thermal modelling of the gearbox detected a fault, whereas nothing was obvious with just the temperature differences. Zhao and Zhang [34] used a prediction method, using temperature to detect faults by comparing the actual running condition of the gearbox, with the predicted condition and flagging any deviation. Gearbox oil temperature was used by Zeng et al. [35] in an anomaly detection method, based on the Sparse Bayesian Learning and hypothesis testing. A Support Vector Machine (SVM) regression model, along with SCADA parameters was used to model the gearbox oil temperature by Zhang and Qian [36] and it was concluded that a warning approximately ten days before the fault was achieved. A deep neural network algorithm was “applied to model the lubricant pressure" by Wang et al. [37] and it was found that gearbox failures could

be predicted approximately two to three days in advance. They also concluded that monitoring lubricant pressure provided more accurate results than monitoring gearbox oil temperature.

Specifically tested on a generator rear bearing, Hu et al. [38] established a performance degradation model using the Wiener process, with the maximum likelihood estimation method used for the model parameters. The “temperature trend data" was determined from the “relative temperature data" using the moving average method. It also established a remaining useful life prediction model, based on the inverse Gaussian distribution. It was concluded that both the degradation model and prediction method were very effective with calculating remaining useful life.

Sudden fault detection of generator bearings was investigated by Velásquez [39]. They firstly used a multi-stage approach consisting of multiple regression models, then probability scores, a search grid validation and then the validated results were ran through “finite element modelling, boroscopy, and vibration analysis". They concluded that failures could be detected five days prior to vibration analysis, with a high accuracy.

Although not related to wind turbines, Apribowo et al. [40] used machine learning models such as an extreme gradient boosting algorithm, along with a temperature variable to predict the RUL of battery energy storage systems. It was concluded that this method provided accurate results.

Most of the existing research reviewed above, employs quite complex data-driven techniques, offering more accurate RUL predictions. However, it was determined that relying solely on temperature data allows for failures to be predicted, only a few months

in advance, at best. In contrast, using vibration data, or combining both temperature and vibration data, could enable failure detection much earlier.

3.3 Model Uncertainty and Error Assessment

Model validation is important and this can be achieved by using measurement chains, to ensure the processes are reproducible, thorough and traceable, as described by Hall and White [41]. A typical measurement chain can consist of: data collection, preprocessing, feature extraction, model prediction, error analysis, feedback.

Four types of uncertainty are described by Bai and Jin [42], including: inherent, measurement, statistical and model. The authors define model uncertainty as “uncertainty due to imperfections and idealizations made in physical model formulations for load and resistance, as well as in the choices of probability distribution types for the representation of uncertainties".

With regards to wind energy and wind turbines, models can serve various purposes, including: predicting wind direction for yaw control, Ouyang et al. [43], modelling of wind speeds to forecast power production, De Giorgi et al. [44], predicting wind speed, Knudsen et al. [45], modelling component failures based upon weather conditions, Reder and Melero [46] and identifying anomalies, Sun et al. [47].

Various types of models are utilised and Barboza et al. [48] found that random forest machine learning models, deliver the highest accuracy. They also concluded that the accuracy increased, with the inclusion of additional variables.

Model uncertainties have been investigated by Jiang et al. [49], Nejad et al. [50],

Tarp-Johansen [51] and Dong et al. [52], amongst others. These studies define model uncertainty as the ratio of the actual or real value of a variable to the predicted value. Bai and Jin [42] explains that bias arises when the mean value does not equal one. They explain that in the absence of detailed information, either lognormal or normal distributions are commonly used. Lognormal distributions for load variables and normal distribution for resistance variables. Dong et al. [52] further emphasizes that lognormal distribution is preferred over Gaussian distribution. Tarp-Johansen [51] highlights that by dividing the standard deviation by the mean, the coefficient of variation can be determined, which is a “convenient measure of the relative error that the model uncertainty represents". Researchers, including Nejad et al. [50], typically use a multiplicative model to account for combined uncertainties, although Tarp-Johansen [51] suggests considering additive errors.

Three different approaches to determine uncertainty in machine learning predictions were investigated by Tavazza et al. [53]. They included the Gaussian process and the quantile approach, which used both the absolute difference and square of the difference, where the difference is defined as the difference between the predicted and observed values. They concluded that whilst the quartile approach was the easiest approach, the Gaussian process provided a reliable estimate. They also determined that the best approach was achieved by using the absolute difference between the predicted and expected values.

An error compensation prediction method was proposed by Jiao et al. [54], based upon an extreme learning machine. This extreme learning machine was designed to predict the error, which is defined as the difference between the predicted and actual

value. This predicted error is derived from a time lag correction model and is then added to the “raw wind speed prediction result", to produce the “final wind speed prediction result".

Confidence intervals can be used for quantifying uncertainty in data-driven models. Pandit and Kolios [55] proposed two approaches incorporating confidence intervals - pointwise and simultaneous - to “measure the uncertainty associated with an SVM-based power curve model". They concluded that pointwise confidence intervals provided the most accurate results, when measuring the uncertainty of the power curve.

Several researchers have utilised Monte Carlo simulations and methods, to account for uncertainties and errors in models. Cao et al. [56] proposed an “uncertainty quantification approach" for determining remaining useful life predictions, which consists of kernel density estimation and Monte Carlo dropout. They concluded a high accuracy based upon this proposed method. Afanasyeva et al. [57] proposed a method combining both a sensitivity analysis and Monte Carlo simulations, in order to try and evaluate how uncertainties may influence the financial risks of wind projects. Gonzaga et al. [58] investigated modelling the effects of both aerodynamic and structural uncertainties on wind turbine blades. They used the Monte Carlo method to characterise the uncertainties in the material properties in a structural model of the blade. Additionally, Liu et al. [59] applied a Monte Carlo simulation to estimate the “annual energy production and its uncertainty for the wind farm".

3.4 References

[1] Amir Rasekhi Nejad, Zhen Gao, and Torgeir Moan. Fatigue reliability-based inspection and maintenance planning of gearbox components in wind turbine drivetrains. *Energy Procedia*, 53:248–257, 2014.

[2] Shuaishuai Wang, Amir R Nejad, and Torgeir Moan. On design, modelling, and analysis of a 10-mw medium-speed drivetrain for offshore wind turbines. *Wind Energy*, 23(4):1099–1117, 2020.

[3] F Zhu and F Li. Reliability analysis of wind turbines. *Stability Control & Reliable Performance of Wind Turbines*, pages 169–186, 2018.

[4] Samet Ozturk, Vasilis Fthenakis, and Stefan Faulstich. Failure modes, effects and criticality analysis for wind turbines considering climatic regions and comparing geared and direct drive wind turbines. *Energies*, 11(9):2317, 2018.

[5] Wei Qiao and Dingguo Lu. A survey on wind turbine condition monitoring and fault diagnosis—part i: Components and subsystems. *IEEE Transactions on Industrial Electronics*, 62(10):6536–6545, 2015.

[6] James Carroll, Alasdair McDonald, and David McMillan. Reliability comparison of wind turbines with dfig and pmg drive trains. *IEEE Transactions on Energy Conversion*, 30(2):663–670, 2014.

[7] James Carroll, Alasdair McDonald, and David McMillan. Failure rate, repair time

and unscheduled o & m cost analysis of offshore wind turbines. *Wind Energy*, 19 (6):1107–1119, 2016.

[8] Kevin Alewine and William Chen. A review of electrical winding failures in wind turbine generators. *IEEE Electrical Insulation Magazine*, 28(4):8–13, 2012.

[9] Katharina Fischer, Thomas Stalin, Hans Ramberg, Torbjörn Thiringer, Jan Wenske, and Robert Karlsson. Investigation of converter failure in wind turbines. *Elforsk report*, 12(58), 2012.

[10] Katharina Fischer, Thomas Stalin, Hans Ramberg, Jan Wenske, Göran Wetter, Robert Karlsson, and Torbjörn Thiringer. Field-experience based root-cause analysis of power-converter failure in wind turbines. *IEEE transactions on power electronics*, 30(5):2481–2492, 2014.

[11] Katharina Fischer, Karoline Pelka, Arne Bartschat, Bernd Tegtmeier, Diego Coronado, Christian Broer, and Jan Wenske. Reliability of power converters in wind turbines: Exploratory analysis of failure and operating data from a worldwide turbine fleet. *IEEE Transactions on Power Electronics*, 34(7):6332–6344, 2018.

[12] Katharina Fischer, Karoline Pelka, Sebastian Puls, Max-Hermann Poech, Axel Mertens, Arne Bartschat, Bernd Tegtmeier, Christian Broer, and Jan Wenske. Exploring the causes of power-converter failure in wind turbines based on comprehensive field-data and damage analysis. *Energies*, 12(4):593, 2019.

[13] Sermed Alsaadi. Comparing the reliability of 2l-vsc and 3l-npc wind turbine power converters. *WESC 2021*, 2021.

[14] Alan Turnbull, James Carroll, Sofia Koukoura, and Alasdair McDonald. Prediction of wind turbine generator bearing failure through analysis of high-frequency vibration data and the application of support vector machine algorithms. *The Journal of Engineering*, 2019(18):4965–4969, 2019.

[15] Alan Turnbull, James Carroll, Alasdair McDonald, and Sofia Koukoura. Prediction of wind turbine generator failure using two-stage cluster-classification methodology. *Wind Energy*, 22(11):1593–1602, 2019.

[16] MJ Gómez, P Marklund, D Strombergsson, C Castejón, and JC García-Prada. Analysis of vibration signals of drivetrain failures in wind turbines for condition monitoring. *Experimental Techniques*, 45:1–12, 2021.

[17] A Joshuva and V Sugumaran. A comparative study of bayes classifiers for blade fault diagnosis in wind turbines through vibration signals. *Structural Durability & Health Monitoring*, 11(1):69, 2017.

[18] Joel Igba, Kazem Alemzadeh, Christopher Durugbo, and Egill Thor Eiriksson. Analysing rms and peak values of vibration signals for condition monitoring of wind turbine gearboxes. *Renewable Energy*, 91:90–106, 2016.

[19] Sajid Hussain and Hossam A Gabbar. Vibration analysis and time series prediction for wind turbine gearbox prognostics. *International Journal of Prognostics and Health Management*, 4(2):69–79, 2013.

[20] Wei Teng, Xian Ding, Shiyao Tang, Jin Xu, Bingshuai Shi, and Yibing Liu. Vi-

bration analysis for fault detection of wind turbine drivetrains—a comprehensive investigation. *Sensors*, 21(5):1686, 2021.

[21] Zijun Zhang, Anoop Verma, and Andrew Kusiak. Fault analysis and condition monitoring of the wind turbine gearbox. *IEEE transactions on energy conversion*, 27(2):526–535, 2012.

[22] James Carroll, Sofia Koukoura, Alasdair McDonald, Anastasis Charalambous, Stephan Weiss, and Stephen McArthur. Wind turbine gearbox failure and remaining useful life prediction using machine learning techniques. *Wind Energy*, 22(3):360–375, 2019.

[23] Wenxian Yang, Richard Court, and Jiesheng Jiang. Wind turbine condition monitoring by the approach of scada data analysis. *Renewable energy*, 53:365–376, 2013.

[24] Alessandro Murgia, Robbert Verbeke, Elena Tsiporkova, Ludovico Terzi, and Davide Astolfi. Discussion on the suitability of scada-based condition monitoring for wind turbine fault diagnosis through temperature data analysis. *Energies*, 16(2): 620, 2023.

[25] Ángel Encalada-Dávila, Bryan Puruncajas, Christian Tutivén, and Yolanda Vidal. Wind turbine main bearing fault prognosis based solely on scada data. *Sensors*, 21(6):2228, 2021.

[26] Jürgen Herp, Mohammad H Ramezani, Martin Bach-Andersen, Niels L Pedersen,

and Esmaeil S Nadimi. Bayesian state prediction of wind turbine bearing failure. *Renewable Energy*, 116:164–172, 2018.

[27] Juchuan Dai, Wenxian Yang, Junwei Cao, Deshun Liu, and Xing Long. Ageing assessment of a wind turbine over time by interpreting wind farm scada data. *Renewable energy*, 116:199–208, 2018.

[28] Ravi Pandit, Davide Astolfi, Jiarong Hong, David Infield, and Matilde Santos. Scada data for wind turbine data-driven condition/performance monitoring: A review on state-of-art, challenges and future trends. *Wind Engineering*, 47(2): 422–441, 2023.

[29] Yanhui Feng, Yingning Qiu, Christopher J Crabtree, Hui Long, and Peter J Tavner. Monitoring wind turbine gearboxes. *Wind Energy*, 16(5):728–740, 2013.

[30] Yanhui Feng, Yingning Qiu, Christopher J Crabtree, Hui Long, and Peter J Tavner. Use of scada and cms signals for failure detection and diagnosis of a wind turbine gearbox. In *European Wind Energy Conference and Exhibition 2011, EWEC 2011*, pages 17–19. Sheffield, 2011.

[31] Zhai Yongjie, Wang Dongfeng, Zhang Junying, and Han Yuejiao. Research on early fault diagnostic method of wind turbines. *TELKOMNIKA Indonesian Journal of Electrical Engineering*, 11(5):2330–2341, 2013.

[32] B Corley, J Carroll, and A Mcdonald. Fault detection of wind turbine gearbox using thermal network modelling and scada data. In *Journal of Physics: Conference Series*, volume 1618, page 022042. IOP Publishing, 2020.

[33] Becky Corley, Sofia Koukoura, James Carroll, and Alasdair McDonald. Combination of thermal modelling and machine learning approaches for fault detection in wind turbine gearboxes. *Energies*, 14(5):1375, 2021.

[34] Hong-shan Zhao and Xiao-tian Zhang. Early fault prediction of wind turbine gearbox based on temperature measurement. In *2012 IEEE International Conference on Power System Technology (POWERCON)*, pages 1–5. IEEE, 2012.

[35] XJ Zeng, M Yang, and YF Bo. Gearbox oil temperature anomaly detection for wind turbine based on sparse bayesian probability estimation. *International Journal of Electrical Power & Energy Systems*, 123:106233, 2020.

[36] Dongdong Zhang and Zheng Qian. Probability warning for wind turbine gearbox incipient faults based on scada data. In *2017 Chinese Automation Congress (CAC)*, pages 3684–3688. IEEE, 2017.

[37] Long Wang, Zijun Zhang, Huan Long, Jia Xu, and Ruihua Liu. Wind turbine gearbox failure identification with deep neural networks. *IEEE Transactions on Industrial Informatics*, 13(3):1360–1368, 2016.

[38] Yaogang Hu, Hui Li, Pingping Shi, Zhaosen Chai, Kun Wang, Xiangjie Xie, and Zhe Chen. A prediction method for the real-time remaining useful life of wind turbine bearings based on the wiener process. *Renewable energy*, 127:452–460, 2018.

[39] Ricardo Manuel Arias Velásquez. Bearings faults and limits in wind turbine generators. *Results in Engineering*, 21:101891, 2024.

[40] Chico Hermanu Brillianto Apribowo, Sasongko Pramono Hadi, Francisco Danang Wijaya, Mokhammad Isnaeni Bambang Setyonegoro, et al. Early prediction of battery degradation in grid-scale battery energy storage system using extreme gradient boosting algorithm. *Results in Engineering*, 21: 101709, 2024.

[41] BD Hall and DR White. Digital representation of measurement uncertainty. *Measurement: Sensors*, 18:100074, 2021.

[42] Yong Bai and Wei-Liang Jin. Random variables and uncertainty analysis. *Marine structural design*, 12:615–625, 2016.

[43] Tinghui Ouyang, Andrew Kusiak, and Yusen He. Predictive model of yaw error in a wind turbine. *Energy*, 123:119–130, 2017.

[44] Maria Grazia De Giorgi, Antonio Ficarella, and Marco Tarantino. Error analysis of short term wind power prediction models. *Applied Energy*, 88(4):1298–1311, 2011.

[45] Torben Knudsen, Thomas Bak, and Mohsen Soltani. Prediction models for wind speed at turbine locations in a wind farm. *Wind Energy*, 14(7):877–894, 2011.

[46] Maik Reder and Julio J Melero. Modelling the effects of environmental conditions on wind turbine failures. *Wind Energy*, 21(10):876–891, 2018.

[47] Peng Sun, Jian Li, Caisheng Wang, and Xiao Lei. A generalized model for wind turbine anomaly identification based on scada data. *Applied Energy*, 168:550–567, 2016.

[48] Flavio Barboza, Herbert Kimura, and Edward Altman. Machine learning models and bankruptcy prediction. *Expert Systems with Applications*, 83:405–417, 2017.

[49] Zhiyu Jiang, Weifei Hu, Wenbin Dong, Zhen Gao, and Zhengru Ren. Structural reliability analysis of wind turbines: A review. *Energies*, 10(12):2099, 2017.

[50] Amir Rasekhi Nejad, Zhen Gao, and Torgeir Moan. On long-term fatigue damage and reliability analysis of gears under wind loads in offshore wind turbine drivetrains. *International Journal of Fatigue*, 61:116–128, 2014.

[51] Niels Jacob Tarp-Johansen. Examples of fatigue lifetime and reliability evaluation of larger wind turbine components. 2003.

[52] Wenbin Dong, Torgeir Moan, and Zhen Gao. Fatigue reliability analysis of the jacket support structure for offshore wind turbine considering the effect of corrosion and inspection. *Reliability Engineering & System Safety*, 106:11–27, 2012.

[53] Francesca Tavazza, Brian DeCost, and Kamal Choudhary. Uncertainty prediction for machine learning models of material properties. *ACS omega*, 6(48):32431–32440, 2021.

[54] Xuguo Jiao, Daoyuan Zhang, Xin Wang, Yanbing Tian, Wenfeng Liu, and Liping Xin. Wind speed prediction based on error compensation. *Sensors*, 23(10):4905, 2023.

[55] Ravi Pandit and Athanasios Kolios. Scada data-based support vector machine wind turbine power curve uncertainty estimation and its comparative studies. *Applied Sciences*, 10(23):8685, 2020.

[56] Lixiao Cao, Hongyu Zhang, Zong Meng, and Xueping Wang. A parallel gru with dual-stage attention mechanism model integrating uncertainty quantification for probabilistic rul prediction of wind turbine bearings. *Reliability Engineering & System Safety*, 235:109197, 2023.

[57] Svetlana Afanasyeva, Jussi Saari, Martin Kalkofen, Jarmo Partanen, and Olli Pyrhönen. Technical, economic and uncertainty modelling of a wind farm project. *Energy Conversion and Management*, 107:22–33, 2016.

[58] Paulo Gonzaga, Henrik Toft, Keith Worden, Nikolaos Dervilis, Lars Bernhammer, Nevena Stevanovic, and Alejandro Gonzales. Impact of blade structural and aerodynamic uncertainties on wind turbine loads. *Wind Energy*, 25(6):1060–1076, 2022.

[59] Ruili Liu, Liuliu Peng, Guoqing Huang, Xuhong Zhou, Qingshan Yang, and Jifeng Cai. A monte carlo simulation method for probabilistic evaluation of annual energy production of wind farm considering wind flow model and wake effect. *Energy Conversion and Management*, 292:117355, 2023.

Chapter 4

State-of-the-Art Approaches to Lifetime Extension in Wind and Other Industries

After researching all the various equipment/components that are located within the nacelle and that form the drivetrain, along with their layouts and the loads/forces that they are subjected to, the next step is to review all existing literature, which is in the public domain and establish what are the current processes of determining lifetime extension. The wind industry, as well as other industries, such as: oil and gas, vessels etc. are reviewed within this chapter. Other industries are investigated because they have been in operation a long time, most of them much longer than the modern wind industry, so have tried and tested techniques in place with regards to determining lifetime extension. Therefore, it is extremely useful and important to learn from other industries, to identify their transferable knowledge, when trying to establish a

methodology.

4.1 Lifetime Extension Methods in the Wind Industry

Classification societies such as DNV and Bureau Veritas, have both issued guidelines related to lifetime extension of wind turbines as a whole.

Bureau Veritas issued the “Guidelines for Wind Turbines Lifetime Extension" [1] in 2017, which recommends carrying out inspections on the components of the turbine to determine the quantitative lifetime extension (LTE). For the structural components which include: the tower, blades and main shaft, lifetime extension calculations are also required to be carried out. With regards to the drivetrain, the gearbox, shrink disk, torque arms, rotor locking system, brake disc and caliper, high speed coupling, hoses and oil ancillaries and the generator mount are listed along with the inspection requirements.

DNV-GL issued both the “Lifetime Extension of Wind Turbines (DNVGL-ST-0262)" [2] and the “Certification of Lifetime Extension of Wind Turbines (DNVGL-SE-0263)" [3], in 2016, with an amendment in 2021. Document DNVGL-ST-0262 recommends four methods for determining if the wind turbine is suitable for lifetime extension. The first method is called the lifetime extension inspection (LEI). For this method, a visual inspection is carried out on all load-transferring or safety-relevant components. Maintenance and inspection reports are reviewed, along with some simple tests and consideration of both SCADA data and type related field experience. The next three methods, which are the Simplified, Detailed and Probabilistic Approach, are all carried

out to determine proof of strength and stability. Each approach consists of an analytical and practical part. The analytical part involves new and/or additional calculations to assess the lifetime extension of the wind turbine. The calculations should take into consideration the location of the wind turbine, including the site-specific installation, local conditions and the field experience related to the type of turbine. The practical part involves wind turbine inspections, which should include all components that are load transferring and the control and protection system. In addition to the inspections, the maintenance/operational history and field experience related to the type of turbine, should also be taken into account. The Simplified Approach is typically carried out when the original design documentation is not readily available. The Detailed Approach uses a deterministic approach and requires the original design documentation. Finally, the Probabilistic Approach uses stochastic methods to determine the structural integrity of the wind turbine. The practical parts for each method are very similar but the analytical part varies depending on which method is chosen. With regards to the drivetrain, it has been broken down into eleven components, including: the hub, main shaft, coupling, main shaft bearings, gearbox, torque support, high speed shaft, generator, cooling system/circuit, bolted connection and protective covers. Each component has its individual test that should be conducted. Document DNVGL-SE-0263 explains the main deliverables including: a report, statement of compliance and/or certificate, obtained from carrying out one of the methods for lifetime extension described in document DNVGL-ST-0262. The document confirms that the possible lifetime extension is determined from load calculations and inspections. Each wind turbine should be inspected and the scope of the inspection will depend on the results obtained from

the analytical part. Results obtained from both the analytical and practical parts, will determine whether the wind turbine is suitable for lifetime extension. These DNV-GL guidelines list components associated with the whole wind turbine but appears mainly focused on the structural elements. TUV Nord [4] recommends the use of both the DNV-GL guidelines discussed above, for assessing the lifetime extension of wind turbines. In addition, they provide an expert analysis service, which includes: an inspection, examination and evaluation of the wind turbine, load determination over their lifetime, analysis and calculations, concluding with determining the period of life remaining.

DNV also provides a service to estimate the lifetime of a wind turbine and wind farm. Their lifetime assessment of the asset can include: “wind turbine fatigue life, asset economic lifetime, wind farm asset integrity and wind farm asset depreciation".

MegaVind issued a report called “Strategy for Extending the Useful Lifetime of a Wind Turbine" [5] in 2016. They have described four different scenarios based upon the amount of data available, from no design basis and operational measurements being available (Scenario 1), to having access to a full range of information including the design basis, the history of load measurements, wind speed details and condition monitoring measurements (Scenario 4). The accuracy of the lifetime extension assessment increases from Scenario 1 through to Scenario 4. This report also mentions that it is important to have information on the environmental conditions that the wind turbine has been operating in, in order to more accurately determine the remaining useful life (RUL) of the turbine. They also discuss conducting a component-by-component analysis, which explains the requirements for the lifetime extension calcu-

lations, the various failure modes and ways to improve both the inspection and condition monitoring. The nacelle section is split into the shaft and main bearing, frame, electrical components and yaw systems.

The “Basic Principles for Performing an Assessment and Verification of the Lifetime Extension of Onshore Wind Energy Converters (BPW)" [6] was issued by BWE. They state that the stability of the tower, foundations and load-transferring components and functionality of the safety, control and brake systems all need to be assessed in order to determine the lifetime extension. They also state that in order to determine the lifetime extension of a wind turbine, then both an analytical part and practical part needs to be carried out. Where the analytical part is determined using the available documentation and practical part involves an inspection. All of the above standards/guidelines [1], [2], [5] and [6] are useful for recommending both the proposed methods in determining lifetime extension i.e. analytical and practical and the components that the process should be applied to.

Performing fatigue assessments on a select number of wind turbines in a wind farm, using site specific environmental data during the design phase and then comparing them with fatigue reassessments carried out on the turbines at the end of the designed service life when the environmental conditions were known, was investigated by Bouty et al. [7]. Differences in the aero- and hydro- dynamic loading, which were caused by certain environmental parameters were adjusted. The fatigue reassessment results were then extrapolated to the entire wind farm. Extrapolation could not be applied to every parameter such as corrosion. Safety factors were also applied to compensate for uncertainties in the model. They concluded that this is an efficient

method for determining lifetime extension of offshore wind turbines.

Splitting the lifetime extension approach into two was suggested by Rubert et al. [8]. The first being data evaluation using SCADA data, maintenance reports, survey reports, wind history and CMS. The second is inspections of the drivetrain, NDI of any connections that are bolted and welded, corrosion areas, blades and electrical components.

Specifically looking at structures and particularly offshore platforms, Pérez et al. [9] discuss a methodology for damage detection. They used the Submatrices Damage Method to establish damage indicators in terms of stiffness degradation. It works by comparing the structural stiffness of the baseline conditions with the damaged conditions. To detect the location of the damage, limited modal information was used. They concluded that the proposed methodology identifies and locates the damage in terms of stiffness degradation. Both the Baruch and Bar Itzhack [10] and the Berman and Nagy [11] methodologies were used and both enabled the Submatrices Damage Method to accurately locate the damage.

Lifetime extension for onshore wind turbines across various countries in Europe, by carrying out a thorough literature review and interviewing a number of operators was carried out by Ziegler et al. [12]. They looked at conducting load simulations along with technical assessments and concluded that the analytical part of the assessment is conducted by using both structural models and actual site conditions. Obtaining the actual site conditions at present is costly, so this needs to be reviewed further to establish a more cost-effective method. The practical part of the assessment determines the current condition but doesn't determine the structural safety level.

A methodology for determining the lifetime extension of onshore wind turbine towers was developed by Amiri et al. [13]. The tower was assumed to be the key structural component. They used a joint aeroelastic-finite element analysis, ensuring that they took into consideration the wind direction, operational history and stress magnification present around the door of the tower.

Data collected from structural health monitoring (SHM) to establish a lifetime extension strategy was used by Rubert et al. [14]. They explain that data analysis, inspections, aero-elastic simulations and data from SHM systems can all be used to determine the lifetime extension of the turbine. The first three methods can be lacking in information or costly, which can be avoided by using data from SHM. They concluded that determining the lifetime extension of a turbine depends highly on it's location and thus the site specific conditions, and that it is extremely important to establish an appropriate strategy for lifetime extension.

Using the measured strain data to link measured oceanographic data to fatigue damage was investigated by Mai et al. [15], as well as using the Bayesian approach to "update the joint distribution of the oceanographic data". By carrying out the process each year, the remaining fatigue life that has been calculated can be updated in order to "adapt the operation to real loading conditions". They concluded that the proposed methodology worked well in predicting the remaining fatigue life of the support structures. The size of the stress-ranges at the "hot-spots" is the main component that affects the remaining fatigue life.

A geographic information system to assist the operators in deciding on the best course of action for wind turbines nearing the end of their design operational life,

was proposed by Piel et al. [16]. This system will process “topographic, wind, turbine and finance data within an integrated system of resource simulations, spatial planning analyses and economic viability assessments". The results of the spatial analysis will provide the operators with the most economic solution.

A method proposed by Saathoff and Rosemeier [17], compared damage equivalent loads (DEL) of site conditions, against the design conditions to predict the lifetime extension. They compared the DEL-based approach to a stress-based approach. They focused on the blade bolts, blade root laminate and main shaft. They concluded that there was a difference between both approaches, with the stress-based approach providing a more reliable model for lifetime assessments.

Bolts, blade erosion and the effective repair of faults were identified by Natarajan et al. [18], as the main inspection points, from which the results can determine the lifetime extension. They confirm that the standards issued focus on fatigue limit states. They are proposing to use SCADA data and aeroelastic design basis to estimate the shaft torsional load, using the collage method and Tikhonov method. Once the shaft torsional load has been determined, the damage equivalent loads (DEL) can then be calculated on all major structural components. They mention that the DEL values calculated from measurements are much more accurate, so provide a more accurate estimate of fatigue life, which in turn will be more efficient for estimating the lifetime extension of older turbines. They also conducted interviews with owners and they confirmed that critical components include the tower and drivetrain, which is classed as the most critical component.

Attempts have been made to particularly study the wind turbine’s drivetrain dam-

age and it's lifetime extension potential, by studying the internal loads on the drivetrain, which are caused by "excitations from both the wind and generator". Girsang et al. [19] discusses the use of a modelling tool that can model the impacts of electrical transients, wind turbulence and shear on the wind turbine's drivetrain. They recommend using the FAST [20] CAE tool along with Simscape to model the drivetrain, to look at ways of extending the life of the gearbox by testing advanced control schemes.

Dvorak [21] has discussed how turbulent winds, effect the wind turbine's drivetrains. The author experiences a wide range of dynamic loads, which may reduce the predicted life of the components in the drivetrain. Transient torque reversals cause strong oscillations, so need to be taken into account, as they affect the bearings and gears in the gearbox, especially in transient or fault events [22].

Combining physics-based and data-driven models to estimate the RUL of the drivetrain was recommended by Keller et al. [23].

A Reliability Block Diagram (RBD) model was proposed by Eriksson [24], in order to determine wind turbine failures and predict their future behaviour along with the cost. They looked at failure rates, failure types, repair times, cost of spare parts, labour costs etc. They concluded that while lifetime extension is beneficial, it is difficult to pinpoint an ideal length of extension because factors such as: wind resource, turbine availability and the increasing operating and maintenance costs, all have an effect.

4.2 Lifetime Extension Methods in Other Industries

4.2.1 Oil and Gas

According to Sintef [25], a number of activities should be conducted in order to make sure that the technical, operational and organisational *integrity of the asset* is maintained throughout the lifetime extension period. The main activities include: updating procedures as per the latest regulations, collecting data and information on the asset to determine the current condition and how the level of integrity has been affected during the operational life, establish a lifetime extension management plan which will detail how to maintain the asset during the additional operational lifetime, to keep the integrity level of the asset at an acceptable level.

As per Palkar and Markeset [26], certain guidelines may be followed to assess the lifetime extension and to maintain both the technical and operational integrity of the asset. They identify key aspects of ageing such as material degradation, obsolescence and organizational issues. They state that the main objective is to confirm whether the equipment is still fully functional and *fit-for-purpose*. In order to do this, it is important to have both past and present information. These tasks include: collection of data, breakdown of the system, screening, monitoring and testing, detailed analysis, evaluation of risks, outline of challenges and a lifetime extension management plan. They concluded that the lifetime extension process should not compromise on safety standards, that regular inspections with thorough documentation will keep the operators informed of the condition of the equipment and that communication is extremely important, along with lessons learned and sharing knowledge. Finally, they state that

a software system is useful with analysing data and detecting changes.

The age of the equipment is not the only factor for ageing according to Ratnayake [27], it is also important to know how the equipment changes over time in its condition. They state that performing efficient inspections is a key component in lifetime extension. Inspection methodologies are determined based upon the applications, as well as the input and output data.

It is important to develop an efficient asset integrity management (AIM) approach, which will not compromise on safety, integrity or the environment but achieve the required reliability and availability, as per Hudson [28]. They mention that the approach needs to include AIM on all components and systems within the asset, which affect the operation. The aim of the asset life extension study is to determine the location and reason of any deterioration, as well as developing a plan that details how the equipment's integrity can be maintained. The method proposed, begins with the normal design life, which is determined from the original design standards and best practices. Maintenance practices, inspection methods and history, operating practices and environmental conditions then aid in the determination of the impact of deterioration mechanisms. From these two assessments, the assessed asset life can then be determined.

Lifetime extension studies were carried out by Abu Dhabi National Oil Company (ADNOC) liquefied natural gas (LNG) team. Sabry [29] explains how they initially split the asset into five sections, which were: static equipment, safety critical equipment, rotating equipment, civil and structures and electrical and instrumentation. Then data was collected for the static equipment from a variety of systems, such as: risk based

inspection, risk based assessment, focused integrity reviews, computerized maintenance management system (CMMS), root cause analysis, fitness for service exercise and major turn around reports. From here the inspection and failure history, degradation rates, probability of failure and fitness for service results were all analysed, to determine if the static equipment would continue to operate until a set date.

For assessing the structural integrity of offshore oil and gas structures Aeran et al. [30], have proposed a framework for estimating the remaining life. The framework consists of four blocks, the first being “Data Collection, Screening and Selection of Fatigue Assessment Approach", the second is “Simulation of Degradation and Development of Degraded FE Models", third is “Simulation of Loading and Analysis" and the final block “Stress Evaluation and Estimation of Remaining Fatigue Life".

DNV-GL codes along with other relevant codes, specifically related to degradation caused by internal corrosion have been used in a risk-based approach to determine the remaining life and life extension of gas pipelines. Tronskar [31] carried out a case study by conducting leak and burst assessments of a gas pipeline, along with “a structural reliability assessment method".

There are many challenges with regards to maintaining the reliability and integrity of ageing equipment. In order to assess the lifetime extension, Khan et al. [32] explains that there are many factors that need to be taken into account, such as: erosion, corrosion, fatigue, obsolescence and change in standards, to name a few. The method they have described to assess suitability of the asset for lifetime extension first begins with data and information, then criticality screening, analysis of failures and challenges, risk reducing measures, overall risk picture and finally lifetime extension

management. They describe that at each stage, the asset must prove that they are fit-for-purpose and meet the As Low As Reasonably Practicable (ALARP) criteria.

4.2.2 Marine Vessels and Floating Production Installations

Marine vessels operate in harsh and challenging environments, so it is important that they are designed, constructed, maintained and operated according to strict standards, in order to operate safely and efficiently, as well as to protect the environment. Classification societies including: Bureau Veritas (BV), Lloyds Register (LR) and the American Bureau of Shipping (ABS), issue regulations and standards that the marine vessel owner's must comply with, in order for their vessels to be classed. Therefore, if they are to operate beyond their designed service life then reviews, surveys and structural analyses are required, in order to prove that they can continue to operate safely and efficiently.

ABS issued regulations for lifetime extension of floating production installations (FPI) [33], in 2017. They state that the lifetime extension process consists of three phases. The first being the investigation phase, which involves data collection, engineering assessments and a baseline survey. The second phase is the determination phase, which involves reassessment and provision of conditions for lifetime extension and the third phase is the implementation phase, which is where the conditions are implemented.

A reliability-based approach consisting of a structural assessment, met-ocean assessment, vessel hydrodynamic modelling and reliability calculation, have been used to determine lifetime extension of floating production unit moorings. Rosen et al. [34]

concluded that there were many benefits to using this type of approach, which included quick implementation, provided the vessel data and environmental conditions are known. Compared to typical “deterministic design event approaches", there is a more in-depth understanding of the system. Finally, it is of high fidelity, selecting the “most likely failure scenario".

4.2.3 Electrical Machines

The use of condition monitoring of the stator insulation system via on-line partial discharge analysis (PDA) systems is discussed by Zhu et al. [35]. Insulation degradation of the stator can cause failures and reduce the life of the equipment. They looked at two case studies, a generator and a motor with degraded insulation, where both had an on-line partial discharge (PD) testing system applied. They concluded that using on-line partial discharge testing as a condition monitoring tool was extremely useful in determining the condition of the winding insulation of the stator. It gave the operators confidence in using the equipment and allowed lifetime extension of the stator winding insulation in both motors and generators. By monitoring the deterioration of the insulation by a condition monitoring system, extends the service lifetime of the machine.

Temperature affects the insulation material in transformers and induction machines, by ageing the insulation, which in turn affects the life, according to Fuchs and Masoum [36]. For magnetic devices, they explain the three phases that can be used to estimate the lifetime. The first being modelling of additional losses caused by harmonics of either voltage or current. The second phase is to establish the rises in temperature

and the third phase is to determine the lifetime reduction as a percentage against the rated lifetime.

Nonlinear models are recommended by Huger and Gerling [37] for dynamic electric and thermal machine behaviour. They simulated certain behaviour over the life of the machine, such as winding resistance and magnet temperatures. They concluded that the end windings were the most critical part of the winding insulation and that the most likely component to fail was the bearings.

4.2.4 Mechanical Rotating Equipment

Analytical modelling is one way of determining the lifetime extension of ageing equipment. Sire and Hopkins [38] state that it is important to select the most appropriate usage parameter for use in damage modelling. Damage parameters can come in many forms, such as crack length and structural wall thickness for structures. Loading can be defined as either cyclic or constant. Fatigue is an example of cyclic loading and creep or stress corrosion are examples of constant loading. Exposure time and/or loading cycles are examples of usage parameters. Upon selecting components for lifetime extension, “materials data characterizing damage progression as a function of usage" should be taken from either testing in a laboratory or from a materials database. Validation of the lifetime prediction model should be carried out by field experience. They concluded that suitable candidates for lifetime extension should be the components that have extensive remaining life, which have been determined from reliable detection of damage. In order to carry out accurate predictions of the component’s life, multiple tools exist.

There are various methods of assessing the remaining useful life (RUL) of ageing mechanical equipment, which were investigated by Hu et al. [39]. They looked at three methods, the first being a physics-based model, the second a data-driven based model and the third a hybrid model of both methods. As the name suggests, the physics-based model is built upon engineering principles and/or physics dynamics. This model can easily adapt to new or unexpected operations. The data-driven based model operates by comparing the “status assessments of the system during testing with all other learned occurrences", therefore historical data must be used to train the model. They concluded that modelling and assessment of RUL is becoming more important and that the decreasing RUL of all equipment is caused by physics performance degradation. It is difficult to see physics degradation, so RUL evaluation is recommended for determining the degradation process, by using physics performance data that is available. Typically, the two processes that are used in the RUL evaluation are, “the hidden degradation process and observation of measurable processes". The observation process and data are used to determine the degradation process, as well as converting the degradation state into a probability density distribution. This then produces the hidden Markov model (HMM) mechanism and Bayesian recursive estimation, which is conveyed in a state space model. Modelling of both the system and observation equation of the state space model is best achieved by using a mixture of “the physics model based method and historical data fitting for parameter initiation-a data driven hybrid method."

4.2.5 Bearings and Gears

A data-driven approach based on E-Support Vector Regression can be used to estimate the remaining useful life of rolling element bearings. Loutas et al. [40] concluded, that the methodology that they proposed can be used for any task for predicting probabilistic RUL.

Another method for determining the remaining useful life of bearings is by using the extended Kalman filtering method, as described by Singleton et al. [41]. It is difficult to predict the RUL of bearings because accurate physical degradation models are lacking. They propose using a data-driven methodology, which will use both time and time-frequency domain features to monitor any bearing faults. After the features are extracted, an analytical function is developed and then used to learn the extended Kalman filter parameters. This is then used on test data to predict faults under different operating conditions.

NREL have recently joined forces with a number of operators to investigate both the causes and solutions of gearbox failures. The outcome of their research will provide valuable assistance in the lifetime extension of wind turbine gearboxes.

4.2.6 Nuclear Power Plants

The Economic and Social Council issued a “Progress Report on the Development of Guidance on the Application of the Convention to the Lifetime Extension of Nuclear Power Plants" [42] in 2019. The report explains that for nuclear power plants, the lifetime extension not only needs to look at nuclear safety, which is extremely impor-

tant but also about any effects on the surrounding environment. Safety reviews and environment impact assessments both need to be carried out.

The Nuclear Energy Agency [43] discusses that prior to applying to extend the operating license of nuclear power plants, the operators typically plan to make technical improvements, upgrade the safety systems and modify the fuel characteristics, performance and refuelling timetables.

It is not practical to shut down nuclear power plants to carry out tests and inspections to determine whether their lifetime can be extended, according to Bellona [44], so instead a number of programs can be implemented. One such program recommended is called an ageing management program, which should aim to identify any deterioration related to the age of the equipment. Another method of assessing the plant's suitability for lifetime extension is by research, modelling and simulations of different scenarios related to degradation. They also emphasize how important it is to collect and monitor information on accidents and incidents, by installing a monitoring system to gather all this information.

Mitigation strategies for nuclear power plants lifetime extension are discussed by Thevenet [45]. The strategies include: a theoretical approach, potential solutions, mitigation techniques acting on tensile stress level and isolating processes.

4.3 Remaining Useful Life Methods

In order to determine lifetime extension, it is essential to establish the analysis of remaining useful life (RUL) of the components, which make up the system, including:

bearings, gearbox, generators and power converters. Therefore, the existing RUL determination methods used for various components situated within the drivetrain has been studied in the following Subsections. Perception of RUL estimation varies among different studies. Depending on the methods used, RUL can refer to the detection of state of damage or an expected time for failure, which are in some cases irrespective of the specific operational conditions.

In general, the various RUL methods used data from either SCADA data or condition monitoring and the modelling methods were either physics-based or data-driven and in rare cases a hybrid approach.

In order to determine the remaining useful life of a component, like all calculations, requires both data as well as a method/process. With regards to data, either SCADA and/or condition monitoring (CM) data can be used. Out of all the literature consulted the majority used a combination of both, with the common parameters being vibration from the CM data and wind speed, power and rotor speed from the SCADA data. With regards to the method/process, either a physics-based or data-driven approach are used, with a data-driven approach the most popular approach used.

4.3.1 Bearings

For the main bearing, a physics-based model has been used for determining remaining useful life, [46], taking inputs from blade root bending moments and rotor speed. While data-driven models such as a stochastic method including: the moving average method, a performance degradation model established with the Wiener process, the maximum likelihood estimation method and inverse Gaussian distribution, [47] and a

method combining the interval whitenization method with a Gaussian process (GP) algorithm, [48] have been employed for generator bearings. The input parameters included temperature [47] and vibration [48].

A data-driven method, involving spectral Kurtosis-derived indices and support vector regression (SVR) based on the vibrations taken from the condition monitoring, have also been used for determining the RUL of high speed stage bearings within the gearbox [49].

For determining the RUL of bearings in general, a data-driven approach involving a Principal Component Analysis (PCA) technique, regression models such as Support Vector Regressor (SVR) and Random Forest (RF) and Weibull Hazard Rate Function [50] have been employed, taking vibration as the input. Another approach/method that can be used which also takes vibration as the input, is a hybrid approach involving monotonicity, Spearman rank correlation analysis, hierarchical clustering, fusion, principal component analysis and T-test [51].

4.3.2 Gearbox

The remaining useful life of bearings, gears and high speed shafts within the gearbox have all been investigated.

For determining the bearing forces in the intermediate-speed shaft of a three-stage WT gearbox, a physics-based approach, using both SCADA data and design data as the inputs for the rigid beam models, have been used [52]. Whereas data-driven approaches have been employed for determining the remaining useful life of the gearbox bearings. Normal behaviour modelling, pattern recognition models, classification and

degradation models were all used to determine the RUL of the planet bearing [53]. A Generalized Cauchy Process to establish a degradation model has also been used [54]. Another data-driven approach using the vibration data as the input, is an artificial neural network to train models and predict the RUL [55]. As an alternative, physics-based calculations, i.e torque, axial and angular misalignment, pinion loads, coupling hub loads, bearing loads, can be employed using SCADA, CM data, as well as high-speed stage (HSS) component dimensions as their input [56]. Both physics-based and data-driven models can be used for determining the RUL of the helical gear within the gearbox, using a combination of SCADA and CM data. “The loads were computed by means of physical relations, damage sensitive parameter (feature extractor) and the transformation of this parameter to the size of misalignment (classification)" [57].

For determining the RUL of the gearbox in general, data-driven approaches using both SCADA and CM data as the inputs dominate. One method is a particle-filtering model [58]. A statistical approach including the Miner’s Rule, cumulative damage calculation and RUL estimation using regression model is another method that has been employed [59]. Machine learning algorithms have also been used [60]. A slightly different method which just uses SCADA data is the particle filtering (PF) method (recursive Bayesian algorithm based on the concept of sequential importance sampling and Bayesian theory), [61].

4.3.3 Generator

Calculating the remaining useful life of the generator by using SCADA and design data can be achieved by using thermal, electrical and mechanical models [52].

SCADA data such as rotor speed, wind speed and output power, along with a data-driven approach using a time-based sliding window/Bin method and state model have also been used to determine RUL [62].

Another data-driven approach used to determine the RUL specifically of the generator bearings, involves the Empirical Mode Decomposition and Support Vector Regression Prediction Model using vibration data from condition monitoring as the input [63].

4.3.4 Power Converter

In all the literature reviewed, the insulated-gate bipolar transistors (IGBT's) were identified as having the highest failure rate within the power converter.

Physics-based approaches have been used for calculating the remaining useful life of power converters. Methods include: mathematical models along with a failure modes and effects analysis (FMEA) [64], as well as a risk assessment from the FMEA, wind profile, integrated aero elastic servo control code, Miners rule, induction generator model, thermal model for junction and case temperature prediction, rain flow counting method and digital twin [65].

A data-driven approach, which included computation of the time-domain features to extract the degradation behaviour of the IGBT device and the Gaussian process regression technique have been used [66].

4.4 Key Steps/Take-Away Points for Determining Lifetime Extension

From the literature presented in the previous subsections, the key steps in lifetime extension and comparison across different industries can be summarised in Figures B.1 and B.2 and further condensed in Table 4.1.

Table 4.1: Condensed Summary of Lifetime Extension in Industries.

Title	Description	Oil & Gas	Marine Vessels	Nuclear	Wind
LTE Objectives	Maintain reliability, integrity and operational safety	X	X	X	X
	Economically beneficial	X	X	X	X
	Environmental impacts			X	
RUL Approaches	Physic-based modelling	X			X
	Data-driven modelling	X			X
	Hybrid modelling	X			
	Survey-based practical		X		
Methodology	Data collection	X	X	X	X
	Risk assessment	X	X	X	X
	System breakdown	X	X		X
	Aging management plan	X		X	
	Environmental re-assessment			X	
	Simulation of degradation scenarios			X	

These key take-away points are items that have been identified as being applicable/transferable for use in determining the lifetime extension process, specifically for wind turbine drivetrains.

The lifetime extension process can be split into a number of stages. The first stage of the process is data collection. The more data available and collected, then the more accurate the final results will be, was a common conclusion throughout. Typically, the data comes from SCADA data, condition monitoring system, design drawings, man-

ufacturing drawings, installation reports, maintenance reports, failure records, operational history etc.

The next stage is to establish the type of assessment. Analytical and/or practical assessments appear to be the most common assessments used across many industries. Utilising both seems to provide the most accurate results. Analytical assessments can include: modelling, simulations, calculations etc., whereas practical assessments refer to surveys and inspections of the assets.

Based upon the methods determined from the equipment/system/plant type and data available, the assessments are then carried out, which is the next stage. The depth of each type of assessment will vary, depending on the industry and the amount of data collected. It is important to consider environmental conditions within this stage, as well as the conditions that the components have been operating in throughout their lifetime.

Regarding the analytical assessments, a number of approaches/methods were mentioned, including:

1. Physics-Based.
2. Data-Driven.
3. Hybrid.

A physics-based approach uses fundamental principles to model the behaviours and operation of the wind turbine, such as aerodynamics, mechanics etc. The data-driven approach uses historical data and real-time data, along with statistical techniques to predict the future behaviour of wind turbines. They aim to determine any pat-

terns and/or anomalies. Typical machine learning models include: regression models, support vector machine models, decision trees etc. Whilst the hybrid approach uses a combination of both physics-based and data-driven approaches, [39].

The outcome from the assessments will then determine the remaining useful life, whether the operational life of the equipment/plant/system can be extended and by how long. It will also establish whether any additional operating and maintenance practices (e.g. additional oil checks, additional measurements, applying protective coating, etc.) will need to be implemented and the frequency of them.

4.5 References

[1] Bureau Veritas. *Guidelines for Wind Turbines Lifetime Extension*. Bureau Veritas, France, latest edition, 2017.

[2] DNV-GL. *DNVGL-ST-0262 - Lifetime extension of wind turbines*. DNV-GL, Norway, latest edition, 2016.

[3] DNV-GL. *DNVGL-ST-0263 - Certification of lifetime extension of wind turbines*. DNV-GL, Norway, latest edition, 2016.

[4] TUV Nord. Certification of Lifetime Extension. `www.tuev-nord.de/en/company/energy/renewables/wind-energy/`, May 2017.

[5] Megavind. Strategy for Extending the Useful Lifetime of a Wind Turbine. `https://megavind.winddenmark.dk/sites/megavind.winddenmark.dk/files/media/document/Strategy.for.Extending.the.Useful.Lifetime.of.a.Wind.Turbine.pdf`, 2016. Online; accessed 23-Apr.-2021.

[6] BWE Grundsätze. Basic Principles for Performing an Assessment and Verification of the Lifetime Extension of Onshore Wind Energy Converters (BPW). `https://www.wind-energie.de/fileadmin/redaktion/dokumente/publikationen-oeffentlich/arbeitskreise/weiterbetrieb/Grundsaetze_Weiterbetrieb_04.2017_V6.3_final.pdf`, 2017. Online; accessed 23-Apr.-2021.

[7] Corantin Bouty, Sebastian Schafhirt, Lisa Ziegler, and Michael Muskulus. Lifetime extension for large offshore wind farms: Is it enough to reassess fatigue for selected design positions? *Energy Procedia*, 137:523–530, 2017.

[8] Tim Rubert, Lisa Ziegler, Elena Gonzalez, David McMillan, Ursula Smolka, and Julio J. Melero. The UK's state-of-the-art of lifetime extension of onshore wind turbines. `https://events.renewableuk.com/images/documents/OAM17/A3-Tim-Rubert.pdf`, 2017.

[9] José Enrique R Pérez, Ramsés Rodríguez, and Alberto Omar Vázquez-Hernández. Damage detection in offshore jacket platforms with limited modal information using the damage submatrices method. *Marine Structures*, 55:78–103, 2017.

[10] Menahem Baruch and Itzhack Y Bar Itzhack. Optimal weighted orttiogonalization of measured modes. *AIAA journal*, 16(4):346–351, 1978.

[11] A Berman and EJ Nagy. Improvement of a large analytical model using test data. *AIAA journal*, 21(8):1168–1173, 1983.

[12] Lisa Ziegler, Elena Gonzalez, Tim Rubert, Ursula Smolka, and Julio J Melero. Lifetime extension of onshore wind turbines: A review covering germany, spain, denmark, and the uk. *Renewable and Sustainable Energy Reviews*, 82:1261–1271, 2018.

[13] A Kazemi Amiri, R Kazacoks, D McMillan, J Feuchtwang, and W Leithead. Farm-wide assessment of wind turbine lifetime extension using detailed tower model

and actual operational history. In *Journal of Physics: Conference Series*, volume 1222, page 012034. IOP Publishing, 2019.

[14] T Rubert, G Zorzi, G Fusiek, P Niewczas, D McMillan, J McAlorum, and M Perry. Wind turbine lifetime extension decision-making based on structural health monitoring. *Renewable Energy*, 143:611–621, 2019.

[15] Quang A Mai, Wout Weijtjens, Christof Devriendt, Pablo G Morato, Philippe Rigo, and John D Sørensen. Prediction of remaining fatigue life of welded joints in wind turbine support structures considering strain measurement and a joint distribution of oceanographic data. *Marine Structures*, 66:307–322, 2019.

[16] JH Piel, C Stetter, M Heumann, M Westbomke, and MH Breitner. Lifetime extension, repowering or decommissioning? decision support for operators of ageing wind turbines. In *Journal of Physics: Conference Series*, volume 1222, page 012033. IOP Publishing, 2019.

[17] Matthias Saathoff and Malo Rosemeier. Stress-based assessment of the lifetime extension for wind turbines. In *Journal of Physics: Conference Series*, volume 1618, page 052057. IOP Publishing, 2020.

[18] Anand Natarajan, Nikolay Krasimirov Dimitrov, Dheelibun Remigius William Peter, Leonardo Bergami, Jens Madsen, Niels Olesen, Thomas Krogh, Jannie Nielsen, John Dalsgaard Sørensen, Mikael Pedersen, et al. *Demonstration of Requirements for Life Extension of Wind Turbines Beyond Their Design Life*. DTU Wind Energy, 2020.

[19] Irving P Girsang, Jaspreet S Dhupia, Eduard Muljadi, Mohit Singh, and Lucy Y Pao. Gearbox and drivetrain models to study dynamic effects of modern wind turbines. *IEEE Transactions on Industry Applications*, 50(6):3777–3786, 2014.

[20] J. M. Jonkman and M. L. Buhl. Fast user's guide. In *Nat. Renew. Energy Lab., Golden, CO, USA, Tech. Rep. NREL/EL-500-38230*. National Renewable Energy Laboratory, 2005.

[21] Paul Dvorak. How turbulent winds abuse wind turbine drivetrains. `https://www.windpowerengineering.com/how-turbulent-wind-abuse-wind-turbine-drivetrains/`, 2015.

[22] Amir Rasekhi Nejad, Zhiyu Jiang, Zhen Gao, and Torgeir Moan. Drivetrain load effects in a 5-mw bottom-fixed wind turbine under blade-pitch fault condition and emergency shutdown. In *Journal of physics: conference series*, volume 753, page 112011. IOP Publishing, 2016.

[23] Jonathan Keller, Shuangwen Sheng, Jason Cotrell, and Aaron Greco. Wind turbine drivetrain reliability collaborative workshop: A recap. 8 2016. doi: $10.2172/1314863$.

[24] Robert Eriksson. Lifetime extension of offshore wind farms, 2022.

[25] Per Hokstad, Solfrid Håbrekke, Roy Johnsen, and Sigbjørn Sangesland. Ageing and life extension for offshore facilities in general and for specific systems. *SINTEF Report for the Petroleum Safety Authority Norway*, 2010.

[26] Sushil Palkar and Tore Markeset. Extending the service life span of ageing oil and

gas offshore production facilities. In *IFIP International Conference on Advances in Production Management Systems*, pages 213–221. Springer, 2011.

[27] RM Chandima Ratnayake. Challenges in inspection planning for maintenance of static mechanical equipment on ageing oil and gas production plants: The state of the art. In *International Conference on Offshore Mechanics and Arctic Engineering*, volume 44939, pages 91–103. American Society of Mechanical Engineers, 2012.

[28] Brian Hudson. Offshore Installation Life Assessment and Extension. `https://www.maintenanceandengineering.com/2015/01/01/offshore-installation-life-assessment-and-extension/`, January 2015.

[29] Houssam Sabry. Aging lng static equipment life extension - a case study. In *Abu Dhabi International Petroleum Exhibition & Conference*. Society of Petroleum Engineers, 2018.

[30] Ashish Aeran, Sudath C Siriwardane, Ove Mikkelsen, and Ivar Langen. Life extension of ageing offshore structures: A framework for remaining life estimation. In *ASME 2017 36th International Conference on Ocean, Offshore and Arctic Engineering*. American Society of Mechanical Engineers Digital Collection, 2017.

[31] Jens P Tronskar. Remaining life assessment and life extension of offshore pipelines. In *ASME 2018 37th International Conference on Ocean, Offshore and Arctic Engineering*. American Society of Mechanical Engineers Digital Collection, 2018.

[32] Riaz Khan, Ammeran B Mad, Khairil Osman, and Mohd Asyraf Abd Aziz. Maintenance management of aging oil and gas facilities. In *Maintenance Management*. IntechOpen, 2019.

[33] ABS. Life extension methodology for floating production installations. `https://ww2.eagle.org/content/dam/eagle/rules-and-guides/current/offshore/217_lifeextensionmethodology_floatingproductioninstallations_2017/FPI_Life_Extension_GN_e-May17.pdf`, 2017.

[34] J Rosen, D Johnstone, P Sincock, AE Potts, and D Hourigan. Application of reliability analysis to re-qualification and life extension of floating production unit moorings. In *ASME 2016 35th International Conference on Ocean, Offshore and Arctic Engineering*. American Society of Mechanical Engineers Digital Collection, 2016.

[35] H Zhu, V Green, and D Huynh. Lifetime extension experience on rotating machine insulation using on-line pd testing. In *Conference Record of the the 2002 IEEE International Symposium on Electrical Insulation (Cat. No. 02CH37316)*, pages 561–564. IEEE, 2002.

[36] E.F Fuchs and M.A.S. Masoum. Chapter 6 - lifetime reduction of transformers and induction machines. In *Power Quality in Power Systems and Electrical Machines*, pages 227–260. Academic Press, 2008.

[37] D Huger and D Gerling. An advanced lifetime prediction method for permanent

magnet synchronous machines. In *2014 International Conference on Electrical Machines (ICEM)*, pages 686–691. IEEE, 2014.

[38] RA Sire and SW Hopkins. Analytical modeling for life extension of aging equipment. *International journal of fatigue*, 19(93):261–266, 1997.

[39] Yawei Hu, Shujie Liu, Huitian Lu, and Hongchao Zhang. Remaining useful life model and assessment of mechanical products: a brief review and a note on the state space model method. *Chinese Journal of Mechanical Engineering*, 32(1): 15, 2019.

[40] Theodoros H Loutas, Dimitrios Roulias, and George Georgoulas. Remaining useful life estimation in rolling bearings utilizing data-driven probabilistic e-support vectors regression. *IEEE Transactions on Reliability*, 62(4):821–832, 2013.

[41] Rodney K Singleton, Elias G Strangas, and Selin Aviyente. Extended kalman filtering for remaining-useful-life estimation of bearings. *IEEE Transactions on Industrial Electronics*, 62(3):1781–1790, 2014.

[42] United Nations. *Progress report on the development of guidance on the application of the Convention to the lifetime extension of nuclear power plants*. United Nations, Geneva, latest edition, 2018. See also URL `https://www.unece.org/fileadmin/DAM/env/documents/2019/ece/Meeting_of_Parties_-_2019/G-Doc_documents/1819196E.pdf`.

[43] Nuclear Energy Agency. *Ad hoc Expert Group on the Impact of Nuclear Power Plant Life Extension*. Nuclear Energy Agency, France, latest edition. See also

URL https://www.oecd-nea.org/jcms/pl_29405/ad-hoc-expert-group-on-the-impact-of-nuclear-power-plant-life-extension.

[44] Bellona. *Nuclear Power Plant Lifetime Extension: A creeping catastrophe*. Bellona, Norway, latest edition, 2020. See also URL https://bellona.org/publication/nuclear-power-plant-lifetime-extension-a-creeping-catastrophe-2.

[45] Re´ mi Thevenet. Nuclear pwr plants mitigation of reactor coolant system areas to consider plants aging management and/or life extension. In *ASME Pressure Vessels and Piping Conference*, volume 43703, pages 355–374, 2009.

[46] Hólmfríður Haraldsdóttir and Maria Sandström. Lifetime analysis of a wind turbine component. Master's thesis, 2016.

[47] Yaogang Hu, Hui Li, Pingping Shi, Zhaosen Chai, Kun Wang, Xiangjie Xie, and Zhe Chen. A prediction method for the real-time remaining useful life of wind turbine bearings based on the wiener process. *Renewable energy*, 127:452–460, 2018.

[48] Lixiao Cao, Zheng Qian, Hamid Zareipour, David Wood, Ehsan Mollasalehi, Shuangshu Tian, and Yan Pei. Prediction of remaining useful life of wind turbine bearings under non-stationary operating conditions. *Energies*, 11(12):3318, 2018.

[49] Lotfi Saidi, Jaouher Ben Ali, Eric Bechhoefer, and Mohamed Benbouzid. Wind

turbine high-speed shaft bearings health prognosis through a spectral kurtosis-derived indices and svr. *Applied Acoustics*, 120:1–8, 2017.

[50] Apakrita Tayade, Sangram Patil, Vikas Phalle, Faruk Kazi, and Satvasheel Powar. Remaining useful life (rul) prediction of bearing by using regression model and principal component analysis (pca) technique. *Vibroengineering PROCEDIA*, 23: 30–36, 2019.

[51] Ping Wang, Zhiqiang Long, and Gao Wang. A hybrid prognostics approach for estimating remaining useful life of wind turbine bearings. *Energy Reports*, 6: 173–182, 2020.

[52] Michael Pagitsch, Georg Jacobs, and Dennis Bosse. Remaining useful life determination for wind turbines. In *Journal of Physics: Conference Series*, volume 1452, page 012052. IOP Publishing, 2020.

[53] Sofia Koukoura. Failure and remaining useful life prediction of wind turbine gearboxes. In *Annual Conference of the PHM Society*, volume 10, 2018.

[54] He Liu, Wanqing Song, Yuhui Niu, and Enrico Zio. A generalized cauchy method for remaining useful life prediction of wind turbine gearboxes. *Mechanical Systems and Signal Processing*, 153:107471, 2021.

[55] Wei Teng, Xiaolong Zhang, Yibing Liu, Andrew Kusiak, and Zhiyong Ma. Prognosis of the remaining useful life of bearings in a wind turbine gearbox. *Energies*, 10(1):32, 2017.

[56] Damian P Rommel, Dario Di Maio, and Tiedo Tinga. Calculating loads and lifetime reduction of wind turbine gearbox and generator bearings due to shaft misalignment. *Wind Engineering*, page 0309524X20914022, 2020.

[57] Dick Breteler, Christos Kaidis, Tiedo Tinga, and Richard Loendersloot. Physics based methodology for wind turbine failure detection, diagnostics & prognostics. *EWEA 2015 Annual Event*, 2015.

[58] Xiaoliang Fan, Xiao Yang, Xinli Li, and Jianming Wang. A particle-filtering approach for remaining useful life estimation of wind turbine gearbox. In *International Conference on Chemical, Material and Food Engineering*, pages 198–200. Atlantis Press, 2015.

[59] R Srinivasan and T Robert. Remaining useful life prediction on wind turbine gearbox. *International Journal of Recent Technology and Engineering*, 9:57–65, 01 2021. doi: $10.35940/\mathrm{ijrte.E5145.019521}$.

[60] James Carroll, Sofia Koukoura, Alasdair McDonald, Anastasis Charalambous, Stephan Weiss, and Stephen McArthur. Wind turbine gearbox failure and remaining useful life prediction using machine learning techniques. *Wind Energy*, 22(3):360–375, 2019.

[61] Fangzhou Cheng, Liyan Qu, and Wei Qiao. Fault prognosis and remaining useful life prediction of wind turbine gearboxes using current signal analysis. *IEEE Transactions on Sustainable Energy*, 9(1):157–167, 2017.

[62] Fan Zhang, Zejun Wen, Deshun Liu, Jie Jiao, Hengzheng Wan, and Bing Zeng.

Calculation and analysis of wind turbine health monitoring indicators based on the relationships with scada data. *Applied Sciences*, 10(1):410, 2020.

[63] Lixiao Cao, Zheng Qian, and Yan Pei. Remaining useful life prediction of wind turbine generator bearing based on emd with an indicator. In *2018 Prognostics and System Health Management Conference (PHM-Chongqing)*, pages 375–379. IEEE, 2018.

[64] Marco Sepulveda, Peter Davies, Mark Spring, Jonathan Shek, PR Thies, and Erkan Oterkus. Risk assessment of an offshore wind turbine and remaining useful life estimation of the power converter. improving availability by prioritising failures with higher risk to operation. 2016.

[65] Krishnamoorthi Sivalingam, Marco Sepulveda, Mark Spring, and Peter Davies. A review and methodology development for remaining useful life prediction of offshore fixed and floating wind turbine power converter with digital twin technology perspective. In *2018 2nd International Conference on Green Energy and Applications (ICGEA)*, pages 197–204. IEEE, 2018.

[66] Adla Ismail, Lotfi Saidi, Mounir Sayadi, and Mohamed Benbouzid. Remaining useful lifetime prediction of thermally aged power insulated gate bipolar transistor based on gaussian process regression. *Transactions of the Institute of Measurement and Control*, 42(13):2507–2518, 2020.

Chapter 5

Developing a Methodology for Determining Lifetime Extension

In the previous chapter, lifetime extension and remaining useful life assessment practices executed within a variety of industries have been investigated. Aspects that have been identified as being easily adoptable, have been noted and taken into consideration when constructing the methodology proposed within this chapter, to again ensure a comprehensive approach and accurate outcome.

5.1 Methodology

Based on the findings from Chapter 4 and a systematic approach, a methodology to determine the feasibility of wind turbine drivetrain lifetime extension has been proposed and summarized in Figure 5.1.

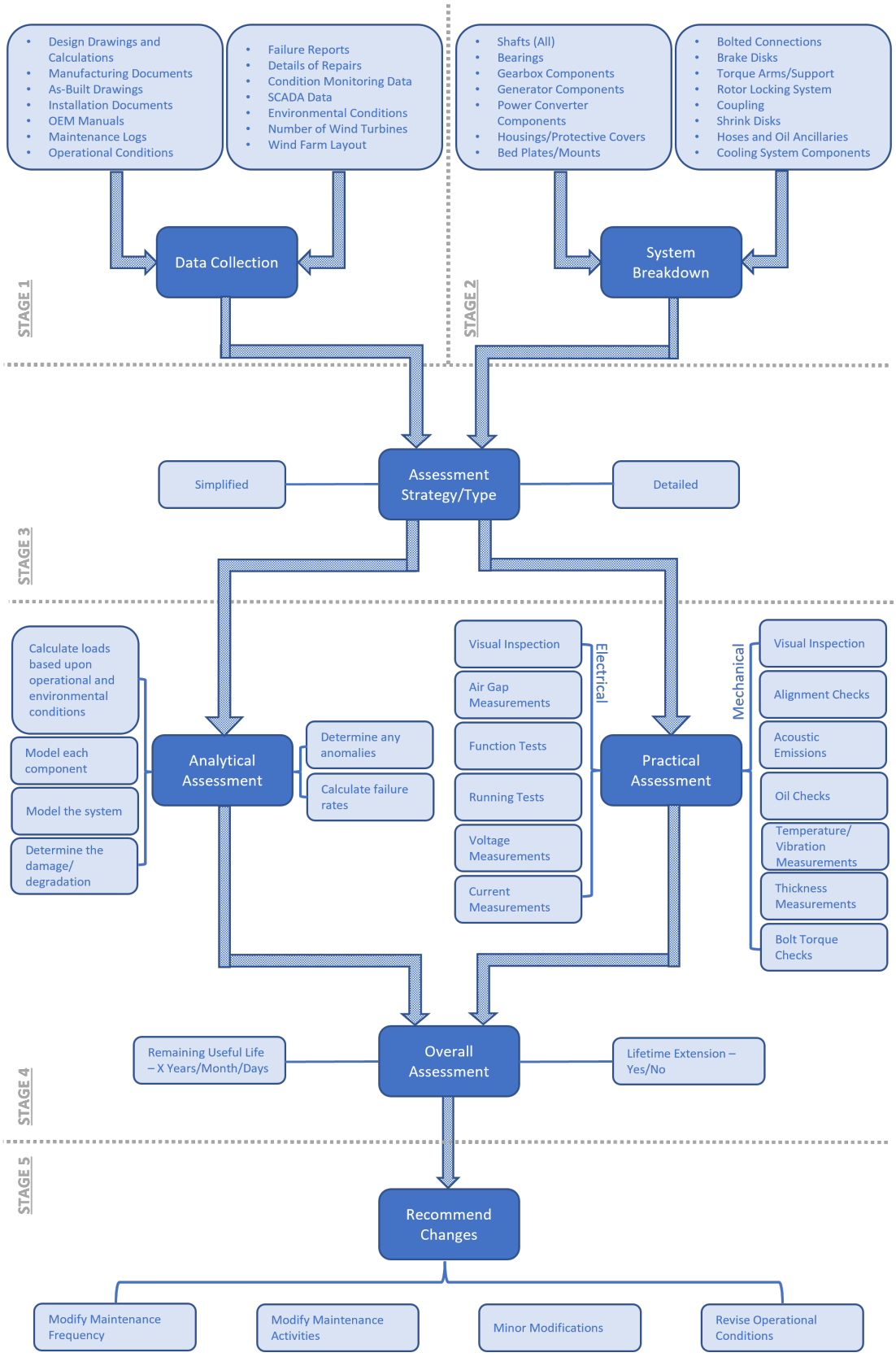

Figure 5.1: Flowchart of Proposed Methodology for Lifetime Extension of Wind Turbine Drivetrains.

5.1.1 Stage 1: Data Collection

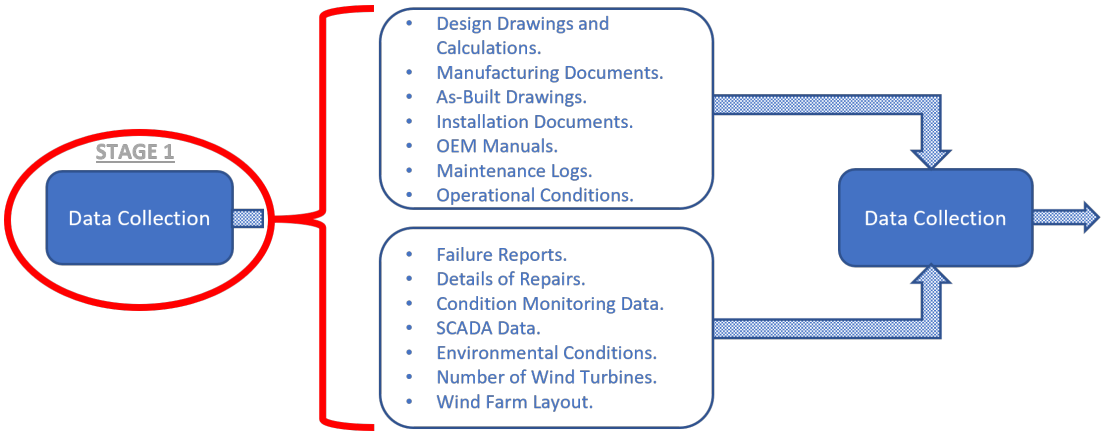

Figure 5.2: Data Collection

Data that can be used to assist with determining the remaining useful life/lifetime extension of the wind turbine drivetrains are listed in Table 5.1. As discussed earlier, in theory the more data available then the more accurate the results will be. All the documents listed, aid in the assessment in some way or another.

Table 5.1: Breakdown of Data Collection Documents

ORIGINAL	OPERATIONAL	MAINTENANCE	ENVIRONMENT	LOCATION
Manufacturing Documents / As-Built Drawings	Operational Conditions	Maintenance Logs	Environmental Conditions	Number of Wind Turbines in Wind Farm
Design Calculation	SCADA Data	Failure Reports		Layout of the Wind Farm
Design Drawings	Condition Monitoring Data	Details of Repair		
Installation Docs	OEM Manuals			

The recommended minimum data required includes: the original manufacturing documents/as-built drawings, operational conditions, maintenance logs, failure reports and SCADA data including power, generator speed and temperature measurements.

Some older turbines may only have SCADA data available, so it is important to be able to determine if an accurate assessment can be carried out using only SCADA data.

5.1.2 Stage 2: System Breakdown

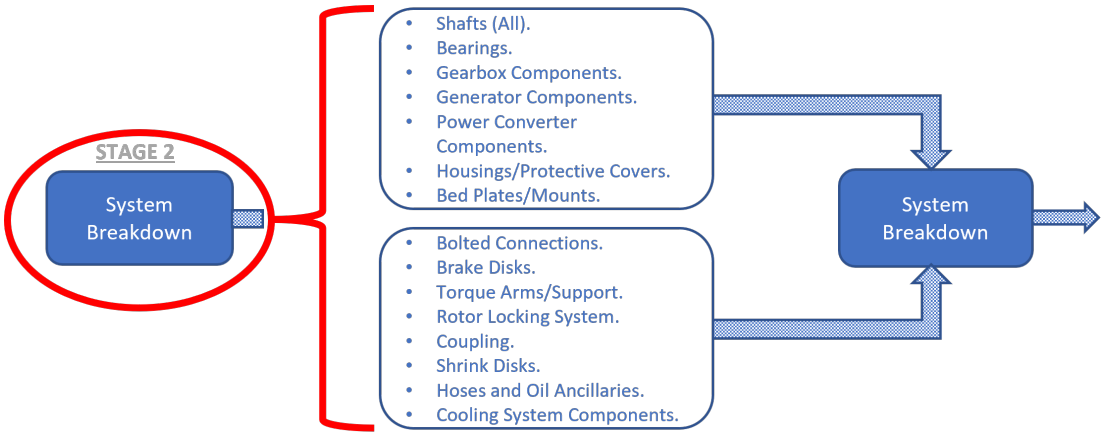

Figure 5.3: System Breakdown

The drivetrain system will then be divided into individual components or groups, as shown in Table 5.2.

The brake disk, rotor locking system and shrink disk have been placed in a separate column, labelled "Safety" because even though they can be classed as "Mechanical" components, their primarily function is related to safety, as opposed to just mechanical power transmission. They are typically used to protect the wind turbine and maintenance personnel from various risks, including excessive motion or uncon-

Table 5.2: Breakdown of Drivetrain Components

STRUCTURAL	MECHANICAL	ELECTRICAL	HYDRAULICS & COOLING	SAFETY
Bedplates / Mounts	Gearbox	Generator Components	Hoses	Brake Disk
Bolted Connections	Bearings	Power Converter Components	Cooling System Components	Rotor Locking System
Housing / Protective Casing	Shafts (HSS, LSS, Output)		Oil Ancillaries	Shrink Disk
Torque Arms / Supports	Couplings			

trolled rotation.

This stage is carried out in order to assist with the ranking of equipment and in turn it's components, starting with those more prone to failure.

5.1.3 Stage 3: Assessment Type

The type and amount of data collected in Stage 1, will determine the type and level of assessment carried out. For example, if either no or only minimum data is available a simplified approach will be implemented, with a more detailed approach implemented when more data is available.

The recommended assessment type will consist of:

1. Analytical/Modelling/Calculations.
2. Practical/Surveys/Inspections.
3. Overall Assessment.

The main objective of the assessment process is to determine the remaining useful life of the components, as discussed in Chapter 4.

5.1.4 Stage 4: Assessment

5.1.4.1 Stage 4a: Analytical Assessment

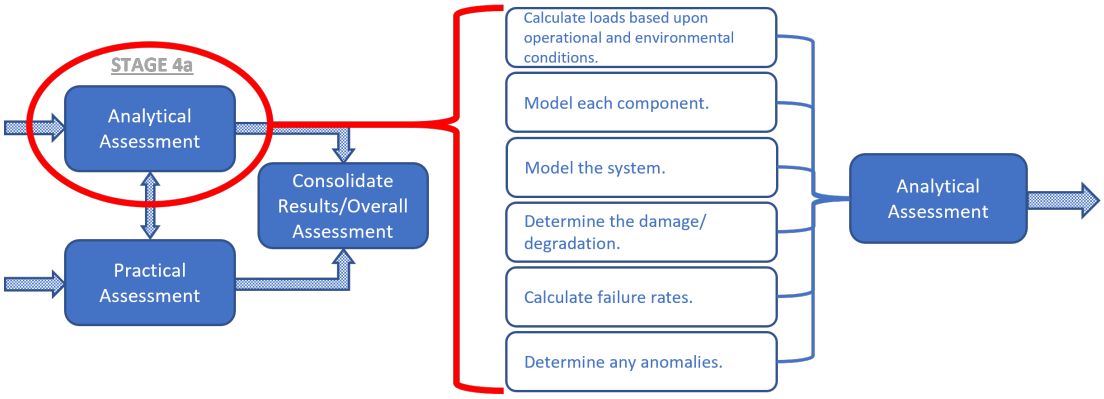

Figure 5.4: Analytical Assessment

As discussed in the previous chapter, the methods used for analytical assessment can include: physics-based, data-driven or hybrid approaches.

Based on these approaches, the recommended analytical assessment will include but not be limited to the following:

1. Calculation of loads that each component has been subjected to throughout its life to date, based upon the operational and environmental conditions (physics-based).

2. Modelling of each component and the system as a whole (e.g. multi-body). This can help identify the interdependencies, by observing how the different components interact and affect each other (physics-based).

3. Determination of the damage/degradation for each component using both the loads calculated and modelling simulations (physics-based).

4. Calculation of failure rates based upon failure reports, in order to identify components more vulnerable to fail (data-driven).

5. Identification of any parameter anomalies, which may signal issues with the components. Monitoring and identifying any variations could indicate that something is wrong (data-driven).

Lifetime extension assessments are typically conducted near the end of an asset's operational design life, requiring the storage of large amounts of SCADA and/or condition monitoring data, which is impractical. Therefore, it is proposed that a smaller analysis be performed annually to assess any deterioration of components from the previous year, with only this information being stored. This approach will also allow for the early detection and resolution of unexpected issues, helping to preserve the components' operational life.

5.1.4.2 Stage 4b: Practical Assessment

The recommended practical assessment will include but not be limited to the following:

1. Visual inspection of the components including: the shaft, coupling, bolted connections, cooling system, protective covers, safety system, etc.

2. Alignment checks of the system including the gearbox and generator.

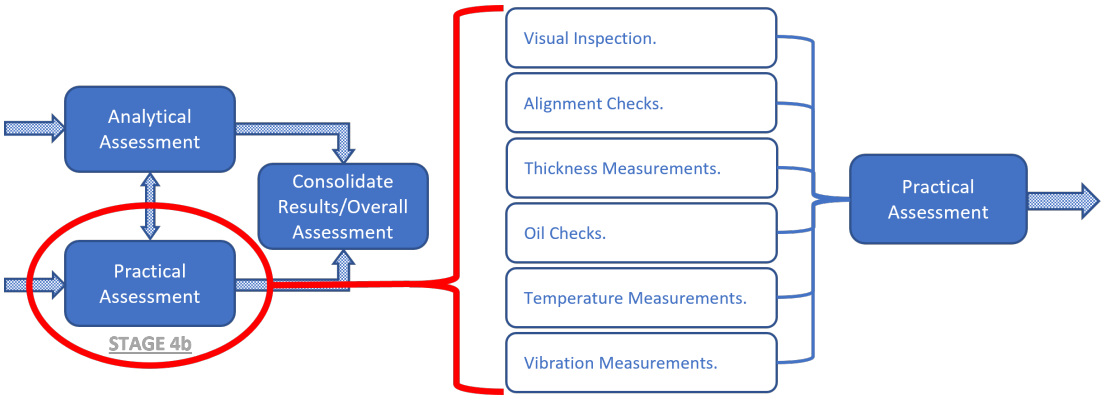

Figure 5.5: Practical Assessment

3. Material thickness measurements on components including: the mechanical brake (e.g. brake disk, brake pad), sliding contacts, gearbox (e.g. gear teeth, casing wall, bearing races and rollers), shrink disk, shaft (e.g. wall), etc.

4. Confirm oil checks have been conducted as part of the maintenance procedures, including: level checks, cleanliness and contamination, viscosity, additive condition check, oxidation and acidity, etc.

5. Check that the temperature and vibration measurements are corresponding with the SCADA data.

The survey or inspection results can be compared with those from the analytical assessment. If significant discrepancies are found, with components in a worse condition than expected, the model can then be updated accordingly. Conducting a practical assessment is crucial to accurately evaluate the system's current condition and ensure the model remains accurate and up to date.

5.1.4.3 Stage 4c: Overall Assessment

After completing both the analytical and practical assessments, the remaining useful life of each component can be determined. A conservative approach is to consider the drivetrain lifetime extension equal to the lowest RUL. In other words, the lowest RUL will determine the possible lifetime extension of the wind turbine drivetrain.

To move from the turbine to the farm level will also be a challenge. In some instances, it may not be possible or practical to analyse and inspect each individual wind turbine. Therefore, a process to assess a certain number of turbines and then use those results to estimate the other turbines is extremely beneficial and will be determined and investigated in future work. Inspections will be one method that will be used to help with uncertainties.

5.1.4.4 Stage 4d: Accounting for Uncertainties and Errors

Uncertainties can be defined as something that is not known or something that is unsure, whereas errors are defined as the difference between the actual and predicted measurements.

With regards to this process, there are a number of uncertainties and errors within the system, including but not limited to the following:

1. Manufacturing and/or installation tolerances.
2. Signal issues or malfunctions.
3. Equipment calibration issues.

4. Calculations.

5. Modelling methods.

6. Environment and/or atmospheric conditions.

Therefore, in order to obtain an accurate outcome, these uncertainties and/or errors need to be taken into account and processes put in place to accommodate these. One method that can be used to take into account certain uncertainties/errors, such as manufacturing and installation tolerances is, inspection. By carrying out thorough inspections of the drivetrain, measurements can be taken to determine the required parameters.

5.1.5 Stage 5: Recommended Changes

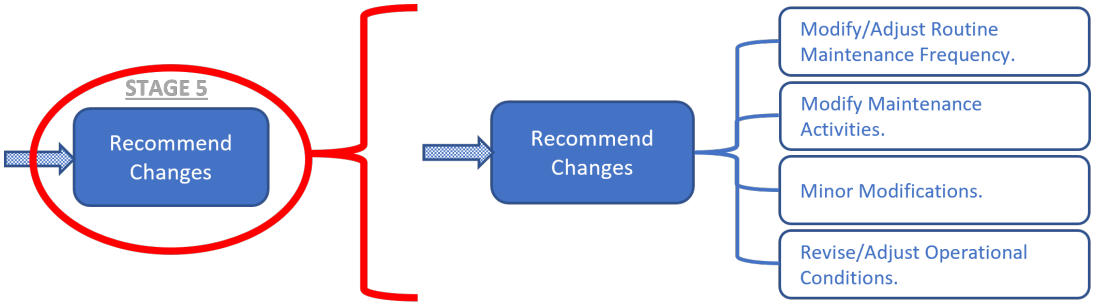

Figure 5.6: Recommended Actions/Changes

Once it has been decided that lifetime extension is applicable, then any necessary conditions, such as additional operational and maintenance procedures to ensure the expected lifetime extension, should be documented. Recommended changes can include:

1. Adjusting the frequency of the maintenance inspections.

2. Modifying the maintenance checklist.

3. Revising the operating procedures.

4. Minor modifications, which may include: upgrading the oil filtration system, installing more temperature and/or vibration sensors, fine-tuning any alarm thresholds, applying protective coating, installing additional dampers, upgrading the cooling system, etc.

5. Change in operation in terms of maximum wind speed, which may include: reducing the cut-out speed, derating the turbine, implementing active load control, adjusting pitch control, etc.

5.2 Theory

As discussed, the ideal situation (Case 1) would be to carry out both practical and analytical assessments, with data from the SCADA system, condition monitoring system and failure/maintenance reports, ideally using a hybrid approach for lifetime extension assessment. However, in some cases, routine practical assessments may not be feasible due to location, hostile environment, cost etc. and the addition of extra sensors required as part of the condition monitoring system are not considered viable due to additional costs, but in all wind turbines, SCADA data is recorded, so the minimum amount of data obtained is SCADA data (Case 2). In this case, it has been assumed that a data-driven approach is ideal, using a readily available machine learning regression model. A data-driven approach has been selected because it is assumed that a

practical, straight-forward method would be more beneficial to owner/operators.

A number of machine learning regression models are available, including but not limited to the following:

1. Linear Regression Model.
2. Polynomial Regression Model.
3. Support Vector Machine (SVM) Regression Model.
4. Regression Tree Ensemble Model.
5. Neural Networks.
6. K-Nearest Neighbours Regression

5.3 Summary

The objective of this chapter was to propose a methodology for determining the feasibility of lifetime extension for wind turbine drivetrains, drawing on key practices from various industries and structuring them into a cohesive process.

The proposed methodology was developed based upon various factors, including:

1. Any recommendations mentioned within the standards.
2. Any processes that were common across various industries (e.g. data collection, system breakdown etc.).
3. The processes implemented in the oil and gas industry. The oil and gas industry has a lot of similarities with the wind industry, particularly their location.

Both are situated in harsh offshore environments, making access for repairs and maintenance more difficult and costly. They are also typically unmanned and whilst oil and gas platforms do not have large moving parts, such as blades, they do contain a variety of mechanical and electrical equipment (e.g. well-heads, pumps, compressors, separators, generators, hydraulic systems, bearings, cranes, switchgear, instrumentation, communication systems, etc.). Plus, their lifetime extension practices have been used for years, so are tried and tested.

Chapter 6

Selection of Critical Components

It was briefly mentioned at the end of Chapter 2, how beneficial it would be to be able to prioritise the drivetrain equipment, as well as the components within the drivetrain's equipment, that are more prone to failure.

One way to do this, is by calculating either the components' failure rates, historical performance or damage and then developing a vulnerability map, as shown in Figure 3.1. A vulnerability map outlines the layout of all sub-assemblies and/or components within a piece of equipment or assembly, indicating the varying levels of damage for each, ranging from low to high [1]. This vulnerability map can then be used during inspections to identify parts at risk of failure, such as in a lifetime extension evaluation.

In addition to assisting with lifetime extension evaluation, the added advantage of a vulnerability map is that the owner/operators can prepare more relevant maintenance plans and adequate spare parts.

Whilst vulnerability maps have been developed for the mechanical equipment located within the drivetrain, they have not yet been created for its electrical equipment.

Therefore, this chapter focuses on developing a vulnerability map specifically for a power converter.

6.1 Method

It is clear from the existing literature, that along with gearboxes and generators, power converters have one of the highest failure rates within the wind turbine drivetrain. Therefore, failure reports/maintenance logs regarding power converters have been obtained. The dataset has data for approximately seven hundred (700) mainly onshore wind turbines, located in various countries and this data will be used to produce a vulnerability map.

The first step is to establish the topology of the power converter. Due to the fact that specific details on the type and layout of the power converters are not available, the Reliawind taxonomy standardisation structure [2] and manufacturer diagrams (Figure 6.1) are used as a starting point.

The relevant components extracted from the “Detailed wind turbine taxonomy" are shown in Table 6.1.

After establishing the layout, the next step is to analyse the dataset. The data is first filtered to include only events caused by unexpected power converter component failures, reducing the list by 47%. From this reduced dataset, failed or malfunctioning components are sorted and grouped, excluding items like oil, cooling liquid, and other consumables, which account for 14% of the total. The number of failures per component are then calculated and ranked from highest to lowest.

Table 6.1: Power Converter Components Selected from “Detailed Wind Turbine Taxonomy" corresponding to Electrical Module a Sub-System of Wind Turbine System [2]

ASSEMBLY	SUB-ASSEMBLY	COMPONENT
Frequency Converter	Converter Auxiliaries	1 Control Board
	Converter Power Bus	2 Branching Unit
		3 Capacitor
		4 Contactor
		5 Generator Side Converter
		6 Generator Side Power Module
		7 Grid Side Converter
		8 Grid Side Power Module
		9 Inductor
		10 Load Switch
		11 Pre-Charge Unit
	Power Conditioning	12 Common Mode Filter
		13 Crowbar
		14 DC Chopper
		15 Generator Side Filter
		16 Line Filter Assembly
		17 Voltage Limiter Unit
Power Electrical System	Power Circuit	18 Cables
		19 Machine Contactor
		20 Machine Transformer
		21 MV Busbar/Isolator
		22 MV Switchgear
		23 Soft Start Electronics

The vulnerability map is then created by colouring the relevant components on the previously established layout, based on the failure rates calculated from the dataset. Since the dataset descriptions are highly specific (e.g., model, part number), assumptions are made about the locations of certain components. Components with the highest failure rates (over 25%) are marked in red, medium/high rates (15%-25%) in orange, low/medium rates (5%-15%) in yellow, and the lowest rates (0%-5%) in green. The map is presented in the following section.

The next analysis examines whether the vulnerability map varies based upon the wind turbine’s location.

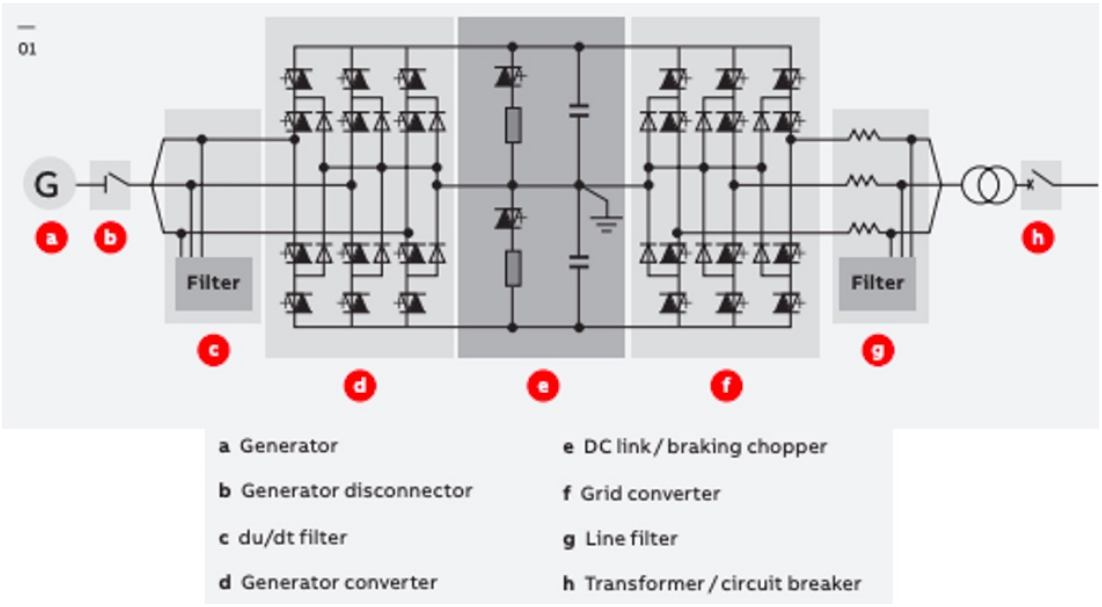

Figure 6.1: ABB's PCS6000 Power Converter Layout [3]

To achieve this, the original list of unexpected failures is sorted and grouped by location, before grouping the failed or malfunctioning components. Six out of the fifteen countries are analysed, chosen for having failures in multiple turbines across over more than ten different wind farms.

Next, the number of failures per component are calculated and ranked from highest to lowest. The results are then compared and analysed by location.

6.2 Results and Discussion

The power converter components that failed or malfunctioned are displayed in the bar chart in Figure 6.2.

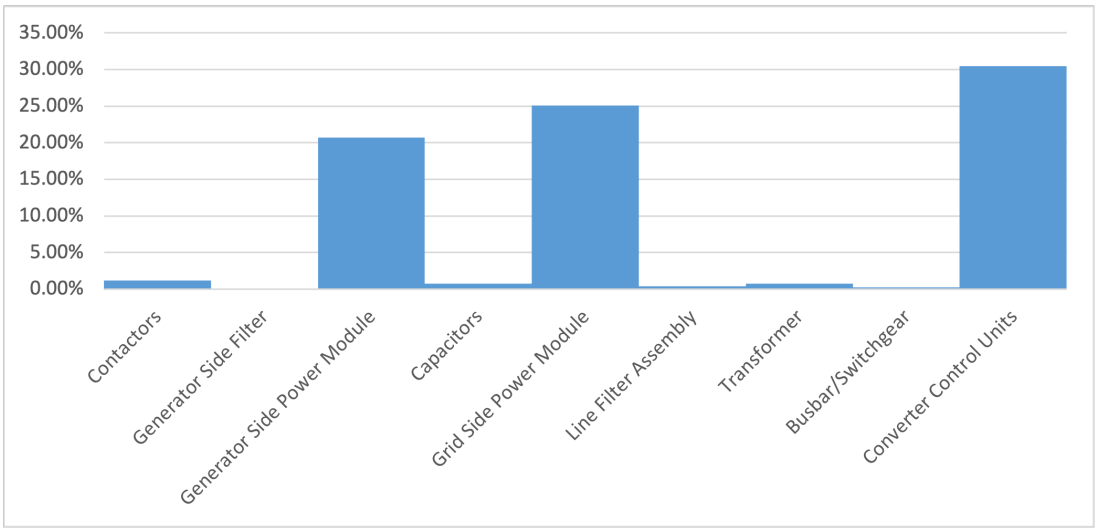

Figure 6.2: Chart Showing Power Converter Failure Rates For All The Data From All Locations

The chart clearly highlights three components with higher failure rates than the others. They are:

1. Converter Control Units (30%).
2. Grid-Side Power Module (25%).
3. Generator-Side Power Module (21%).

During the early design life of nearly four hundred (400) turbines, one hundred and eighty five (185) required converter control unit replacements. Grid-side power modules failed in ninety six (96) turbines and generator-side power modules failed in eighty three (83), with 45% and 43% respectively, of these turbines needing two or

more replacements. Additionally, forty eight (48) turbines had both grid and generator-side power modules replaced.

Data from Figure 6.2 is used to colour the components according to their failure rates. Figure 6.3 presents the vulnerability map created using data from all locations.

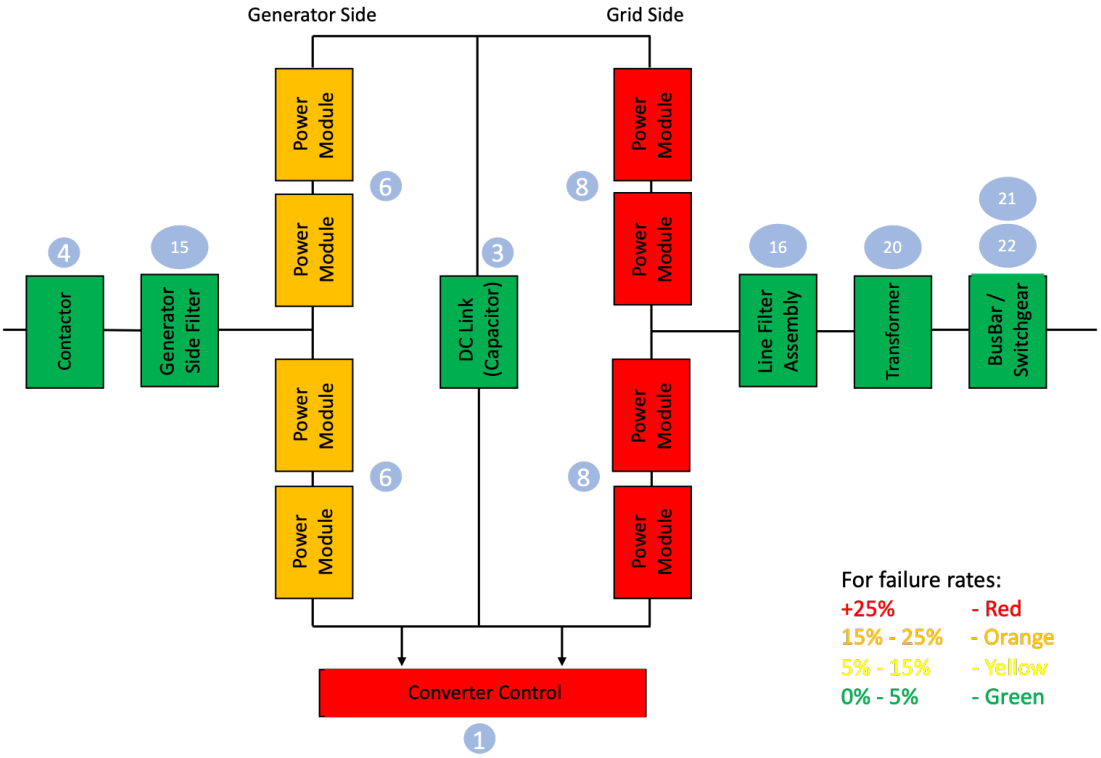

Figure 6.3: Vulnerability Map Built Based On All The Data From All The Locations (NOTE: Numbering refers to components listed in Table 6.1)

To address the question as to whether turbine location affects the vulnerability map, Table 6.2 lists six of the fifteen countries alphabetically and highlights the most frequently failed components in each location.

In all locations, the same three components had the highest failure rates: converter control units, generator-side power modules, and grid-side power modules. However, their ranking varied by location. The grid-side power modules failed most in France,

Table 6.2: Highest Power Converter Component Failures per Location

LOCATION	1st HIGHEST COMPONENT FAILURE	2nd HIGHEST COMPONENT FAILURE	3rd HIGHEST COMPONENT FAILURE
China	Converter Control Units (33.79%)	Generator Side Power Module (29.66%)	Grid Side Power Module (28.97%)
France	Grid Side Power Module (28.00%)	Generator Side Power Module (24.00%)	Converter Control Units (21.71%)
Germany	Converter Control Units (38.46%)	Grid Side Power Module (23.08%)	Generator Side Power Module (15.38%)
Italy	Grid Side Power Module (31.43%)	Generator Side Power Module (22.86%)	Converter Control Units (17.14%)
Poland	Grid Side Power Module (27.91%)	Converter Control Units (27.91%)	Generator Side Power Module (25.58%)
Sweden	Converter Control Units (41.57%)	Grid Side Power Module (18.67%)	Generator Side Power Module (6.63%)

Italy and Poland, while the converter control units had the highest failure rates in China, Germany, and Sweden.

In China and Poland, the failure rates of the top three components: converter control units, generator-side power modules and grid-side power modules, are similar. However, in Germany and Sweden, converter control units have a much higher failure rate than grid-side power modules, which rank second. In Sweden, there is also a significant gap between the failure rates of the second-place grid-side power modules and the third-place generator-side power modules.

Figures 6.4 - 6.9, show the vulnerability maps of the components in each of the six locations.

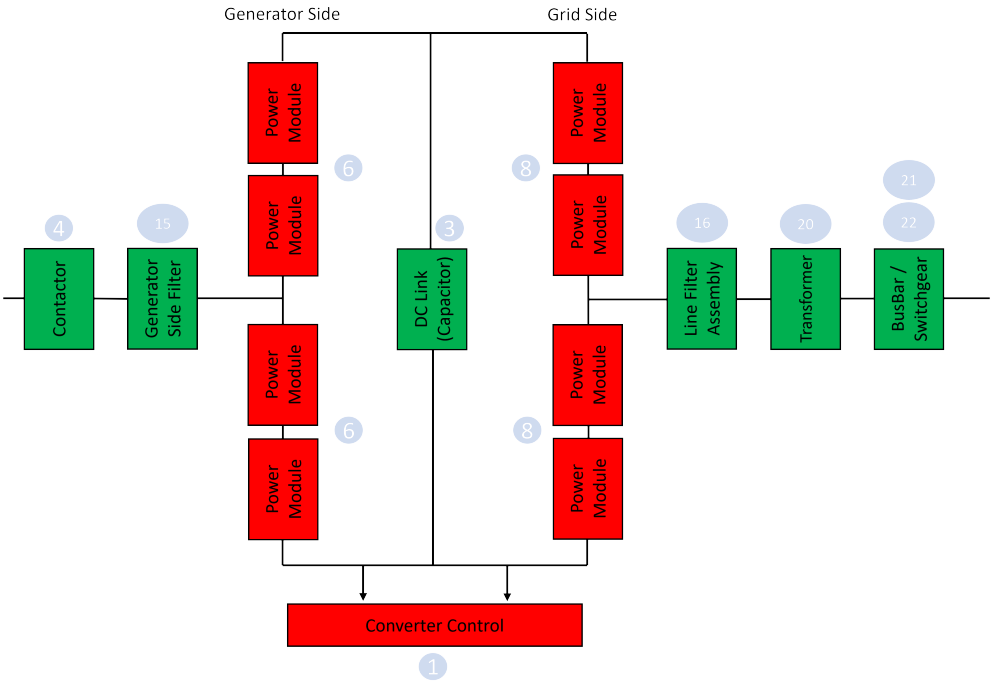

Figure 6.4: Power Converter Vulnerability Map for China

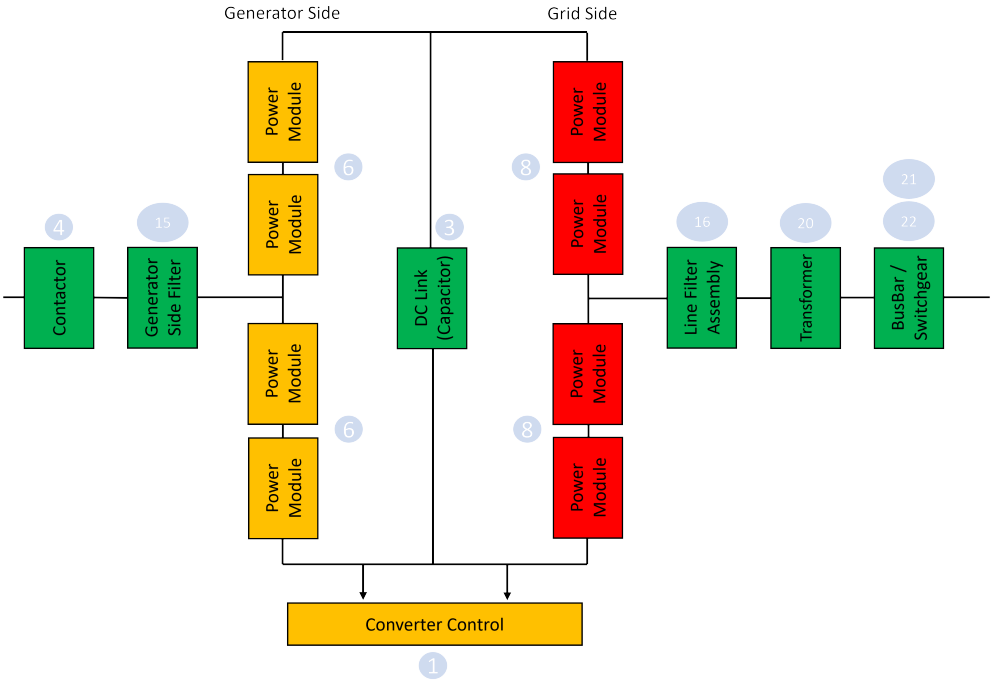

Figure 6.5: Power Converter Vulnerability Map for France

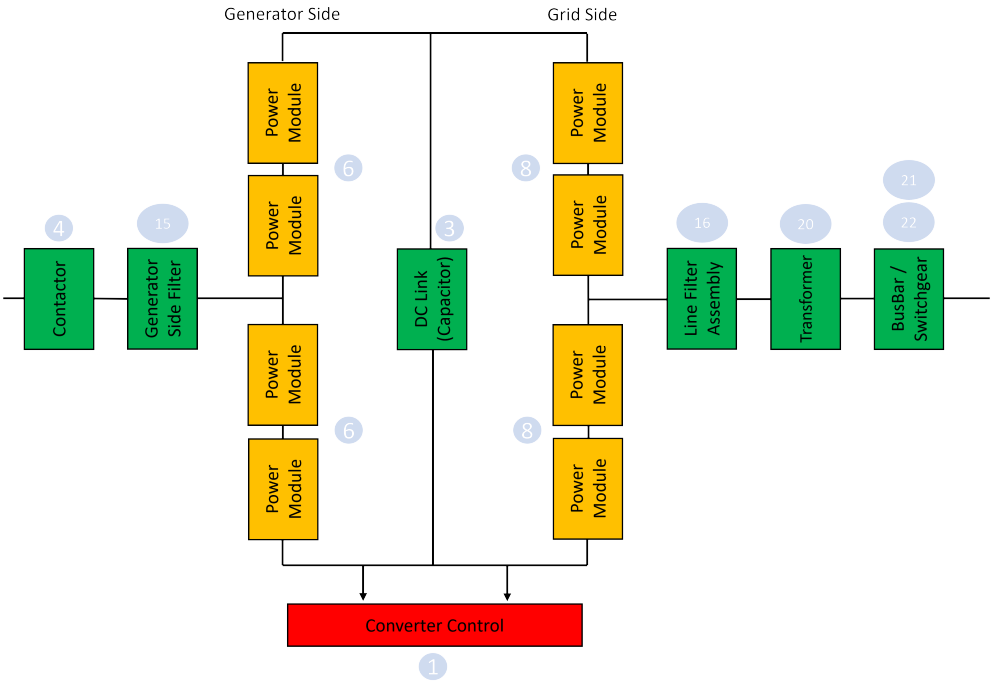

Figure 6.6: Power Converter Vulnerability Map for Germany

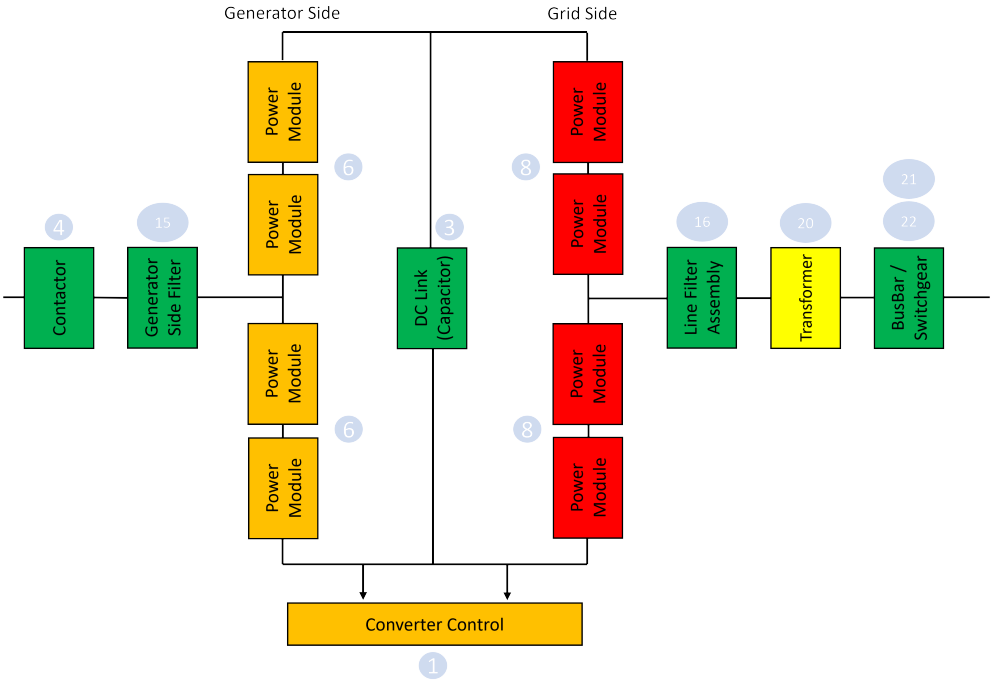

Figure 6.7: Power Converter Vulnerability Map for Italy

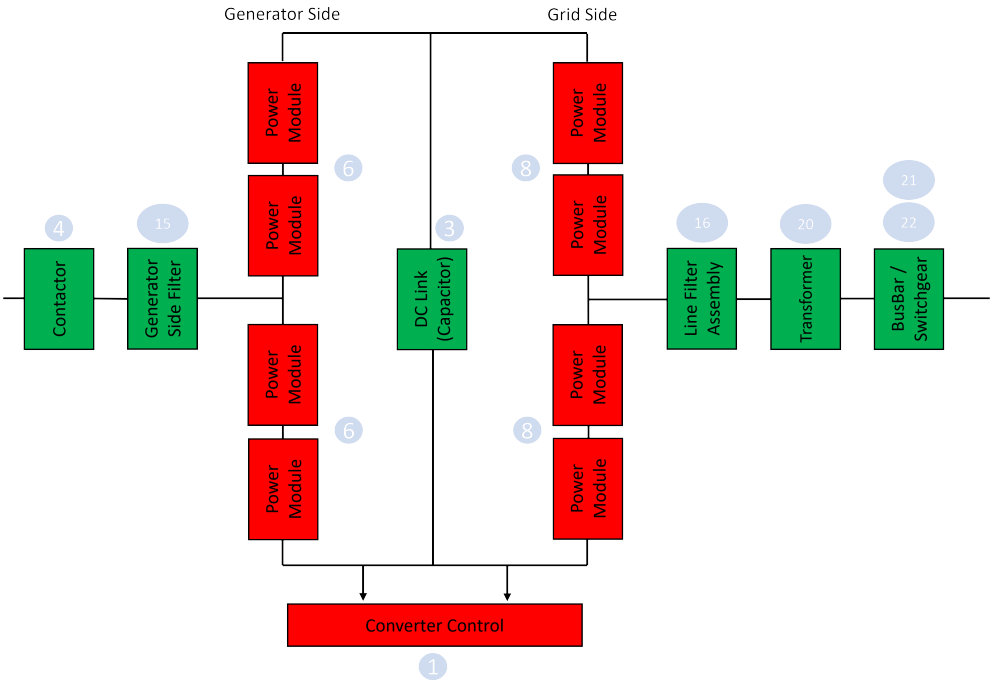

Figure 6.8: Power Converter Vulnerability Map for Poland

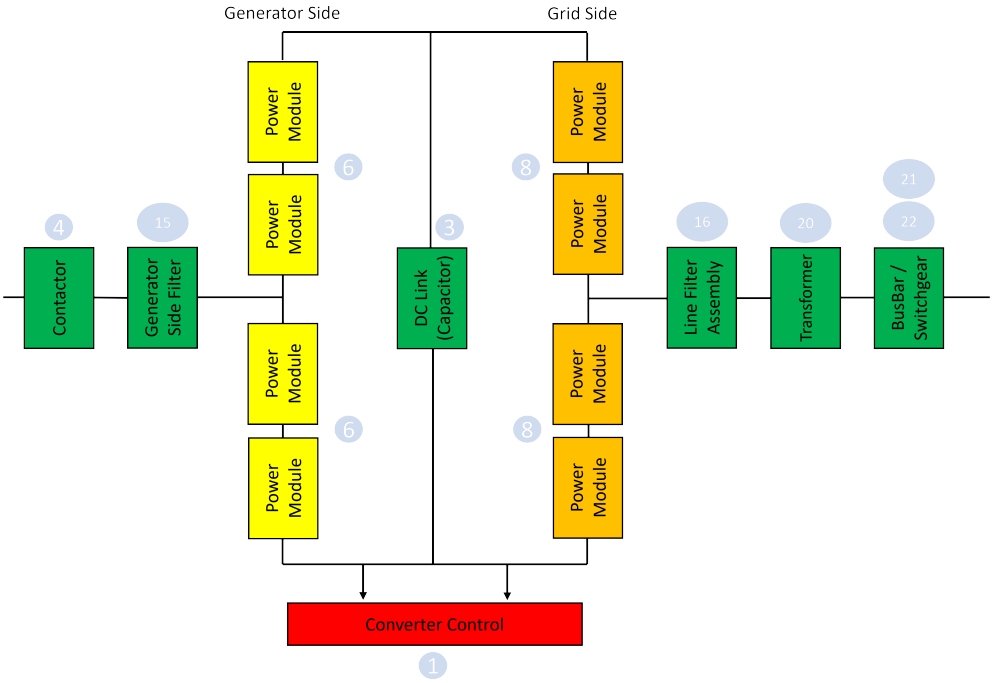

Figure 6.9: Power Converter Vulnerability Map for Sweden

6.3 Summary

This analysis was conducted for a single turbine type, so the vulnerability maps produced cannot be generalized for all turbines because different turbines may contain different types of power converters. However, the results align with multiple studies conducted by Fischer et al., confirming that power modules are among the most failure-prone components. In this study, three components — converter control units, grid-side power modules, and generator-side power modules — consistently had the highest failure rates, regardless of the wind farm location. The only variation was their ranking based upon their failure rates.

By creating a topology of the power converter and calculating the failure rates for each subsystem or component housed within the power converter, they can then be ranked from highest to lowest. Each subsystem or component is then assigned a colour: red for high, yellow for medium and green for low failure rates.

The vulnerability map is easy to interpret and provides sufficient information to clearly identify, which subsystems or components to focus on when determining lifetime extension, by helping to establish an efficient inspection and maintenance strategy.

In the context of lifetime extension assessment, the remaining useful life of these three components, would be critical in determining whether the power converter can continue to operate beyond it's designed service life.

6.4 References

[1] Amir Rasekhi Nejad, Zhen Gao, and Torgeir Moan. Fatigue reliability-based inspection and maintenance planning of gearbox components in wind turbine drivetrains. *Energy Procedia*, 53:248–257, 2014.

[2] Peter Tavner. *Offshore wind turbines: reliability, availability and maintenance*, volume 13. IET, 2012.

[3] ABB. Pcs 6000 for large wind turbines medium voltage, full power converters up to 9 mva. *ABB*, 2012,.

Chapter 7

Implementation of Method for Determining Lifetime Extension: Utilizing SCADA Data

A methodology for determining lifetime extension has been proposed in Chapter 5, so the next step is to implement this proposed method, using real-life data. Obtaining real-life wind turbine or wind farm data is challenging due to owner/operator confidentiality. However, Charlie Plumley and Cubico Sustainable Investments have released some wind farm supervisory control and data acquisition (SCADA) data, along with event status files, which can be used. Therefore, in this case study, “Stage 1 - Data Collection" (Figure 5.2), specifically refers to SCADA data, including temperature measurements and event reports/status logs/data logs.

Wind turbines are equipped with multiple sensors located throughout the turbine, recording data at regular intervals — typically every ten minutes, with some modern

turbines recording every second. SCADA data captures a range of critical parameters, including: wind speed, wind direction, power output and temperature. Temperature measurements may include: ambient, nacelle, main bearing, gearbox and generator temperatures, amongst others.

The work presented within this chapter aligns with “Stage 4 - Assessment" of the proposed methodology. Where it will be investigated whether, by using SCADA data, which is typically the minimum amount of data that is obtained from a wind turbine, useful results regarding determining a component’s end of life can still be obtained.

The primary objective of this chapter is to develop a method or process, that utilises a readily available machine learning model, combined with specific SCADA input parameters, to evaluate a component’s health. This approach aims to identify key indicators, that can help track the condition of components and provide early warnings when a component is approaching the end of it’s operational life. Ideally, these indicators can then be used to compare components across multiple turbines. The advantage of this approach is that it offers a comprehensive yet straightforward process, for determining a component’s end of life based on SCADA temperature data.

7.1 Method

The methods outlined in the following sections (7.1.1 and 7.1.2) fall within the Assessment Stage (Stage 4) depicted in Figure 5.1. They have been developed/proposed based upon the data available, with the aim of providing accurate and useful results regarding determining a component’s end of operational life.

7.1.1 Selecting a Suitable Model Predictor

This initial process is to identify a reliable and user-friendly predictive model. The method of determining a suitable model predictor is shown in a flowchart, in Figure 7.1.

Three models have been selected for evaluation of their suitability and they are:

1. Polynomial Regression Model.
2. Support Vector Machine (SVM) Model.
3. Regression Tree Ensemble Model.

The simplest regression model, which is the linear regression model, was deemed not to be suitable due to the fact that the correlation between power and temperature is not linear.

Labelled data is required for this process, meaning that “healthy" data is needed to identify a suitable model and optimal SCADA input parameters. “Healthy" data in this case is assumed to be all data recorded in 2016, which is when the wind farm began operating.

The first step, as outlined in Step 1 on the flowchart, is to filter the data. This includes: removing any missing data values and replacing any negative power values with the previous or nearest positive value.

Next, Step 2 involves subtracting the nacelle ambient temperature, T_{na}, from the selected component temperature, T_c, in order to normalize the component’s temperature values, T_{norm}, as per Equation 7.1.

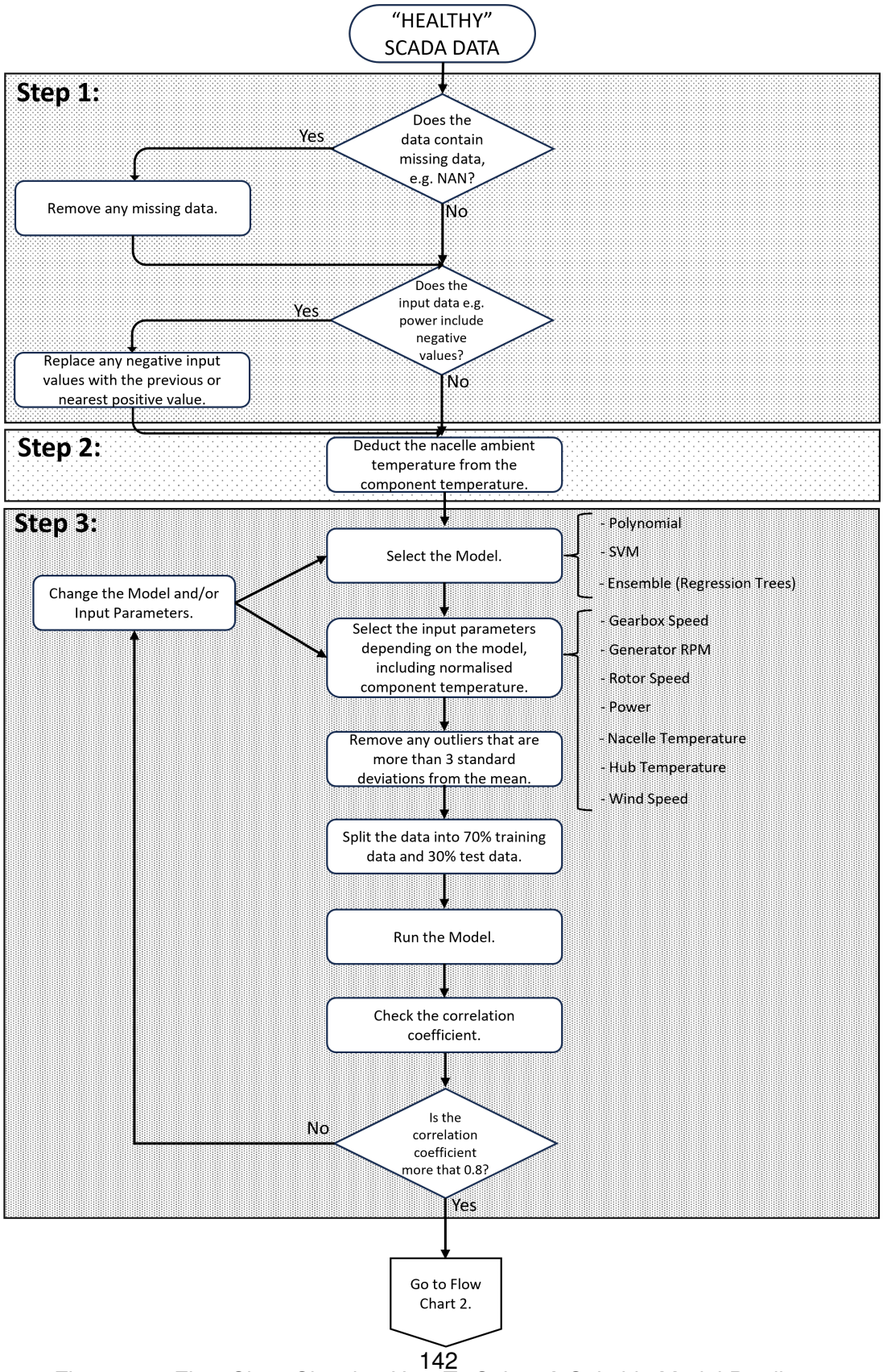

Figure 7.1: Flow Chart Showing How To Select A Suitable Model Predictor

$$T_{norm} = T_c - T_{na} \tag{7.1}$$

In Step 3, input parameters are selected based upon the chosen model. For instance, linear regression and polynomial regression models typically accept only one input parameter along with the component temperature values, whilst support vector machine models and regression tree ensemble models can handle multiple input parameters. After selecting the parameters, any data points that are found to exceed three standard deviations from the mean are removed, as part of the final filtering process. The “healthy" data is then randomly split into 70% training data and 30% test data.

The filtered data is then passed through the model, in order to generate predicted component temperatures as the output.

Based on the results/model output, the correlation coefficient between the actual and predicted temperature values are calculated. If the correlation coefficient is low, the process is repeated using different input parameters and/or models, until a satisfactory correlation coefficient is achieved. A correlation coefficient of 0.8, as shown in Step 3 of Figure 7.1, has been selected because values of 0.8 or higher are considered to indicate strong correlation, [1].

Graphs are also generated to visualize the correlation, including: temperature versus power, actual versus predicted temperature and temperature versus time.

Due to the large volume of data, daily mean values are calculated for each parameter, i.e. power, actual component temperature and predicted component temperature. These averaged values are then used to generate additional graphs to analyse the

correlation, to assess the suitability of the model.

The process is then repeated using the entire filtered “healthy" dataset, for both training and testing the model. The results are plotted to assess the model’s sensitivity.

As previously mentioned, the first model selected is the polynomial regression model to the eighth order. Power, along with the component temperature values from the training dataset, are used as the input parameters to train the model. Then power values from the test dataset are used to predict the component temperature values. This is then repeated using torque in place of power, which is calculated by dividing power by the rotor speed.

The support vector machine model is the next model investigated, chosen for its ability to accept multiple inputs. The same process is followed as described previously, first using power as the sole input parameter, followed by power and rotor speed as the input parameters.

Finally, the regression tree ensemble model is used, again chosen for its ability to accept multiple inputs. Initially, seven different parameters are selected alongside the component temperature, these include: power, rotor speed, generator RPM, gearbox speed, nacelle temperature, hub temperature and wind speed. Various combinations of these parameters are tested with the model, to identify which parameters give the best fit.

After completing the process of selecting a suitable model predictor, the next step is to apply the model to help identify components approaching the end of their operational life, which is described in Section 7.1.2.

7.1.2 Identifying Critical Components in the Drivetrain

Identifying critical components within the drivetrain which are prone to fail earlier, is essential. One approach is to analyse the failure data; however, if this data is not available, then vulnerability maps, like those developed by Nejad et al. [2], Nejad et al. [3], and as described in Chapter 6, may be utilised.

The proposed method for identifying components nearing the end of their life, is summarized in the flowchart shown in Figure 7.2.

The first step involves collecting all the SCADA data from the first turbine. The pre-processing of the data, as outlined in Section 7.1.1 and as shown in Steps 1 and 2 in the flowchart (Figure 7.2), is applied to both the training and test datasets. In this method, the training dataset consists of all of the “healthy" data, which is typically from the turbine’s first year of operation, while the test dataset includes all data from a subsequent year. The pre-processing for both the training and test datasets includes: removing any missing data, replacing any negative power values with either the previous or the nearest positive value and subtracting the nacelle ambient temperature from the component temperature to normalize the temperature values. Additionally, for the training dataset, any outliers beyond three standard deviations from the mean are removed.

After pre-processing the SCADA data, the selected input parameters are then passed into the model (Step 3). As determined in Section 7.1.1, the regression tree ensemble model, using three input parameters from the SCADA data — power, rotor speed and nacelle temperature — along with the component temperature, have been

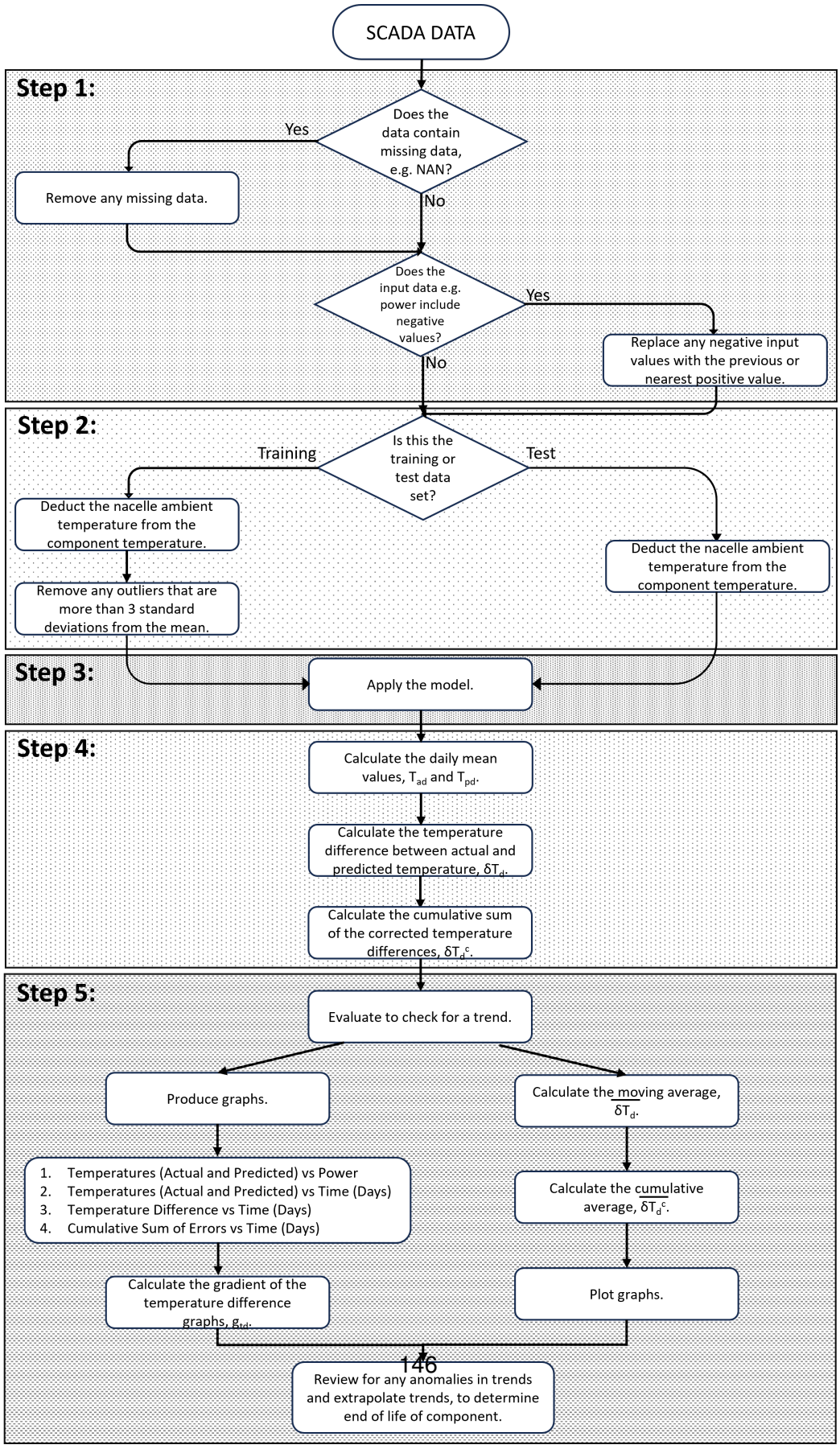

Figure 7.2: Flow Chart Showing Method Used for Identifying Critical Components in the Drivetrain (Flow Chart 2)

identified as being the most effective predictor.

Based on the results, the daily mean values of power, actual component temperature, T_{ad_j} and predicted component temperature, T_{pd_j}, for each day, j, are calculated from the instantaneous values of actual and predicted temperature, T_{a_i} and T_{p_i}, respectively, as shown in Equations 7.2 and 7.3 (Step 4). In this case, n represents the number of ten minute intervals per day (i.e. 6 intervals per hour, 24 hours per day, therefore n = 6x24=144).

$$T_{ad_j} = \frac{\sum_{i=x}^{x+(n-1)} T_{a_i}}{n} \tag{7.2}$$

$$T_{pd_j} = \frac{\sum_{i=x}^{x+(n-1)} T_{p_i}}{n} \tag{7.3}$$

The daily temperature difference, δT_{d_j}, is then calculated as shown in Equation 7.4.

$$\delta T_{d_j} = T_{ad_j} - T_{pd_j} \tag{7.4}$$

After determining the temperature difference, the cumulative sum of the temperature differences, $\delta T^c_{d_M}$, is calculated using Equation 7.5, where M represents the corresponding time, in this case, the day. Calculating the cumulative sum of the temperature differences between the actual and predicted temperatures, provides a simple yet effective method for identifying anomalies or shifts in trends, which may warrant further investigation.

$$\delta T^{c}_{d_M} = \sum_{j=1}^{M} \delta T_{d_j} \tag{7.5}$$

An effective evaluation method involves plotting various graphs using both the temperature difference and cumulative sum values, against the time in days. These graphs are then analysed for any anomalies and/or trends, which could assist in identifying the end of life of the component (Step 5).

The subsequent analysis involves calculating the gradient of the temperature difference, g_{td}, graphs, for all turbines, to assess whether the gradient increases as the component approaches failure.

$$g_{td} = \frac{(\delta T_{d_j+1} - \delta T_{d_j})}{(t_{j+1} - t_j)} \tag{7.6}$$

Initially, the gradient over each day is determined, i.e. $t_{j+1} - t_j = 1$, as shown in Equation 7.6, then the average over five, ten and thirty days are calculated.

The moving average method, is an approach which can be used to identify short-term trends/changes. Therefore, the moving average of the temperature differences, $\overline{\delta T_{d_M}}$, are calculated as shown in Equation 7.7, where x is the size of the window, which in this case is 3.

$$\overline{\delta T_{d_M}} = \frac{\sum_{i=M}^{M+x-1} \delta T_{d_j}}{x} \tag{7.7}$$

Another approach used for identifying trends, typically long-term trends/changes, is the cumulative average method, [4]. This is a straightforward and robust method, which smooths out short-term fluctuations. Therefore, this is the final analysis to be

carried out, where the cumulative average, $\overline{\delta T^c_{d_M}}$, is calculated by dividing the cumulative sum on any given day, $\delta T^c_{d_M}$, by the number of days up to that point, t_M, as shown in Equation 7.8.

$$\overline{\delta T^c_{d_M}} = \frac{\delta T^c_{d_M}}{t_M} \tag{7.8}$$

It is to be noted that the cumulative sum is reset following a repair. This analysis aims to determine whether a threshold value can be identified, indicating that if any turbine exceeds this threshold, then a drivetrain component may be nearing the end of its operational life. This could potentially be defined as the average accumulation of temperature difference.

This model/process is then repeated for all subsequent years, using each new year as the test dataset, while maintaining the "healthy" year as the training dataset. The same procedure is also repeated for all the remaining turbines.

7.1.3 Case Study

7.1.3.1 Data Set

The Kelmarsh wind farm is located in Northamptonshire and consists of six (6) onshore 2.05MW Senvion MM92 wind turbines, as shown in Figure 7.3. SCADA data and event reports/status logs/data logs were collected over a seven (7) year period, from 2016 to the end of 2022.

The event reports/status logs/data logs indicate two faults occurred within the generator in 2022, one in Turbine 2 and one in Turbine 4. Identifying the occurrence and

Figure 7.3: Location of Kelmarsh Wind Farm

location of these faults is crucial for evaluating the proposed life extension approach.

7.1.3.2 Implementation

The methods described in Sections 7.1.1 and 7.1.2, are implemented using the dataset described in Section 7.1.3. The SCADA data from the year 2016 is used as the training dataset and the test dataset are each of the subsequent years, i.e. 2017 - 2022.

Initially, the method/model is run on each component, including the generator rear bearing, generator front bearing, front bearing, rear bearing and gear oil inlet, for each year and each turbine. This is to see if any one component is following a different trend, which may indicate that it may be approaching it's end of life.

Due to the fact that the event reports/status logs/data logs record failures in the generator non-drive end (NDE) bearing, it would be expected for the generator rear bearing to follow a different trend to the rest.

7.2 Results

All the results obtained by applying the dataset from Section 7.1.3 using the methods outlined in Sections 7.1.1 and 7.1.2, are displayed in this Section.

7.2.1 Selecting a Suitable Model Predictor

All the results within this sub-section are produced when using the entire 2016 dataset from one turbine, for both training and testing the model.

The first model that was investigated was the polynomial regression model. Figures 7.4 and 7.5 show the fit/correlation. Figure 7.4 shows the actual and predicted temperatures against power, which was the input parameter and Figure 7.5 displays the actual temperature against the predicted temperature. These graphs show that the correlation is not ideal for this situation.

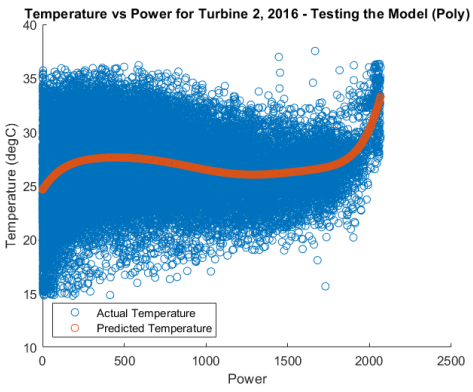

Figure 7.4: Testing the Model - Temperature vs. Power - Polynomial

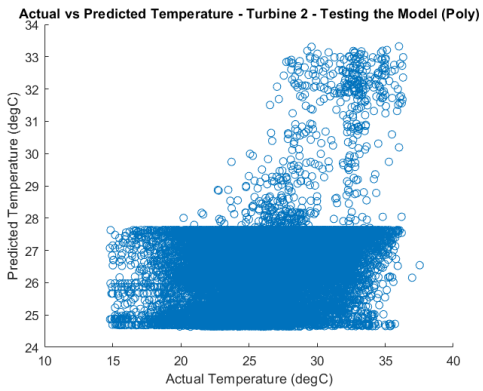

Figure 7.5: Testing the Model - Comparing the Actual vs Predicted Temperature - Polynomial

The next model implemented was the support vector machine (SVM) model. Figures 7.6 - 7.8 illustrate the degree of correlation. Figures 7.6 and 7.7 show the rela-

tionship between the actual and predicted temperatures against both power and rotor speed, respectively, whereas Figure 7.8 displays the actual temperature against predicted temperature.

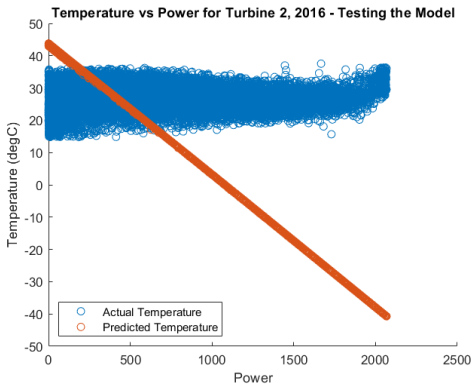

Figure 7.6: Testing the Model - Temperature vs. Power - SVM

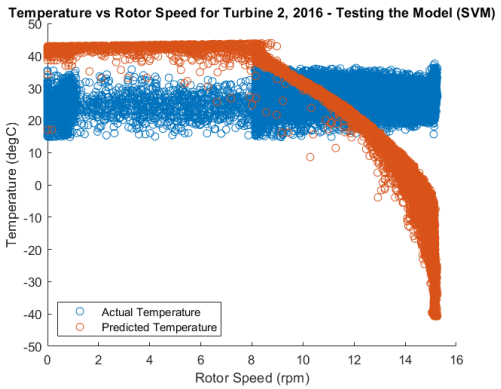

Figure 7.7: Testing the Model - Temperature vs. Rotor Speed - SVM

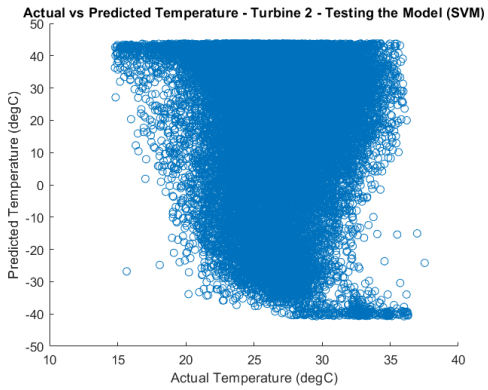

Figure 7.8: Testing the Model - Comparing the Actual vs Predicted Temperature - SVM

These graphs show that this model does not provide a good fit or correlation, so similar to the first model, this model is not a good predictor in this case.

The final model explored is the regression tree ensemble model. Figures 7.9 - 7.13, demonstrate the fit or correlation of the applied regression tree ensemble model. Figure 7.9 shows both the actual and predicted temperatures against power, which is one of the input parameters used. Figure 7.10 illustrates both the actual and predicted temperatures against rotor speed and Figure 7.11 displays the temperatures against the nacelle temperature, which are the other two input parameters. Figure 7.12 presents the actual temperature against the predicted temperature and Figure 7.13 shows both the actual and predicted temperatures per day. All graphs show a good correlation.

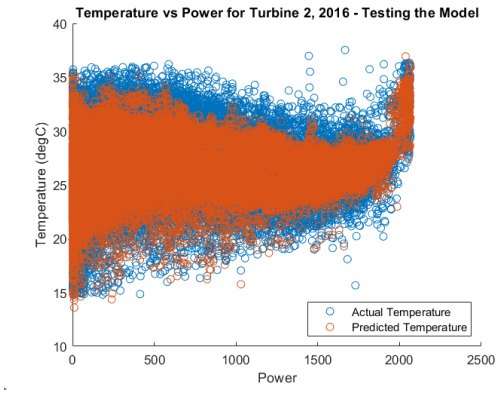

Figure 7.9: Testing the Model - Temperature vs. Power

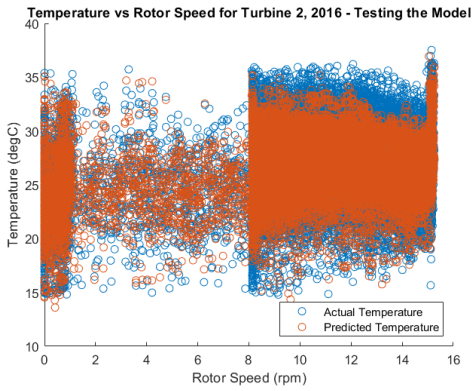

Figure 7.10: Testing the Model - Temperature vs. Rotor Speed

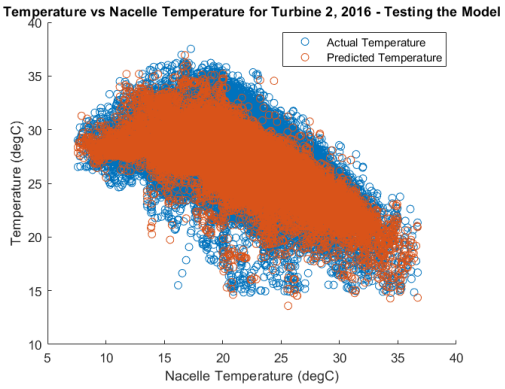

Figure 7.11: Testing the Model - Temperature vs. Nacelle Temperature

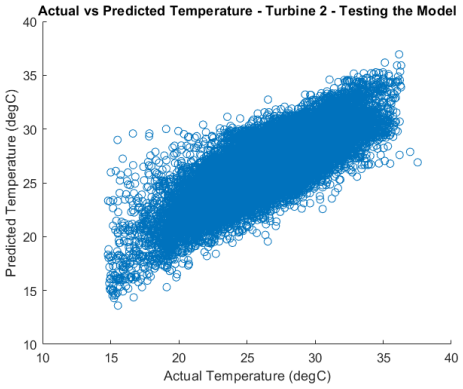

Figure 7.12: Testing the Model - Actual vs Predicted Temperature

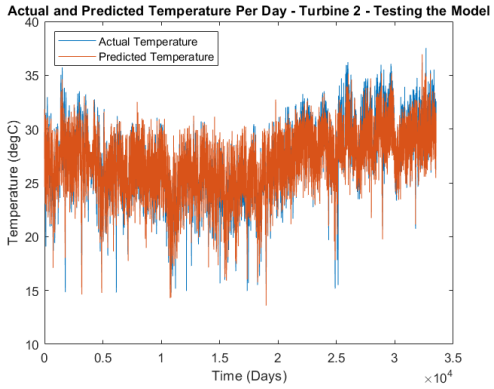

Figure 7.13: Testing the Model - Comparing the Actual vs Predicted Temperature

Based upon these graphs the regression tree ensemble model, using three input parameters: power, rotor speed and nacelle temperature has been selected as a suitable model predictor.

7.2.2 Identifying Critical Components in the Drivetrain

As outlined earlier, the method described in Section 7.1.2 has been applied to a dataset comprising of six wind turbines over a seven-year period. The results of this analysis are discussed below.

Section 7.1.3 discussed implementing the method on a variety of components within the drivetrain, including: the rear generator bearing, front generator bearing, front bearing, rear bearing and gear oil inlet within each turbine and Figures 7.14 - 7.25 show the results for all turbines. Figures 7.14, 7.16, 7.18, 7.20, 7.22 and 7.24 show the temperature differences of the various components in each turbine, while Figures 7.15, 7.17, 7.19, 7.21, 7.23 and 7.25 show the cumulative sum of the temperature differences of the various components in each turbine.

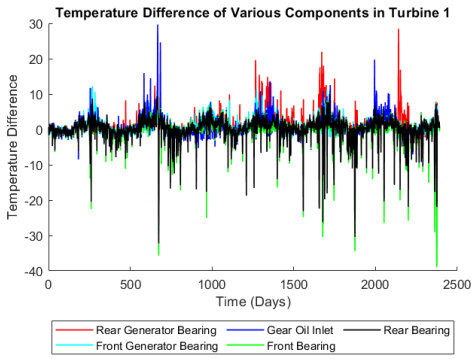

Figure 7.14: Temperature Differences for Various Components in Turbine 1

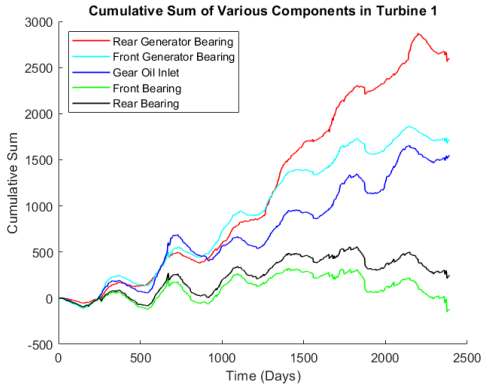

Figure 7.15: Cumulative Sum of the Temperature Differences for Various Components in Turbine 1

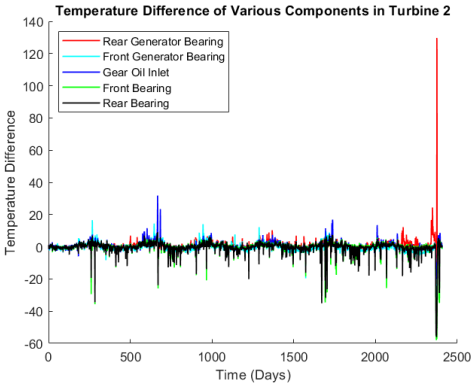

Figure 7.16: Temperature Differences for Various Components in Turbine 2

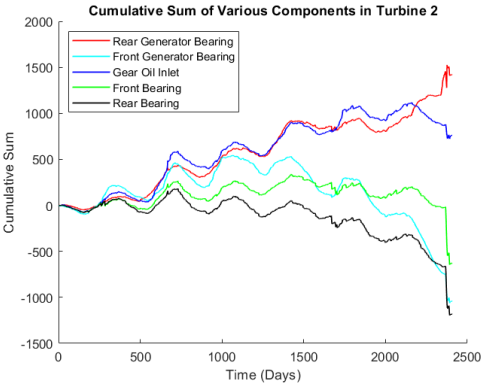

Figure 7.17: Cumulative Sum of the Temperature Differences for Various Components in Turbine 2

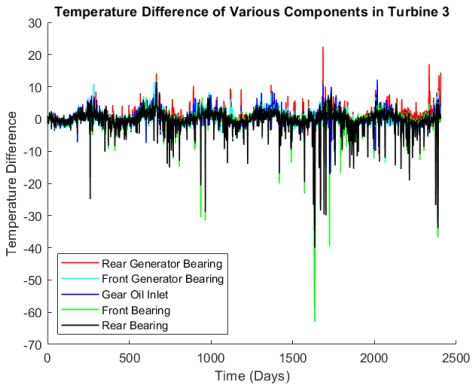

Figure 7.18: Temperature Differences for Various Components in Turbine 3

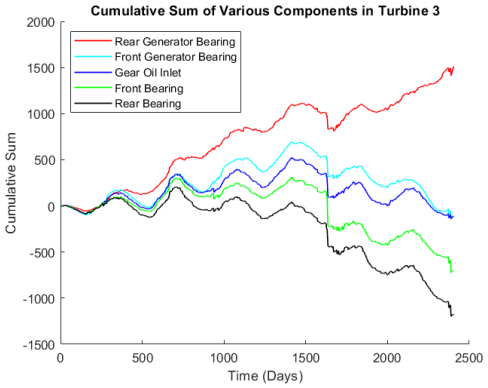

Figure 7.19: Cumulative Sum of the Temperature Differences for Various Components in Turbine 3

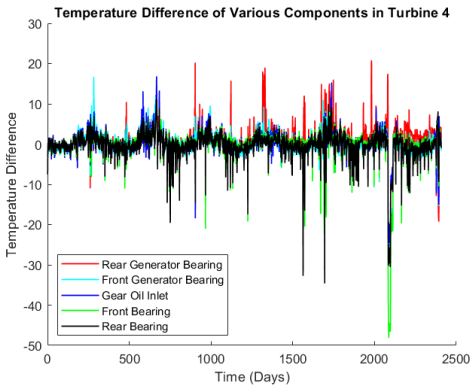

Figure 7.20: Temperature Differences for Various Components in Turbine 4

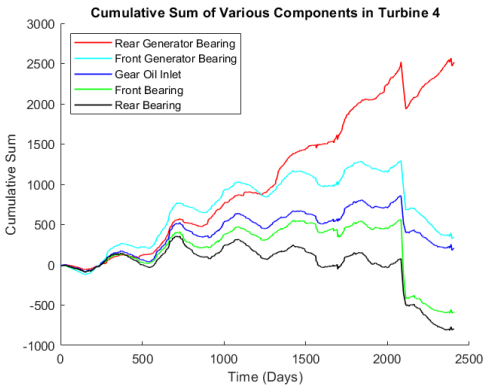

Figure 7.21: Cumulative Sum of the Temperature Differences for Various Components in Turbine 4

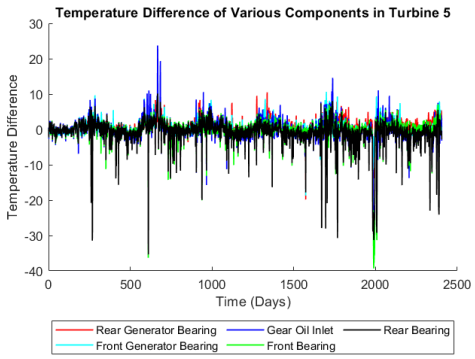

Figure 7.22: Temperature Differences for Various Components in Turbine 5

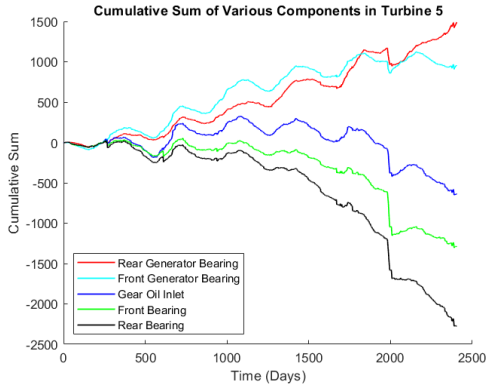

Figure 7.23: Cumulative Sum of the Temperature Differences for Various Components in Turbine 5

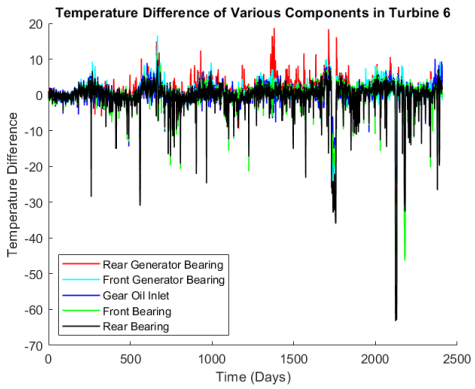

Figure 7.24: Temperature Differences for Various Components in Turbine 6

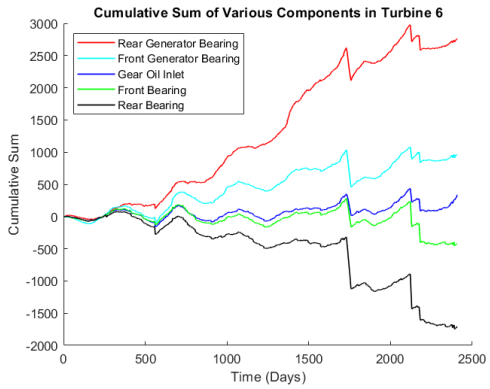

Figure 7.25: Cumulative Sum of the Temperature Differences for Various Components in Turbine 6

All the cumulative sum graphs show that the rear generator bearing appears to follow a different trend to the other components, which corresponds well with the event reports/status logs/data logs indicating failure of these components later on. Therefore, the rear generator bearing has been determined to be the weakest component, so will be investigated further.

Tables 7.1 and 7.2 represent a summary of the scheduled maintenance for each

turbine over the last three years and a summary of the forced outage for each turbine over the last three years, respectively. This data was extracted from the event reports/status logs/data logs included with the turbine data files. The tables display the total downtime hours per turbine over the year, the maximum downtime for a single event and the corresponding month, for instances where the total number of downtime hours exceeded fifty hours.

Table 7.1: Summary of the Scheduled Downtime for each Turbine

	2020 - Downtime Hours		2021 - Downtime Hours		2022 - Downtime Hours	
Turbine	Total	Max	Total	Max	Total	Max
1	30		29		101	25 (June)
2	62	49 (Dec)	26		218	165 (Nov)
3	20		122	77 (Nov)	40	
4	21		36		710	673 (Feb-Mar)
5	14		309	260 (Nov)	58	27 (Oct)
6	23		642	600 (Feb-Mar)	32	

Table 7.2: Summary of the Forced Outage for each Turbine

	2020 - Downtime Hours		2021 - Downtime Hours		2022 - Downtime Hours	
Turbine	Total	Max	Total	Max	Total	Max
1	57	28 (Mar)	118	92 (July)	31	
2	41		3		66	48 (Nov)
3	76	51 (Oct)	21		3	
4	72	48 (Aug)	12		61	60 (Feb)
5	30		300	240 (Nov)	32	
6	45		118	77 (Feb)	605	221 (Mar)

With regards to the rear generator bearing, the graphs shown in Figures 7.26 and 7.27, present both the temperature difference and cumulative sum of the temperature difference respectively, for all six turbines between the years 2016 and 2022.

Figure 7.26 illustrates that the largest temperature differences were observed in

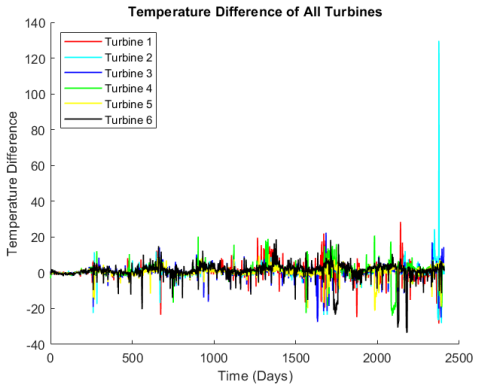

Figure 7.26: Temperature Differences for All Turbines Over All Years

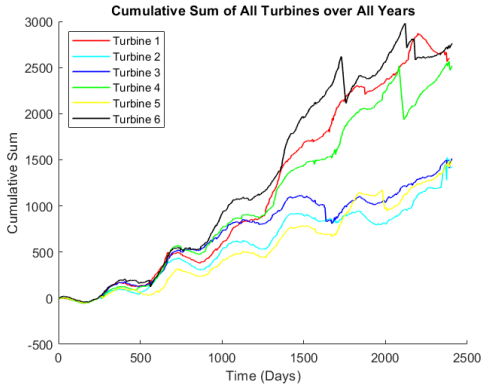

Figure 7.27: Cumulative Sum of the Temperature Differences for All Turbines Over All Years

Turbines 1 (red), 2 (cyan), 4 (green) and 6 (black). The status reports confirm that in 2022, the generator NDE bearing failed in Turbines 2 and 4, so it is expected that the actual component temperature would be higher than the predicted temperature in these turbines. Figure 7.27 shows that the six turbines appear to form two distinct groups, the first group consists of Turbines 1, 4 and 6 and the second group consists of Turbines 2, 3 and 5. The first group has a much higher cumulative sum than the second group and they appear to split into the separate groups around day 1000, which corresponds to the first quarter of 2019. Turbines 1 and 6 follow a similar pattern to Turbine 4, which had a generator NDE bearing failure, indicating that these two turbines also had possible issues, which will be discussed further.

The results for each turbine are now plotted separately to identify any additional trends.

The graphs in Figures 7.28, 7.30, 7.32, 7.34, 7.36 and 7.38 show the cumulative sum of the temperature difference between the actual and predicted rear generator bearing temperature values for all turbines, starting from zero at the start of every year,

whereas Figures 7.29, 7.31, 7.33, 7.35, 7.37 and 7.39 show the cumulative sum of the difference in actual and predicted temperatures, that are a continuation from the previous year. Both graph styles are presented to demonstrate that, regardless of the amount of data available — whether it spans only a few years and starts from zero, or covers many years allowing for a continuous plot — anomalies or trends can still be identified.

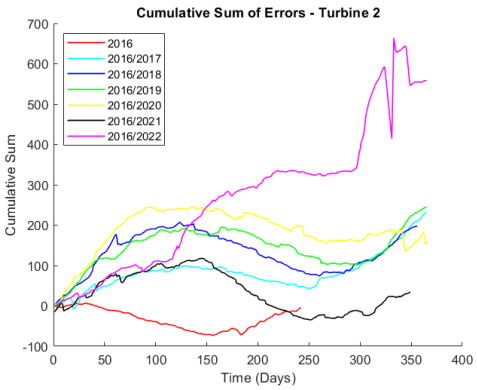

Figure 7.28: Turbine 2 - Cumulative Sum of the Temperature Differences

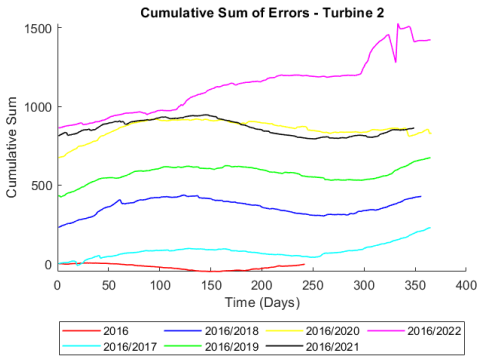

Figure 7.29: Turbine 2 - Cumulative Sum of the Temperature Differences Continuing from Previous Year

Starting with Turbine 2, where a generator NDE bearing failure is known to have occurred, both Figures 7.28 and 7.29, clearly show a noticeable change in trend in 2022. While this was not as apparent in Figure 7.27, a significant change in temperature is observed in Figure 7.26 towards the end of 2022. According to Table 7.1, the scheduled downtime occurred in the second half of November 2022, aligning with the observations in the graphs. The trend appears to initially shift around day 120 in the year 2022, which is roughly 200 days before the failure occurred, followed by another change around day 300.

The next turbine which also experienced a generator NDE bearing failure is Turbine

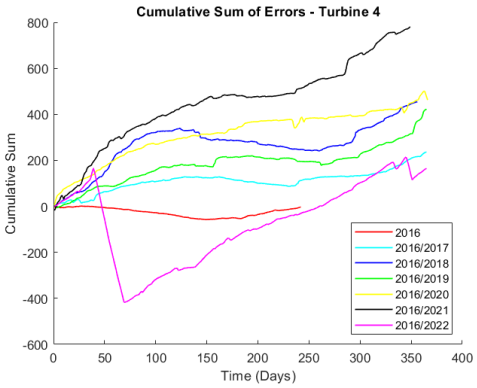

Figure 7.30: Turbine 4 - Cumulative Sum of the Temperature Differences

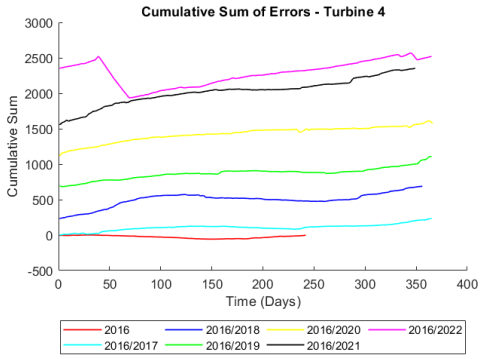

Figure 7.31: Turbine 4 - Cumulative Sum of the Temperature Differences Continuing from Previous Year

4. There is a distinct upward trend for Turbine 4 in year 2021 (Figure 7.30). The cumulative sum for this year is noticeably different and higher than in the other years, with the trend continuing to rise into early 2022 (Figure 7.31), aligning with the timing of the failure and as recorded in the event reports/status logs/data logs. Table 7.1 shows that the downtime occurred in February 2022, with the bearing replacement taking place in March 2022.

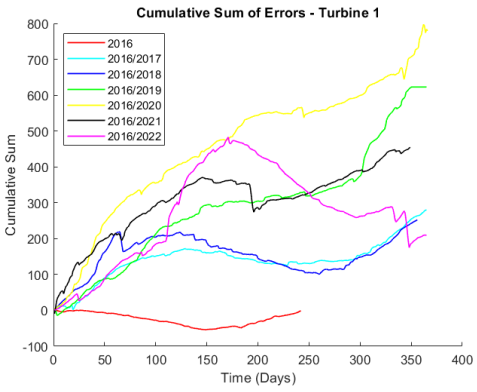

Figure 7.32: Turbine 1 - Cumulative Sum of the Temperature Differences

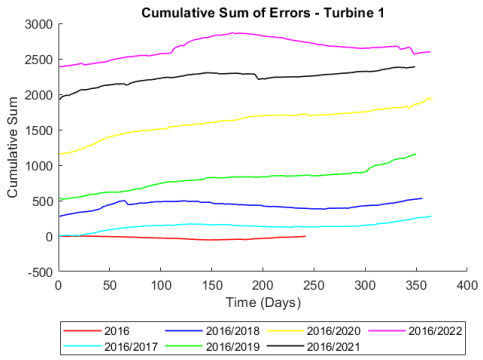

Figure 7.33: Turbine 1 - Cumulative Sum of the Temperature Differences Continuing from Previous Year

Figures 7.32 and 7.33 illustrate the results for Turbine 1, which shows a trend

comparable to Turbine 4 in Figure 7.27, where a bearing failure was confirmed. The abnormal higher operating temperatures of the rear generator bearing in this turbine, begins to emerge towards the end of 2019 (Figure 7.32). This becomes more pronounced in 2020 (Figure 7.32), as indicated by the steep increase in cumulative sum in the same figure. This rise in operating temperature continues in year 2021, which is more obvious in Figure 7.33, with the cumulative sum continuing to climb beyond the previous year's levels. This is followed by a sharp rise in year 2022, starting around day 120, marking a significant shift in the trend, ultimately leading to the scheduled downtime as reported in the event reports/status logs/data logs. According to the event reports/status logs/data logs, Turbine 1 underwent scheduled downtime in June 2022 for the proactive replacement of the NDE bearing. This is the same bearing that failed in Turbines 2 and 4.

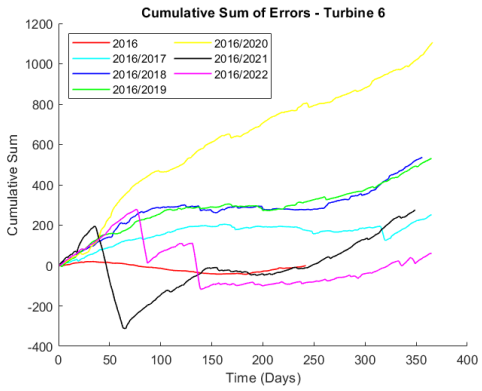

Figure 7.34: Turbine 6 - Cumulative Sum of the Temperature Differences

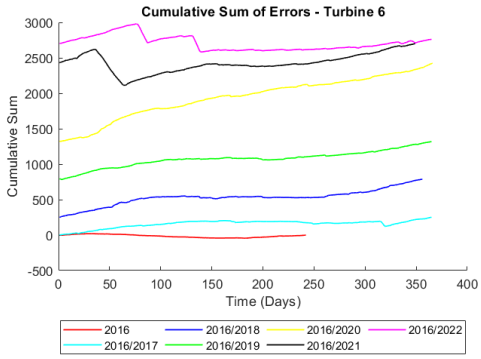

Figure 7.35: Turbine 6 - Cumulative Sum of the Temperature Differences Continuing from Previous Year

The other turbine which exhibits a similar trend to Turbines 1 and 4, is Turbine 6. Figures 7.34 and 7.35 show noticeable anomalies occurring at the beginning of 2021 and 2022. According to Table 7.1, 600 hours of scheduled maintenance took place

in February and March 2021, after which the temperature difference decreased once the turbine was operational again. Additionally, Table 7.2 shows 221 hours of forced outage in March 2022, due to a pitch motor failure and a pitch fault.

Figure 7.27 reveals that the remaining two (2) turbines, Turbine 3 and 5, exhibit a similar trend to Turbine 2. A closer examination, as shown in Figures 7.36 - 7.39 highlights some anomalies in both turbines.

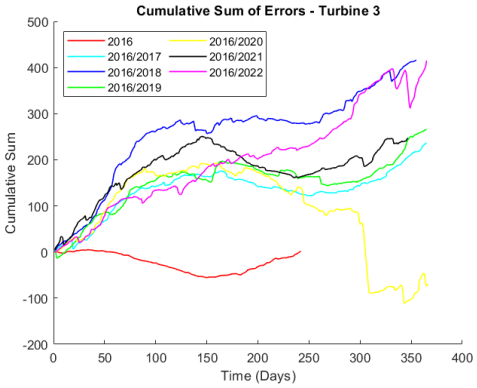

Figure 7.36: Turbine 3 - Cumulative Sum of the Temperature Differences

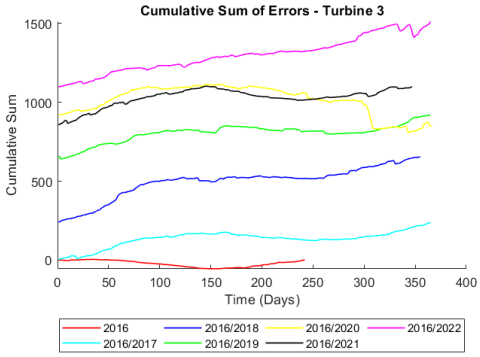

Figure 7.37: Turbine 3 - Cumulative Sum of the Temperature Differences Continuing from Previous Year

Turbine 3 displays an anomaly towards the end of 2020, with decreasing cumulative sum trend (colder temperatures). The cumulative sum trends across the years appear relatively consistent in Figures 7.36 and 7.37. Aligned with this observation, no failures were reported for this turbine.

Regarding Turbine 5, while some anomalies emerge in 2021 characterized by a rising trend, the cumulative sum values are relatively insignificant when comparing Figure 7.39 with Figure 7.35.

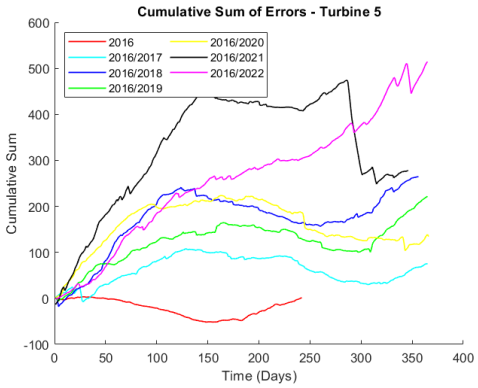

Figure 7.38: Turbine 5 - Cumulative Sum of the Temperature Differences

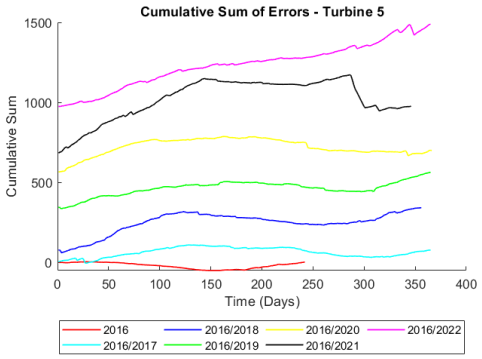

Figure 7.39: Turbine 5 - Cumulative Sum of the Temperature Differences Continuing from Previous Year

Figures 7.40 - 7.45, show plots of the annual cumulative sum values, reset to zero and continued, across six separate figures, for years 2020, 2021 and 2022, respectively. Each figure corresponds to a single year but includes data for all turbines. These comparisons illustrate that turbines with higher cumulative sum values of temperature, are more susceptible to failure.

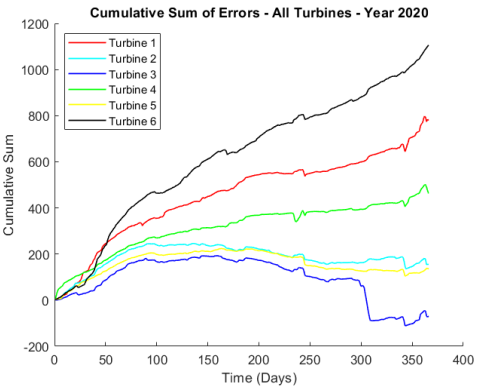

Figure 7.40: All Turbines - Cumulative Sum of the Temperature Differences for Year 2020

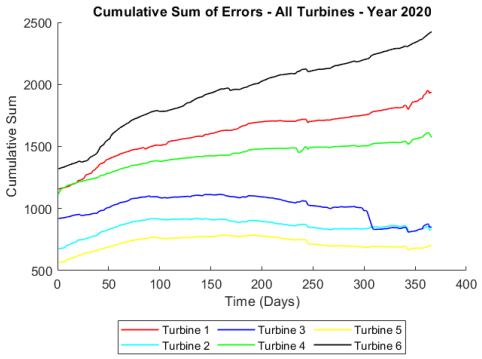

Figure 7.41: All Turbines - Cumulative Sum of the Temperature Differences Continuing from Previous Year for Year 2020

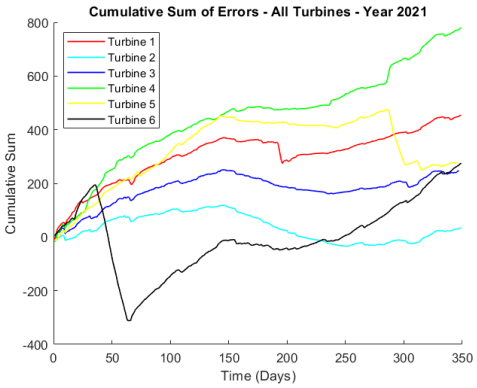

Figure 7.42: All Turbines - Cumulative Sum of the Temperature Differences for Year 2021

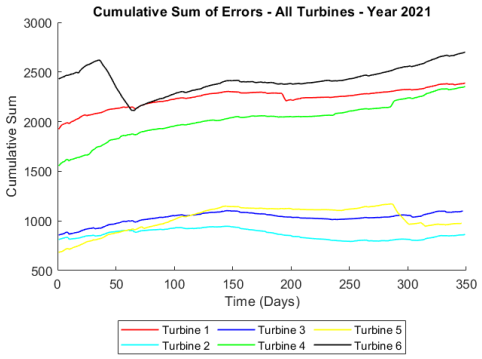

Figure 7.43: All Turbines - Cumulative Sum of the Temperature Differences Continuing from Previous Year for Year 2021

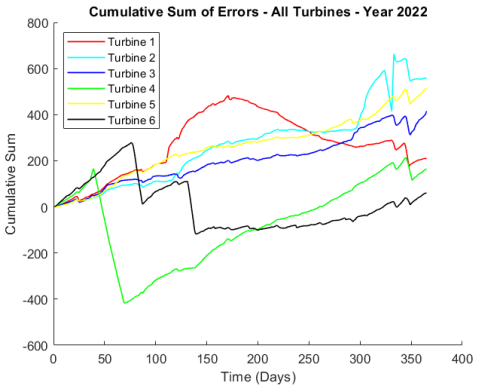

Figure 7.44: All Turbines - Cumulative Sum of the Temperature Differences for Year 2022

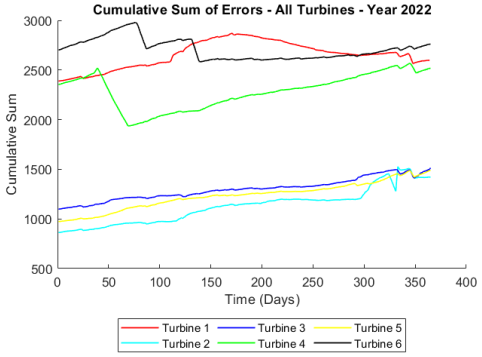

Figure 7.45: All Turbines - Cumulative Sum of the Temperature Differences Continuing from Previous Year for Year 2022

An additional analysis involves calculating the gradient of the temperature difference for all turbines, as shown in Figures 7.26 and 7.27. This analysis aims to determine if the gradient increases the closer you get to the failure.

Figure 7.46 displays the gradient calculated over a single day, while Figure 7.47 uses the gradient value calculated per day, to average the value over thirty days. The graphs indicate that averaging over thirty days smooths out the temperature trends.

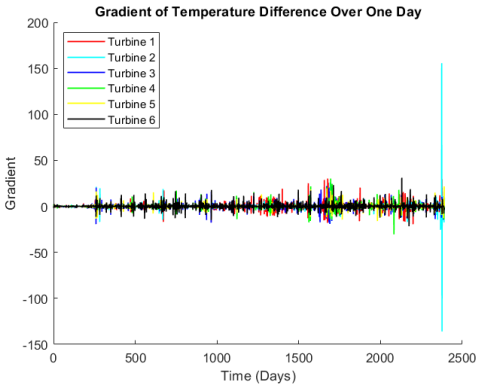

Figure 7.46: Gradient of Temperature Difference for All Turbines Per Day

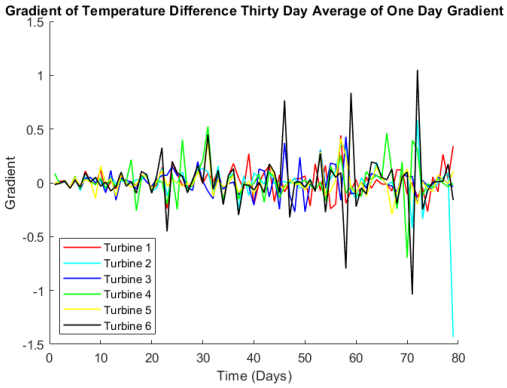

Figure 7.47: Gradient of Temperature Difference for All Turbines As Per Every 30 Days

Figure 7.46 reveals a significant temperature spike in the rear generator bearing of Turbine 2 within a short time-frame, suggesting a different failure mode than those observed in the other turbines; this component failed on day 2370. In Figure 7.47, Turbine 2 failed in November (day 79), Turbine 4 failed in February (day 69) and Turbine 1 had a proactive replacement in June (day 73).

7.2.3 Component Life Predictions

The aim of these final analyses, as outlined in Section 7.1.2, is to calculate both the moving average and cumulative average, in order to identify any potential threshold values, in which if a turbine exceeds this threshold, then it may indicate that a component is nearing the end of its operational life and whether it can be predicted.

Figure 7.48 shows the moving average of the temperature differences. Turbines 1, 2 and 4 all show high values towards the latter half of the graph. These correspond to the two turbines (2 and 4) that had generator NDE bearing failures and Turbine 1, which had a proactive replacement. Their highest values reached 22, 78 and 19

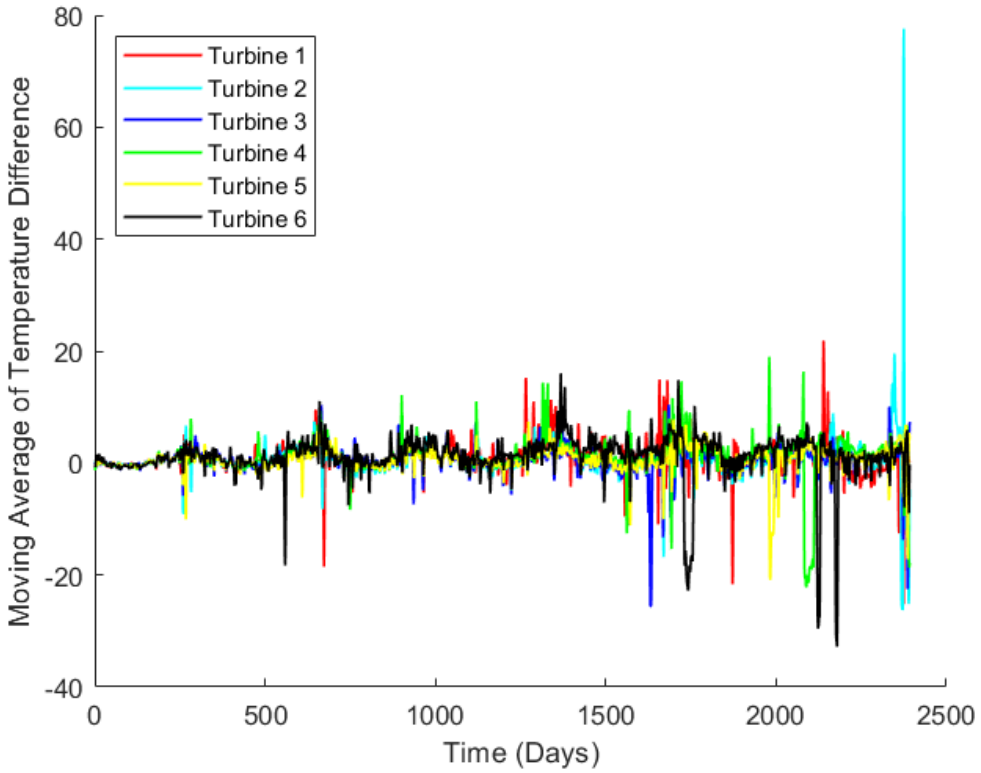

Figure 7.48: Moving Average of Temperature Difference

respectively.

As previously mentioned, Turbines 1, 4 and 6 exhibit similar trends, with two of the Turbines, both 1 and 4, confirmed to have required replacement of the generator NDE bearing. From Figure 7.49, it can be observed that on the day Turbine 4 failed, the cumulative average reached a value of 1.2.

Turbine 1 also crosses this threshold value, around the same time Turbine 4 failed and subsequently had the same component replaced approximately four months later, although the reasons for this proactive replacement are unclear. Turbine 6 surpasses this threshold value much earlier in March 2020 and underwent scheduled maintenance about eleven months later, in early February 2021, although detailed informa-

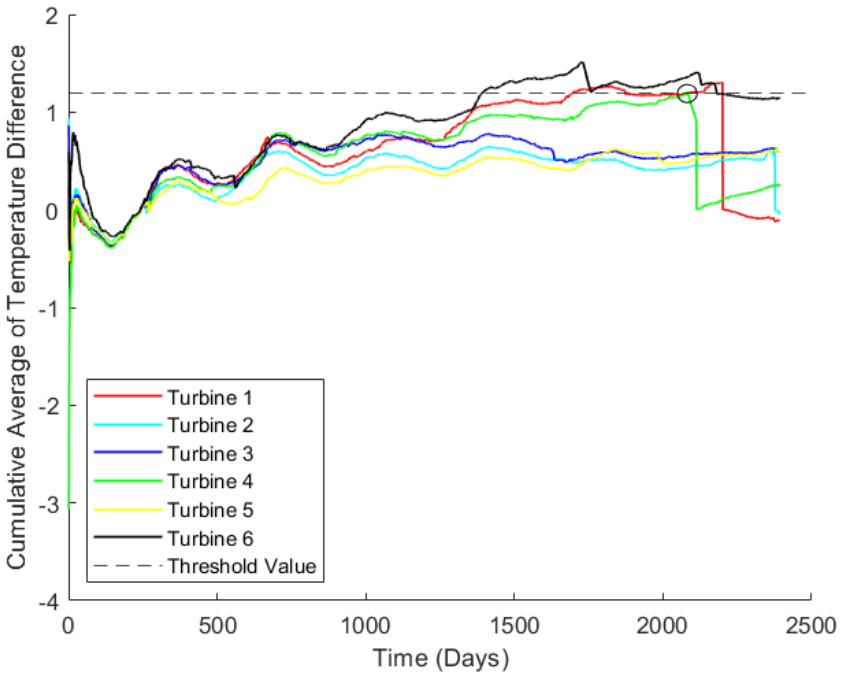

Figure 7.49: Cumulative Average

tion regarding this maintenance is also lacking. Therefore, it can be inferred that a threshold value of approximately 1.2, may indicate that a component is approaching the end of it's operational life within this wind farm. The advantage of employing the proposed cumulative average, over the cumulative sum, is that the values of the latter are influenced by the duration of monitoring up to any given point. In contrast, the former provides a real-time assessment of the rate of accumulated temperature differences. As such, by extrapolating the trend of the cumulative average, it will be feasible to predict when the cumulative average will exceed the threshold, indicating the end of the component's life. It is important to note that this method requires monitoring to commence when the specific components are in a healthy state. Proposing this indicator and discussing its implications aims to offer turbine operators a means

of predicting end-of-life scenarios, as well as highlighting the necessity for additional condition monitoring, to potentially extend the service life of drivetrain components.

7.3 Summary

In conclusion, the methodology that was proposed in Chapter 5 was used to develop a method, which specifically utilised large amounts of annual SCADA temperature data, to assess possible lifetime extension of the drivetrain. This approach focused on identifying any growing trends in temperature difference, which could indicate that a component is reaching the end of it's operational life. By applying a regression tree ensemble model, using three SCADA input parameters: power, rotor speed and nacelle temperature, along with a component temperature, it was possible to predict component temperatures. These predicted component temperatures were then compared to the actual temperatures, providing a way to monitor and evaluate the health of the component over multiple years of wind farm data.

From the dataset which was used to test the proposed method, the rear generator bearing was identified as the most vulnerable component to fail. The results comprising of - the temperature difference between the actual and predicted temperature values and the cumulative sum of these temperature differences - were inconclusive for rear generator bearings that failed due to operating at higher temperatures (e.g. Turbine 4). This may be due to noise or short-term fluctuations (e.g. environmental conditions) in the data, accumulating over time, which obscured any useful trends. However, the method can be useful for identifying components that experience sud-

den, sharp temperature increases, such as Turbine 2, which failed shortly after such an incident. The final analysis, based on the cumulative average, established a threshold value of 1.2. The threshold value was captured at this point because prior to that point, the cumulative average had been increasing but it was only once it reached that point, that the rear generator bearing failed, resulting in turbine downtime. While three turbines exceeded this threshold value and subsequently either failed or underwent maintenance/downtime, the time between crossing the threshold and failure varied significantly. Therefore, an accurate lifetime extension prediction could not be provided. However, each rear generator bearing could be treated individually, which may provide more accurate or useful results because - each turbine may be subjected to slightly different operating conditions, there may be differences in the manufacture and installation, they may have different maintenance histories, etc. - or even a hybrid approach, looking at them both individually and farm wide.

7.4 References

[1] Bruce Ratner. The correlation coefficient: Its values range between+ 1/- 1, or do they? *Journal of targeting, measurement and analysis for marketing*, 17(2): 139–142, 2009.

[2] Amir Rasekhi Nejad, Zhen Gao, and Torgeir Moan. Fatigue reliability-based inspection and maintenance planning of gearbox components in wind turbine drivetrains. *Energy Procedia*, 53:248–257, 2014.

[3] Amir Rasekhi Nejad, Yi Guo, Zhen Gao, and Torgeir Moan. Development of a 5 mw reference gearbox for offshore wind turbines. *Wind energy*, 19(6):1089–1106, 2016.

[4] Trendspider. Cumulative indicators: An overview. Technical report, 2018-2024.

Chapter 8

Model Uncertainty and Error Assessment

Due to the importance of reliable and operational wind turbines, any models, processes or methods that are used to predict outcomes, which in turn are used to make important decisions regarding the future of the turbines, must be as accurate as possible. Inaccurate predictions can lead to serious consequences, such as unnecessary shutdowns and replacement of functional components, or unexpected failures that result in unforeseen downtime.

In the previous chapter, a model/process/method has been proposed and implemented on real-life data, in order to predict a threshold value, which may indicate when a component is coming the end of its operational life, as part of lifetime extension evaluation. Therefore, it is crucial to determine any errors and/or uncertainties within the model and incorporate these, to improve the accuracy of the predicted outcomes.

Model uncertainties can be classed as epistemic or subjective uncertainties, along

with measurement and statistical uncertainties, [1]. These uncertainties stem from a lack of knowledge. Therefore, additional information, data and improved models can all help reduce these types of uncertainties.

Errors in the model refers to the difference between the actual and predicted values, while model uncertainty is the ratio between the actual and predicted values. Errors in the model may be caused by factors such as: model bias, variance, noisy data and model limitations. Model uncertainty may be caused by factors such as: insufficient information, complex models, data variability and inherently ambiguous data patterns. Therefore, model errors refer to specific discrepancies between the actual and predicted values, whereas model uncertainty refers to confidence or lack of within the model and acknowledges that discrepancies may stem from fundamental issues.

In this chapter, both the model errors and uncertainties will be investigated. The main sources of errors/uncertainties in this case, may come from the machine learning model and the measurements recorded in the SCADA data, which are used for the model's input parameters. Errors in the measurements may be caused by sensor failures, malfunction and/or noise.

A method to predict and incorporate these errors has then been proposed, in order to try and obtain a more reliable and accurate predicted value i.e. component temperature and in turn threshold value.

8.1 Method

Depending upon whether the focus is on investigating errors within the model or determining model uncertainty, different methods are applied.

8.1.1 Model Uncertainty

Model uncertainty can be used in stochastic analyses, such as reliability analysis, [2], [3] to represent a probabilistic model of the uncertainty associated with the data-driven model.

The initial step in determining model uncertainty, specifically uses the first year of SCADA data, which in this case is all the data from 2016 because this data is assumed to be “healthy" data. The dataset is randomly split into 70% training data and 30% test data and applied to the previously developed regression tree ensemble model. The model is trained and tested on separate data, to ensure an unbiased view of the model. The input parameters for the training dataset include: power, rotor speed, nacelle temperature and rear generator bearing temperature, whilst the test dataset only uses the first three parameters. The model output is the predicted rear generator bearing temperature. To account for the data split being randomly generated, the process is repeated a total of ten (10) times, generating a range of predicted rear generator bearing temperatures for the test dataset. The predicted temperature values for each 10-minute interval, along with the daily averages, are recorded and stored for all ten runs.

After completing the initial step, the next step is to calculate model uncertainty,

χ, which as defined in Section 3.3, is the ratio of the actual rear generator bearing temperature, X_{true}, to predicted rear generator bearing temperature, $X_{Predicted}$, [2], as shown below.

$$\chi = \frac{X_{true}}{X_{Predicted}} \tag{8.1}$$

The model uncertainty is calculated for each 10-minute averaged data point, as well as for the daily averaged value. The uncertainty is then modelled using a lognormal distribution, to determine the mean and standard deviation. Lognormal distribution is typically used because it only allows the use of positive values, effectively narrowing the range of random variables, [4].

The cumulative distribution function (CDF) of a lognormal distribution can be defined as:

$$F_x(x) = \phi(\frac{lnx - a}{c}) \tag{8.2}$$

Where $\phi()$ is the standard Gaussian CDF, lnx is natural logarithm, a is the mean and c is the standard deviation of lnx.

The next step is to calculate the 95% confidence interval, which is a range of values in which there is a 95% certainty, that the predictions are expected to fall between the upper and lower limits.

This process is then repeated with different dataset splits - 60% training/40% testing and 80% training/20% testing - to assess any potential impact on the predicted values.

If the first year of SCADA data is not available or if after reviewing the data it does not look "healthy", then an alternative could be to try and find a period within the data that is stable and which could be used to calculate the model uncertainty. Another alternative could be to use "healthy" data from a similar turbine or maybe even generate data from a physics-based model.

8.1.2 Errors in Model

8.1.2.1 Error Metrics

The model error can be defined as the difference between the actual and predicted rear generator bearing temperatures, which were determined in the previous section. Once the error has been calculated, key performance indicators such as the Mean Absolute Error (MAE), Mean Squared Error (MSE), Root Mean Squared Error (RMSE) and Mean Absolute Percentage Error (MAPE) can then be determined, as these are all valuable for assessing the regression model's performance.

The Mean Absolute Error (MAE) calculates the average absolute difference or error between the actual and predicted values, [5], so obviously the smaller the value the better.

$$MAE = \frac{1}{n}\sum_{i=1}^{n}|X_{true} - X_{Predicted}| \tag{8.3}$$

The Mean Squared Error (MSE) squares the average absolute difference or error between the actual and predicted values.

$$MSE = \frac{1}{n}\sum_{i=1}^{n}(X_{true} - X_{Predicted})^2 \tag{8.4}$$

The Root Mean Squared Error (RMSE) calculates the root of the mean of the differences between the actual and predicted values squared, [6].

$$RMSE = \sqrt{\frac{1}{n}\sum_{i=1}^{n}(X_{true} - X_{Predicted})^2} \tag{8.5}$$

The Mean Absolute Percentage Error (MAPE) calculates the average magnitude of the difference or error between the actual and predicted values. It is the percentage version of MAE, [7].

$$MAPE = \frac{1}{n}\sum_{i=1}^{n}|\frac{X_{true} - X_{Predicted}}{X_{true}}|x100 \tag{8.6}$$

These error metrics are calculated in order to assess how the model is performing, for example, to identify if there is any bias.

8.1.3 Monte Carlo Anomaly Detection Approaches and Metrics

The subsequent step is to apply the Monte Carlo method to incorporate an 'error' value into any future predictions. This error value is derived from the values of mean and standard deviation, extracted from the calculated error's probability distribution, based on the "healthy" data and detailed later in this Section. The following process is run separately for each turbine.

The data preparation process described previously and which is illustrated in Figure 8.1 is applied to all data from year 2016. For all data from years 2017 to 2022, the

same process is followed, except for the final stage.

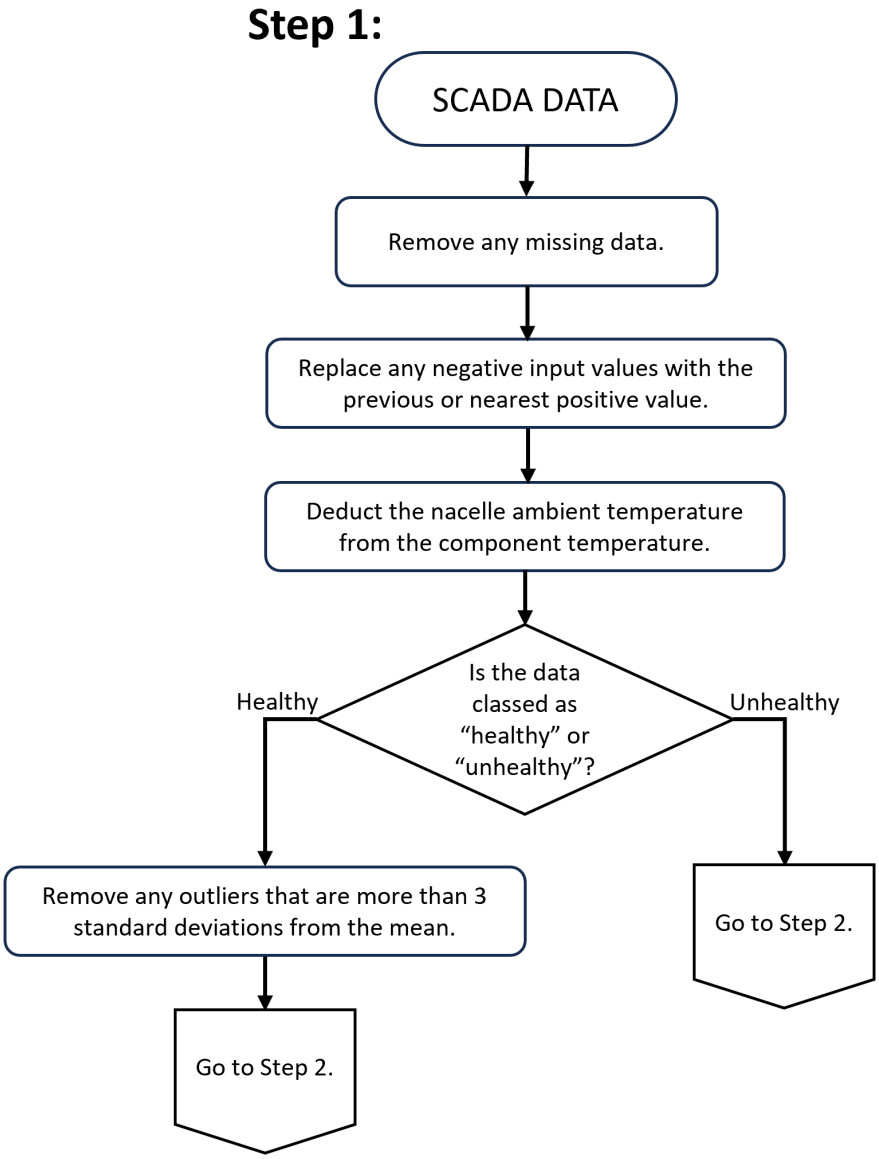

NOTE: "Healthy" data is data from year 2016. "Unhealthy" data refers to data from all other years.

Figure 8.1: Flow Chart Showing the Data Preparation

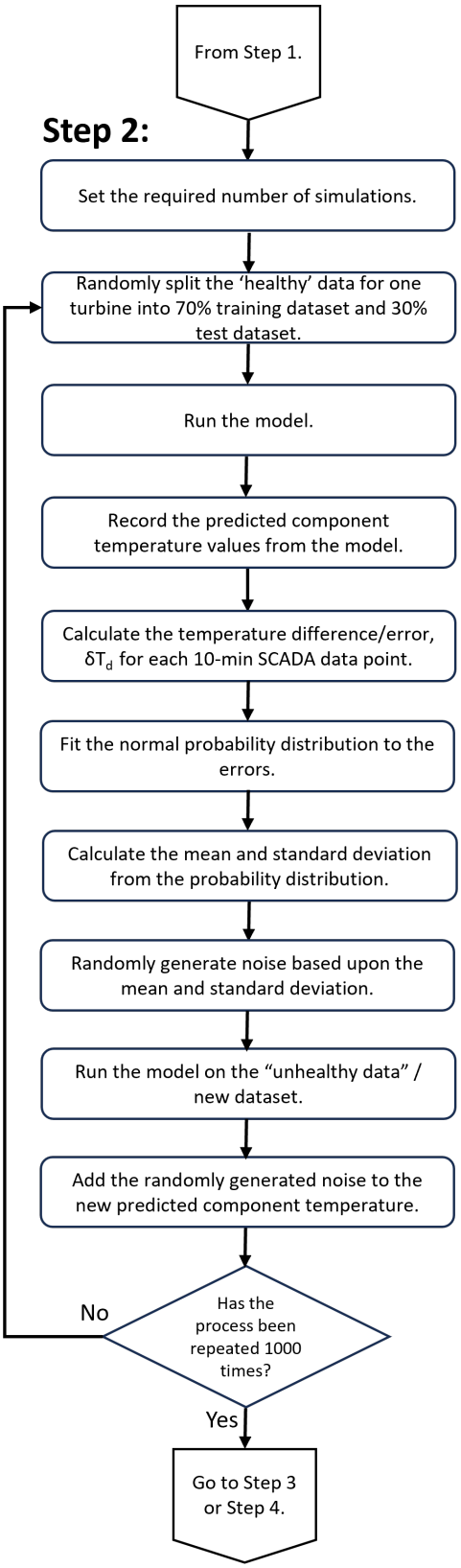

Figure 8.2: Flow Chart Showing the Monte Carlo Method used to Determine Predicted Values

The next step is to set up the Monte Carlo simulation, detailed in a flowchart shown in Figure 8.2. This process is ran separately for each turbine, with the number of simulations set to one thousand (1000). The “healthy" data, which in this case is the 2016 data is randomly split into 70% training data and 30% test data and the model ran. The differences between actual and predicted component temperatures are then calculated and a Matlab tool is used to fit a probability distribution to these errors. From this normal probability distribution, the mean and standard deviation are determined, which are then used to randomly generate an ’error’.

The model is then ran on a new dataset, which consists of the future years data, to predict the component’s temperature, in which the randomly generated ’error’ is added too.

8.1.3.1 Discrete Confidence Interval-Based:

After all the simulations are complete, both the 95% and 99% confidence intervals are calculated from these simulated predictions and the post-processing process is carried out, which is detailed in a flowchart in Figure 8.3. The daily values are then calculated, along with the temperature difference of any actual temperatures which fall outside of the confidence intervals, the cumulative sum of these temperature differences, cumulative average and moving average.

The above process is then repeated with “healthy" training/test data splits of 80%/20% and 60%/40%, to assess if varying the amount of training data impacts the accuracy of the predicted component temperature. Additionally, it is repeated using different amounts of future data, i.e. 1 year - 6 years, to examine if data quantity affects the

reliability and accuracy of the output.

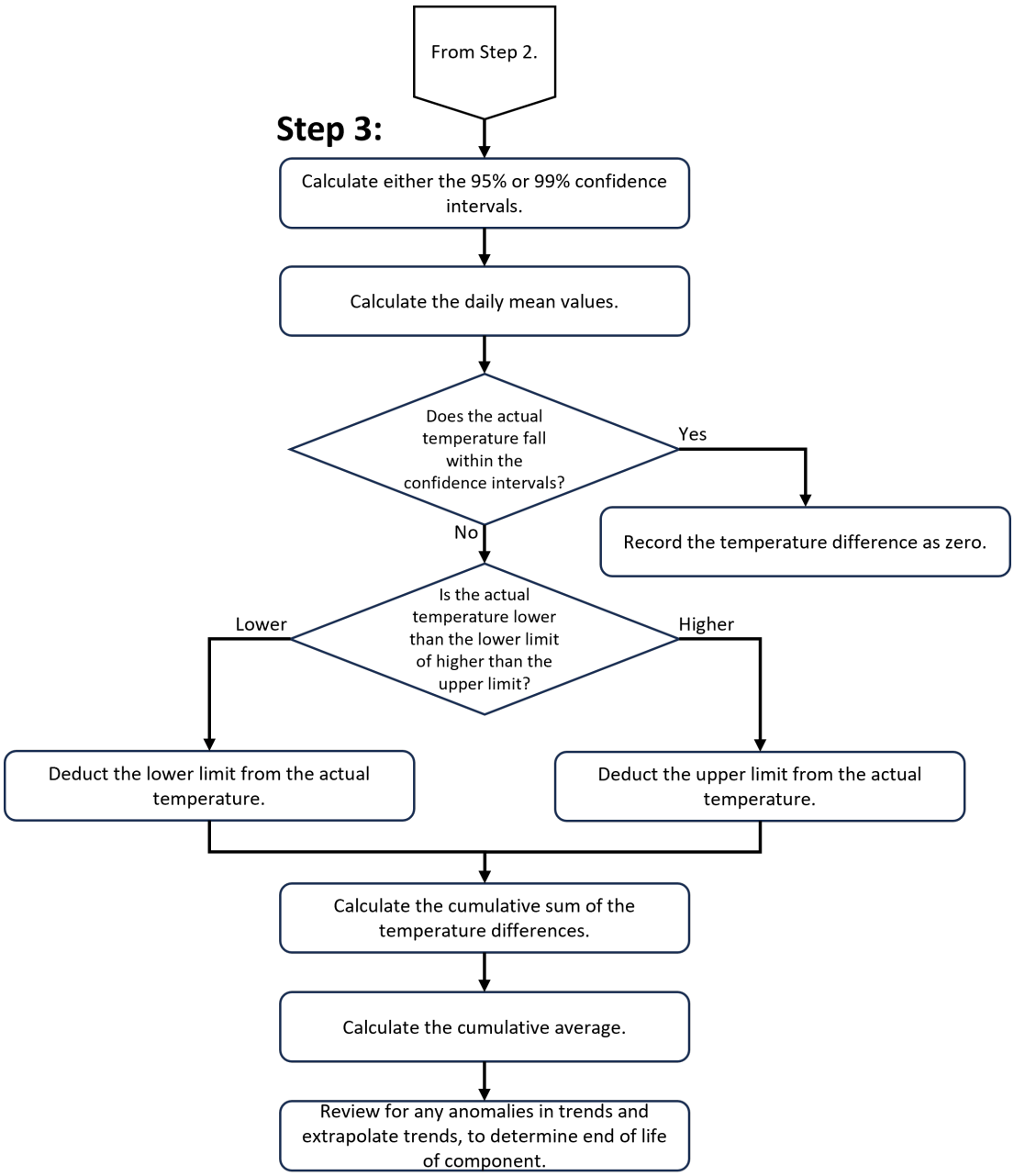

Figure 8.3: Flow Chart Showing the Post-Processing Process Using Discrete Confidence Interval-Based Approach

8.1.3.2 Continuous Probability Distribution-Based:

The next analysis that is carried out is based upon continuous probability distribution, which is detailed in a flowchart in Figure 8.4. After each run, the difference between the actual and predicted temperatures are calculated. Once all the runs are complete, the table that is produced contains the temperature difference for each 10-minute interval, for each of the thousand (1000) runs.

The normal probability distribution is then fit for each row and the mean, along with standard deviation and the 95% confidence intervals are then determined.

The cumulative sum of the temperature differences, along with the cumulative average and moving average of the temperature differences, are then calculated and all the necessary graphs plotted.

The process is then repeated, including: the 2016 data, as well as removing the noise and converting the 10-min data values to daily averages. This was done, so that a direct comparison can be made.

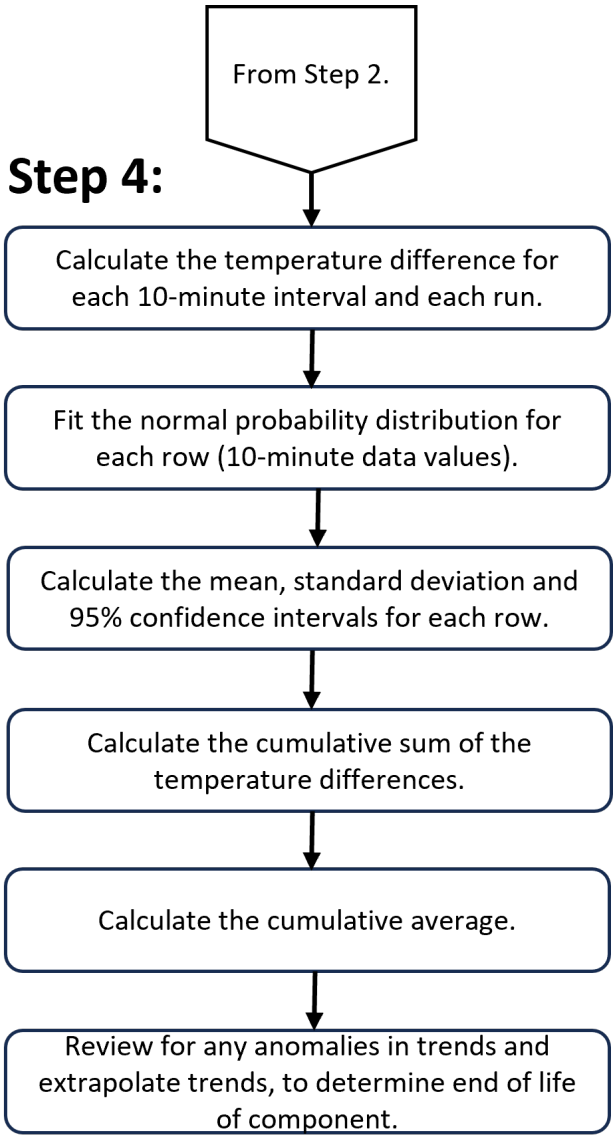

Figure 8.4: Flow Chart Showing the Post-Processing Process Using Continuous Probability Distribution-Based Approach

8.2 Results

8.2.1 Model Uncertainty

Figures 8.5 - 8.10 show the lognormal probability distribution graphs for all wind turbines and they all show similar results.

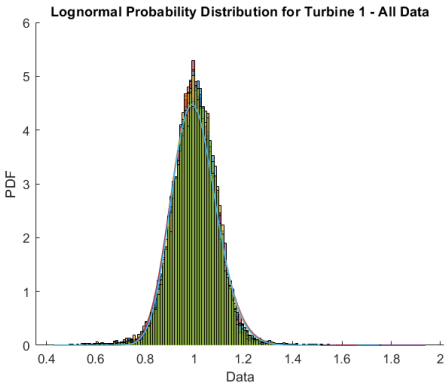

Figure 8.5: Probability Distribution for Turbine 1

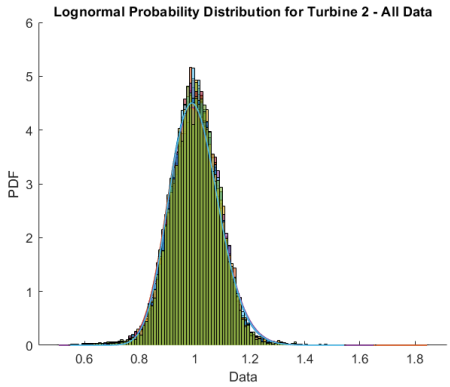

Figure 8.6: Probability Distribution for Turbine 2

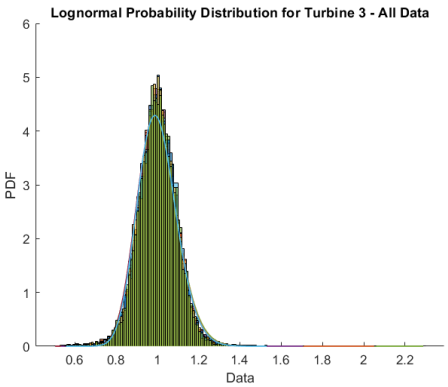

Figure 8.7: Probability Distribution for Turbine 3

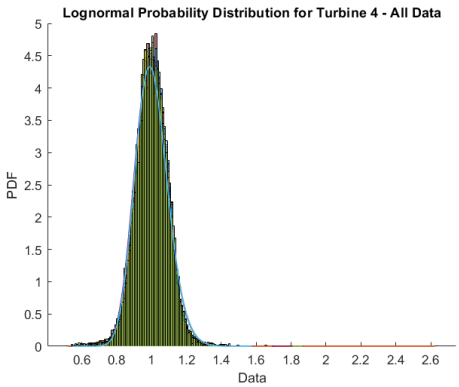

Figure 8.8: Probability Distribution for Turbine 4

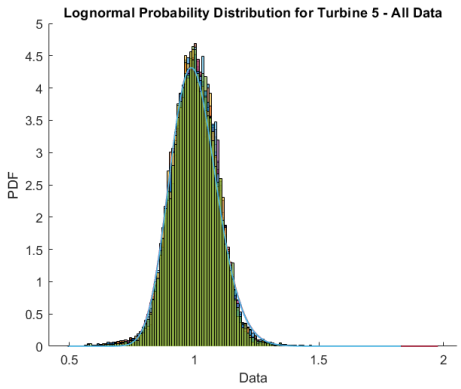

Figure 8.9: Probability Distribution for Turbine 5

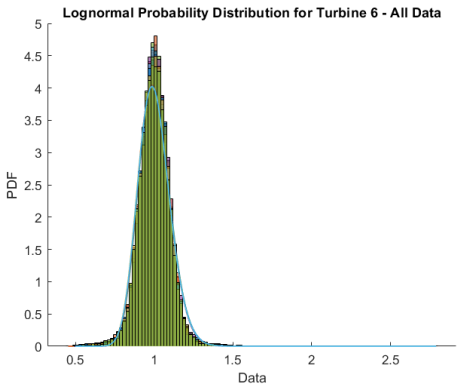

Figure 8.10: Probability Distribution for Turbine 6

The average mean and standard deviation for each 10-minute SCADA data value, which will be referred to as 'all data' going forth and the daily averages of the model uncertainty are shown in Tables 8.1 and 8.2, respectively. They show the mean to be around 1 and standard deviation to be around 0.09 for all data values and 0.03 for the daily average values. All the mean values are slightly above 1, indicating that the model is fairly accurate, although a little conservative. The standard deviation of around 0.09 reflects minimal variability, demonstrating the model's consistency. Converting the 10-minute averages to daily averages, reduces the standard deviation, thus decreasing variability because it smooths out any short-term fluctuations.

Table 8.1: Average Values for All Turbines Using Model Uncertainty

Turbine	Mean	Standard Deviation
1	1.0011	0.0918
2	1.0010	0.0899
3	1.0012	0.0951
4	1.0012	0.0933
5	1.0012	0.0936
6	1.0018	0.0997

Table 8.2: Average Values for All Turbines Using Model Uncertainty (Daily Values)

Turbine	Mean	Standard Deviation
1	1.0010	0.0358
2	1.0005	0.0334
3	1.0017	0.0369
4	1.0010	0.0359
5	1.0014	0.0343
6	1.0017	0.0381

The mean and standard deviation of the model uncertainty when using different training/test data splits, are shown in Tables 8.3 and 8.4. Table 8.3 shows that the standard deviation values are slightly lower when using an 80%/20% split, whereas this is the opposite in Table 8.4, where the average daily values are used. Although in general, changing the percentage split of training/test data, does not change the values significantly.

Table 8.3: Average Mean and Standard Deviation Values for All Turbines Using Different Training/Test Data Split

	Training/Test : 60%/40%		Training/Test : 80%/20%	
Turbine	Mean	Standard Deviation	Mean	Standard Deviation
1	1.0010	0.0929	1.0011	0.0908
2	1.0017	0.0913	1.0012	0.0893
3	1.0014	0.0960	1.0008	0.0940
4	1.0013	0.0941	1.0005	0.0924
5	1.0014	0.0945	1.0011	0.0926
6	1.0017	0.1004	1.0018	0.0978

Table 8.4: Average Mean and Standard Deviation Values for All Turbines Using Different Training/Test Data Split (Daily Values)

	Training/Test : 60%/40%		Training/Test : 80%/20%	
Turbine	Mean	Standard Deviation	Mean	Standard Deviation
1	1.0010	0.0348	1.0012	0.0364
2	1.0014	0.0330	1.0006	0.0352
3	1.0018	0.0369	1.0011	0.0384
4	1.0009	0.0350	1.0005	0.0373
5	1.0017	0.0333	1.0015	0.0366
6	1.0013	0.0371	1.0015	0.0391

8.2.2 Errors in Model

8.2.2.1 Error Metrics

Tables 8.5 and 8.6 show the average error metrics for all data and the average daily values for the ”healthy" (2016) data, respectively.

Table 8.5: Average Error Metrics for All Turbines

Turbine	MAE	MSE	RMSE	MAPE
1	1.8321	5.5723	2.3605	7.0493
2	1.8376	5.4687	2.3385	7.0438
3	1.9485	6.2626	2.5025	7.3174
4	1.9355	6.0592	2.4615	7.2834
5	1.9341	5.9778	2.4449	7.3240
6	1.9411	6.3569	2.5211	7.5029

All the error metrics: MAE, MSE, RMSE and MAPE are reduced when each 10-min data value is transformed into the daily average, which is constructive because obviously the closer each value is to zero the better. This transformation is beneficial because it smooths out any short-term fluctuations, which reduces the error metric

Table 8.6: Average Error Metrics for All Turbines (Daily Values)

Turbine	MAE	MSE	RMSE	MAPE
1	0.7735	0.9453	0.9720	2.9141
2	0.7204	0.8252	0.9082	2.7076
3	0.8035	1.0944	1.0460	2.9460
4	0.7950	0.9927	0.9960	2.9230
5	0.7436	0.9000	0.9483	2.7284
6	0.7982	1.0413	1.0202	2.9999

values, thus indicating a better correlation between the actual and predicted values. Lower error metrics signify improved model accuracy and performance. Therefore, with regards to model evaluation, minimizing these errors is a key objective.

In order to carry out a sensitivity analysis, the training/test data split is adjusted and the process repeated. Tables 8.7 and 8.8 show the error metrics for the “healthy" data only i.e. 2016 data, for the 70%/30%, 60%/40% and 80%/20% data splits, for all data and the average daily values, respectively. Table 8.8 shows that MAE and MSE increases as the training dataset increases from 60% to 80%, but RMSE and MAPE reduce in value as the training dataset increases. Whereas for all the data (Table 8.7), all the error metrics, i.e. MAE, MSE, RMSE and MAPE, reduce in value as the size of the training dataset increases. Again, varying the training/test data split does not alter the results significantly.

Table 8.7: Error Metrics for Different Data Splits for 2016 Data - All Values

Turbine	Error Metric	60%/40%	70%/30%	80%/20%
1	MAE	1.847	1.832	1.817
1	MSE	5.694	5.575	5.460
1	RMSE	2.386	2.361	2.337
1	MAPE	7.126	7.060	7.002
2	MAE	1.854	1.829	1.817
2	MSE	5.560	5.403	5.345
2	RMSE	2.358	2.324	2.312
2	MAPE	7.113	7.022	6.968
3	MAE	1.972	1.946	1.931
3	MSE	6.427	6.282	6.176
3	RMSE	2.535	2.506	2.485
3	MAPE	7.404	7.316	7.254
4	MAE	1.950	1.933	1.920
4	MSE	6.168	6.051	5.948
4	RMSE	2.483	2.460	2.439
4	MAPE	7.340	7.275	7.239
5	MAE	1.951	1.935	1.917
5	MSE	6.107	5.998	5.883
5	RMSE	2.471	2.449	2.425
5	MAPE	7.396	7.339	7.265
6	MAE	1.962	1.949	1.920
6	MSE	6.487	6.423	6.214
6	RMSE	2.547	2.534	2.493
6	MAPE	7.592	7.541	7.414

Table 8.8: Error Metrics for Different Data Splits for 2016 Data - Daily Values

Turbine	Error Metric	60%/40%	70%/30%	80%/20%
1	MAE	0.747	0.770	0.775
1	MSE	0.885	0.935	0.968
1	RMSE	2.386	2.361	2.337
1	MAPE	7.126	7.060	7.002
2	MAE	0.706	0.715	0.751
2	MSE	0.784	0.808	0.890
2	RMSE	2.358	2.324	2.312
2	MAPE	7.113	7.022	6.968
3	MAE	0.791	0.794	0.829
3	MSE	1.052	1.049	1.140
3	RMSE	2.535	2.506	2.485
3	MAPE	7.404	7.316	7.254
4	MAE	0.773	0.796	0.820
4	MSE	0.950	0.994	1.058
4	RMSE	2.483	2.460	2.439
4	MAPE	7.340	7.275	7.239
5	MAE	0.731	0.748	0.781
5	MSE	0.855	0.897	1.014
5	RMSE	2.471	2.449	2.425
5	MAPE	7.396	7.339	7.265
6	MAE	0.782	0.803	0.816
6	MSE	1.009	1.053	1.106
6	RMSE	2.547	2.534	2.493
6	MAPE	7.592	7.541	7.414

8.2.3 Monte Carlo Anomaly Detection Approaches and Metrics

The original graphs of the cumulative sum of the temperature differences and the calculated cumulative average, that were determined in Chapter 7, prior to investigating the model errors and uncertainty, are shown in Figures 8.11 and 8.12.

Figure 8.11 shows the cumulative sum of the temperature differences between the actual and predicted rear generator bearing temperatures, for all turbines, across all years.

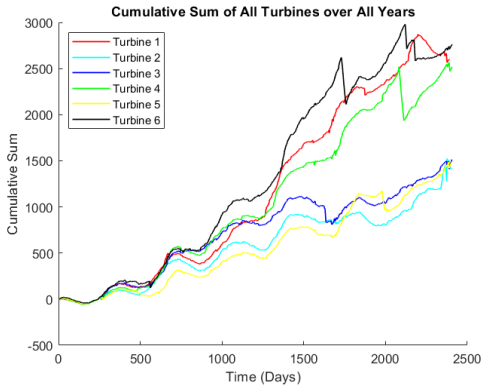

Figure 8.11: Cumulative Sum of the Temperature Differences for All Turbines Over All Years

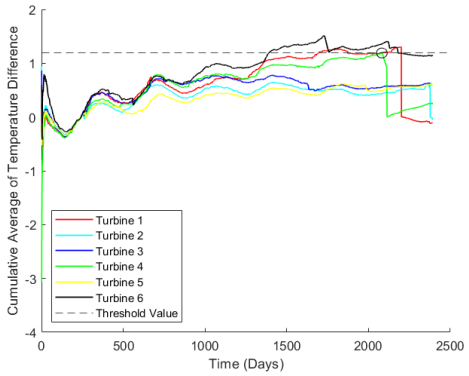

Figure 8.12: Cumulative Average

Figure 8.12 displays the cumulative average, which has been calculated in order to see if there is an obvious threshold value, in which if the turbine crosses then it is reaching its end of life. A suitable threshold value was deemed to be 1.2.

8.2.3.1 Discrete Confidence Interval-Based:

As described in Section 8.1, the proposed Monte Carlo process/method was originally carried out on all turbines, using a training/test data split of 70%/30%. The 95% and

99% prediction or confidence intervals of the predicted component temperatures were then calculated. Figures 8.13, 8.15, 8.17, 8.19, 8.21 and 8.23, show the actual rear generator bearing temperatures, along with the 95% confidence upper and lower limits for the daily values, for all turbines. Figures 8.14, 8.16, 8.18, 8.20, 8.22 and 8.24 show the corresponding confidence bands. It can be seen from the graphs that some actual component temperatures exceed either the upper or lower limits, which may be due to excessive noise, a temporary sensor issue or component failure, especially in the case of Turbine 4, where there are many more values exceeding the upper limit.

The number of daily average data values, that fall outside the upper and lower limits, are shown in Table 8.9, for both 95% and 99% confidence intervals. It shows that for the 95% confidence interval, between 5% to 11% of the total dataset values fall outside the limits, whereas between 2% to 6% fall outside the limits when using the 99% confidence interval.

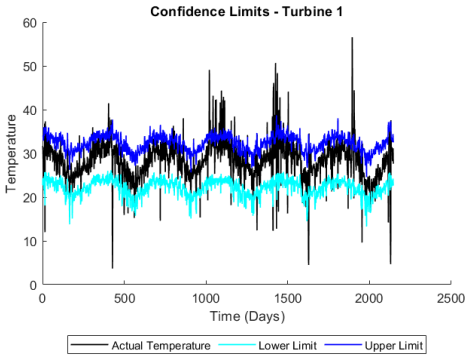

Figure 8.13: Turbine 1 - Actual Temperature and Confidence Limits (95%)

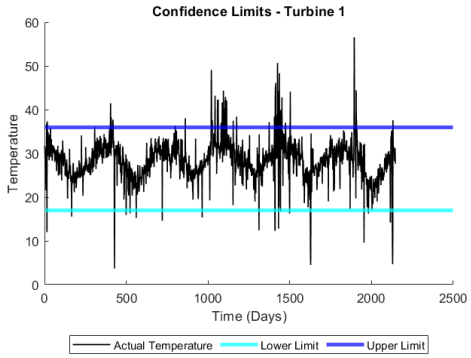

Figure 8.14: Turbine 1 - Actual Temperature and Confidence Bands (95%)

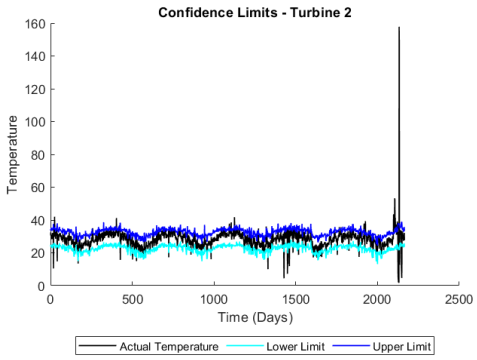

Figure 8.15: Turbine 2 - Actual Temperature and Confidence Limits (95%)

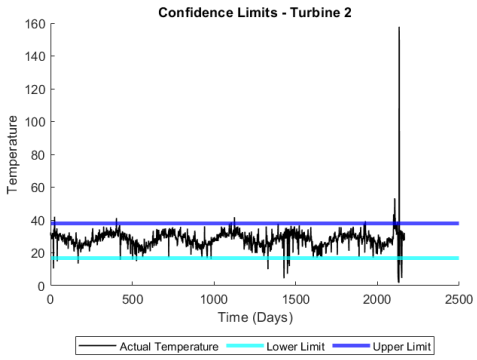

Figure 8.16: Turbine 2 - Actual Temperature and Confidence Bands (95%)

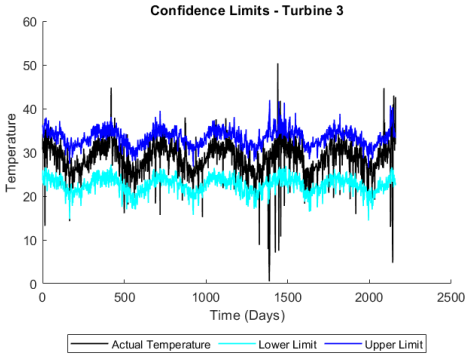

Figure 8.17: Turbine 3 - Actual Temperature and Confidence Limits (95%)

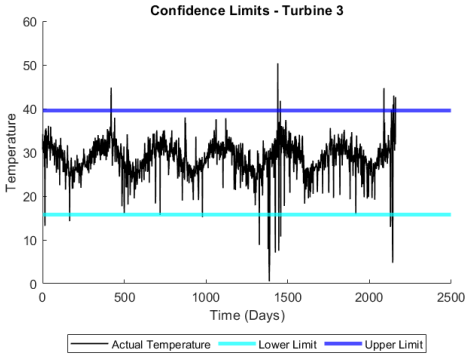

Figure 8.18: Turbine 3 - Actual Temperature and Confidence Bands (95%)

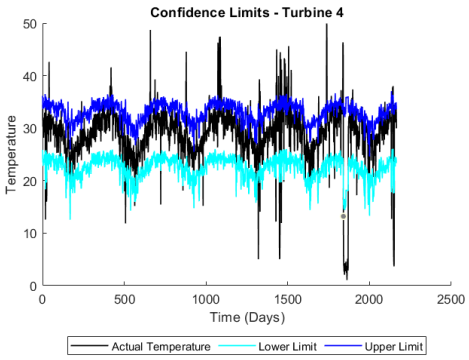

Figure 8.19: Turbine 4 - Actual Temperature and Confidence Limits (95%)

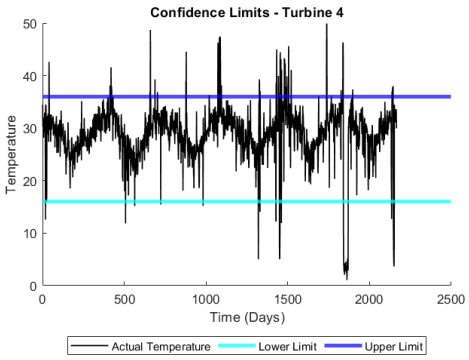

Figure 8.20: Turbine 4 - Actual Temperature and Confidence Bands (95%)

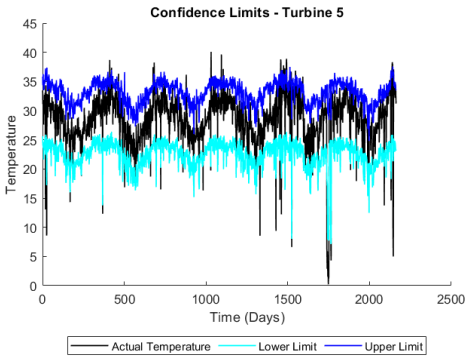

Figure 8.21: Turbine 5 - Actual Temperature and Confidence Limits (95%)

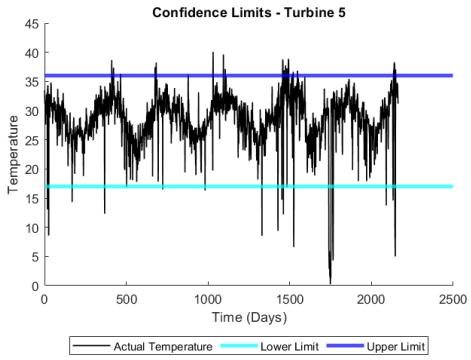

Figure 8.22: Turbine 5 - Actual Temperature and Confidence Bands (95%)

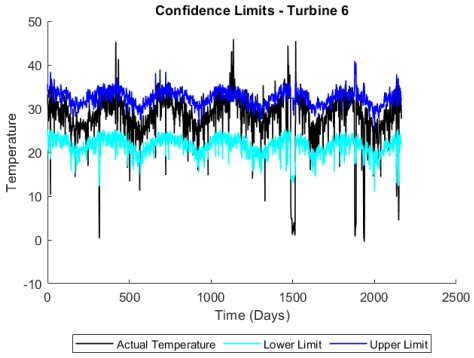

Figure 8.23: Turbine 6 - Actual Temperature and Confidence Limits (95%)

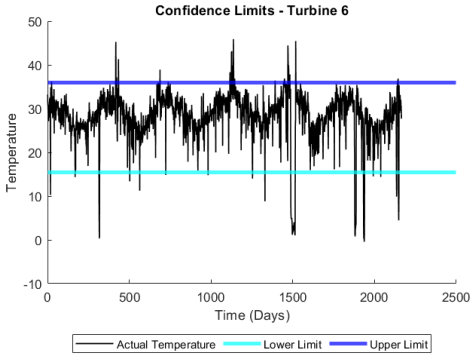

Figure 8.24: Turbine 6 - Actual Temperature and Confidence Bands (95%)

Table 8.9: Number of Data Points that fall outside the Lower and Upper Limits for both 95% and 99% Confidence Intervals

	No. of Values Outside Limits	
Turbine	95%	99%
1	171 (8%)	108 (5%)
2	123 (6%)	73 (3%)
3	108 (5%)	58 (3%)
4	202 (9%)	131 (6%)
5	119 (6%)	52 (2%)
6	236 (11%)	132 (6%)

The new graphs of the cumulative sum of the temperature differences and the cumulative average, for all turbines are displayed in Figures 8.25 - 8.28.

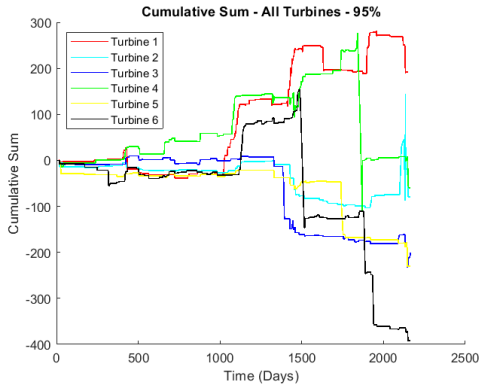

Figure 8.25: Cumulative Sum of the Temperature Differences for All Turbines Over All Years Using the New Process (95% Prediction Level)

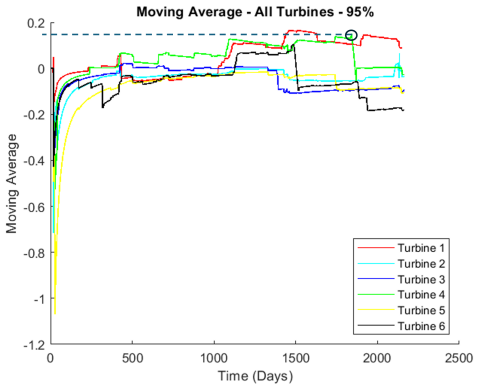

Figure 8.26: Cumulative Average using Discrete Confidence Interval Method (95% Prediction Level)

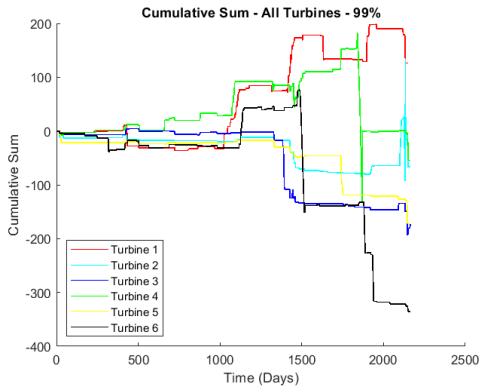

Figure 8.27: Cumulative Sum of the Temperature Differences for All Turbines Over All Years Using the New Process (99% Prediction Level)

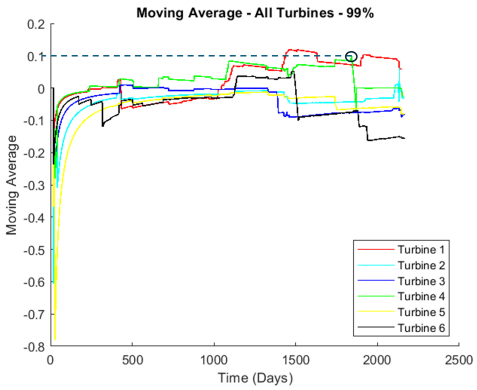

Figure 8.28: Cumulative Average using Discrete Confidence Interval Method (99% Prediction Level)

The graphs appear different to the original because only actual temperatures that do not fall within the prediction/confidence limits for each daily average value, are recorded as having a temperature difference. Any values that fall within the limits, are recorded as having zero temperature difference, which means that the cumulative sum

can stay at the same value for a period of time, until an actual temperature outside the limits is recorded. This explains why there are more horizontal and vertical lines on the new graphs.

From these graphs, it can be seen that by using the same technique that was used to determine the threshold value in Figure 8.12, that the threshold value is approximately 0.15 for 95% confidence interval and 0.1 for 99% confidence interval, as opposed to 1.2 in the original results. They also show that only Turbines 1 and 4 cross the threshold value, which matches the information recorded in the data logs. The data logs recorded generator NDE bearing failures in Turbines 2 and 4, as well as the proactive replacement of the component in Turbine 1. Turbine 6 does not cross the threshold value in this case, even though it gets close. This may be due to the fact that the issues it had were not related to the rear generator bearing, or that maintenance was carried out before it failed.

Some of the error metrics, specifically the mean absolute error (MAE) and mean squared error (MSE), are calculated for the results obtained via the new process and compared with the results from the original method. The results are displayed in Table 8.10. It shows that the proposed discrete confidence interval-based method reduces both the MAE and MSE, in all turbines, which is advantageous.

It can also be seen from the table, that the MSE values for Turbines 2 and 4 are higher than the others, in the new discrete confidence interval-based method, probably due to the fact that failures occurred in both these turbines.

A sensitivity analysis is performed, which involves repeating the process using a different training/test data split for the “healthy" data, a split of both 80%/20% and

Table 8.10: Error Metrics for Original vs. New Process

Turbine	Error Metric	Original Method	New MC Method
1	MAE	2.16	0.37
1	MSE	12.69	3.59
2	MAE	1.90	0.37
2	MSE	23.19	15.43
3	MAE	1.84	0.22
3	MSE	9.81	2.36
4	MAE	2.30	0.50
4	MSE	15.61	5.17
5	MAE	1.71	0.17
5	MSE	7.46	1.34
6	MAE	2.79	0.49
6	MSE	20.88	4.68

60%/40% is applied and the results are shown in Figures 8.29 - 8.32. The tabular results from the sensitivity analysis are shown in Table 8.11.

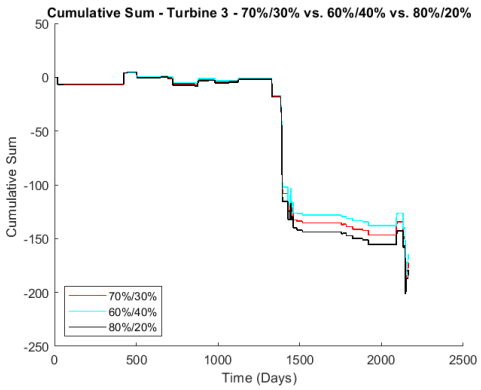

Figure 8.29: Cumulative Sum of the Temperature Differences for Turbine 3 Over All Years: Comparison Using Training/Test Split of 60%/40% vs. 70%/30% vs. 80%/20% (99% Prediction Level)

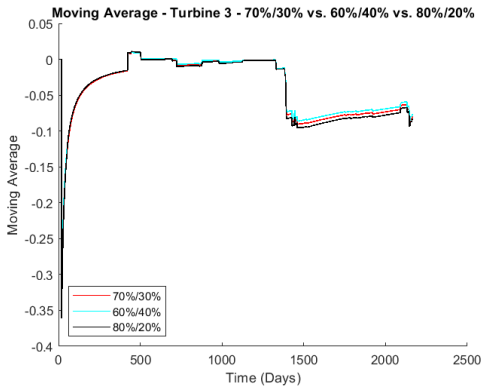

Figure 8.30: Cumulative Average for Turbine 3 Over All Years: Comparison Using Training/Test Split of 60%/40% vs. 70%/30% vs. 80%/20% (99% Prediction Level)

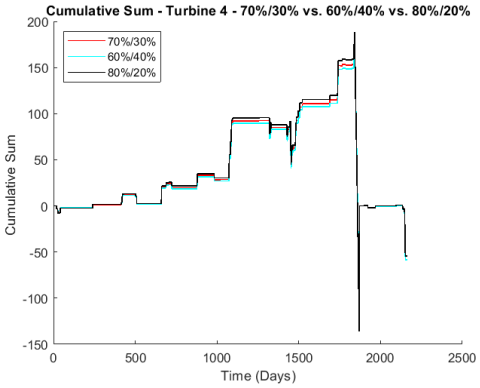

Figure 8.31: Cumulative Sum of the Temperature Differences for Turbine 4 Over All Years: Comparison Using Training/Test Split of 60%/40% vs. 70%/30% vs. 80%/20% (99% Prediction Level)

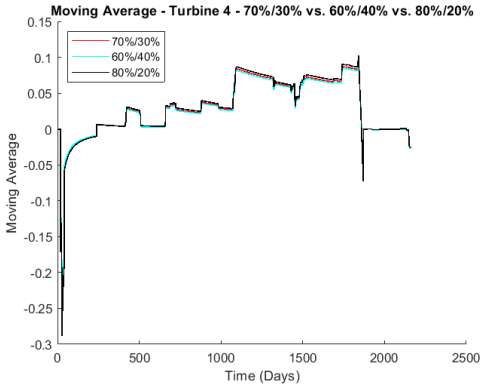

Figure 8.32: Cumulative Average for Turbine 4 Over All Years: Comparison Using Training/Test Split of 60%/40% vs. 70%/30% vs. 80%/20% (99% Prediction Level)

Table 8.11: Error Metrics for Different Data Splits - Daily Values for All Years

Turbine	Error Metric	60%/40%	70%/30%	80%/20%
1	MAE	0.36	0.37	0.38
1	MSE	3.50	3.59	3.67
2	MAE	0.36	0.37	0.38
2	MSE	15.32	15.43	15.63
3	MAE	0.21	0.22	0.23
3	MSE	2.24	2.36	2.40
4	MAE	0.49	0.50	0.52
4	MSE	5.08	5.17	5.36
5	MAE	0.17	0.17	0.19
5	MSE	1.27	1.34	1.48
6	MAE	0.47	0.49	0.49
6	MSE	4.47	4.68	4.76

The error metrics for the complete process, i.e. the error calculated from applying the proposed discrete confidence interval-based method to years 2017 - 2022, using the different “healthy" dataset splits are calculated and are shown in Table 8.11. The table shows that both the MAE and MSE increase as the training dataset increases

from 60% to 80% and testing dataset reduces from 40% to 20%.

With regards to the amount of data required to obtain accurate results, the process is repeated and the model applied to different durations, i.e. 1-6 years, to Turbine 4. The results for years 1, 3 and 5 are shown in Figures 8.33 - 8.38.

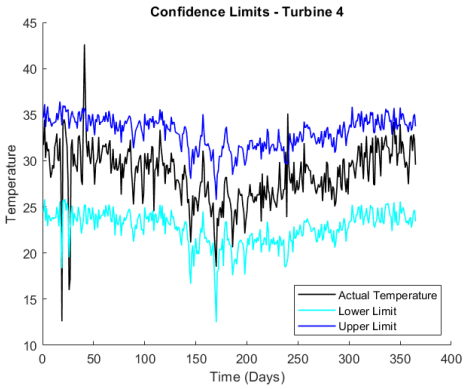

Figure 8.33: Actual Temperature and Confidence Intervals for 1 Year Data for Turbine 4

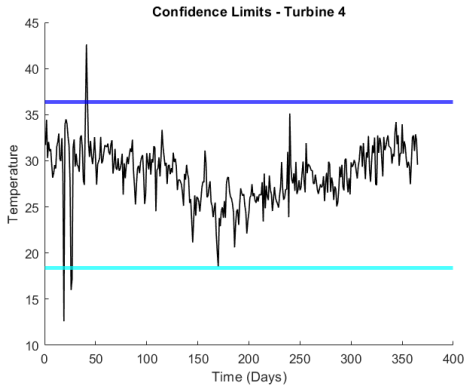

Figure 8.34: Actual Temperature and Confidence Bands for 1 Year Data for Turbine 4

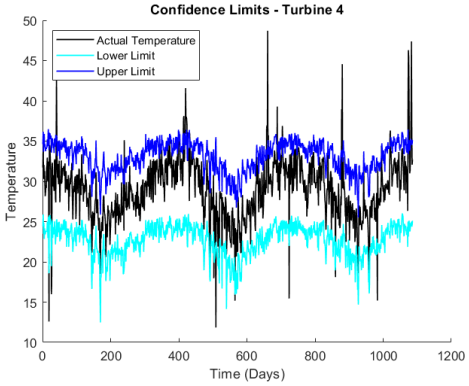

Figure 8.35: Actual Temperature and Confidence Intervals for 3 Years of Data for Turbine 4

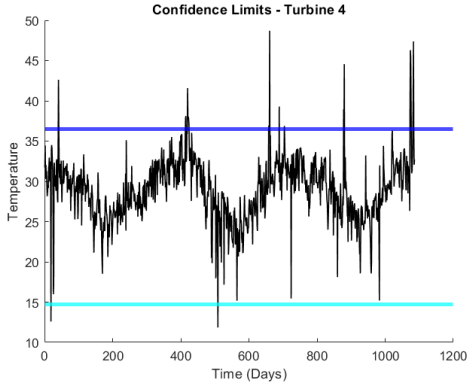

Figure 8.36: Actual Temperature and Confidence Bands for 3 Years of Data for Turbine 4

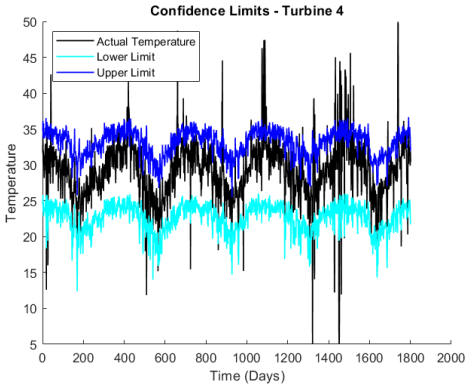

Figure 8.37: Actual Temperature and Confidence Intervals for 5 Year Data for Turbine 4

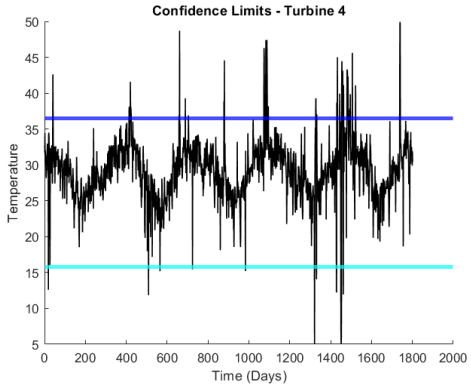

Figure 8.38: Actual Temperature and Confidence Bands for 5 Year Data for Turbine 4

8.2.3.2 Continuous Probability Distribution-Based:

Figures 8.39 - 8.41 show the temperature difference, cumulative sum of the temperature difference and cumulative average, respectively, based upon the continuous probability distribution-based method.

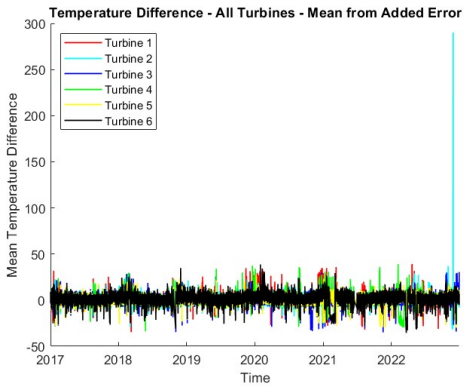

Figure 8.39: All Turbines - Temperature Difference Using Continuous Probability Distribution Method

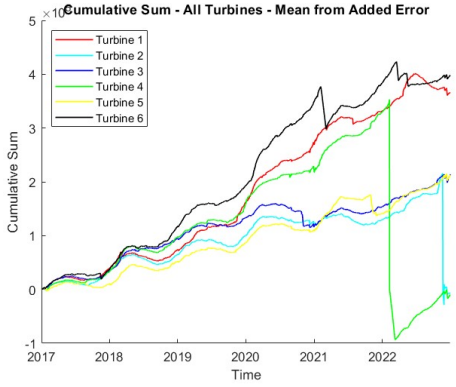

Figure 8.40: All Turbines - Cumulative Sum of the Temperature Difference Using Continuous Probability Distribution Method

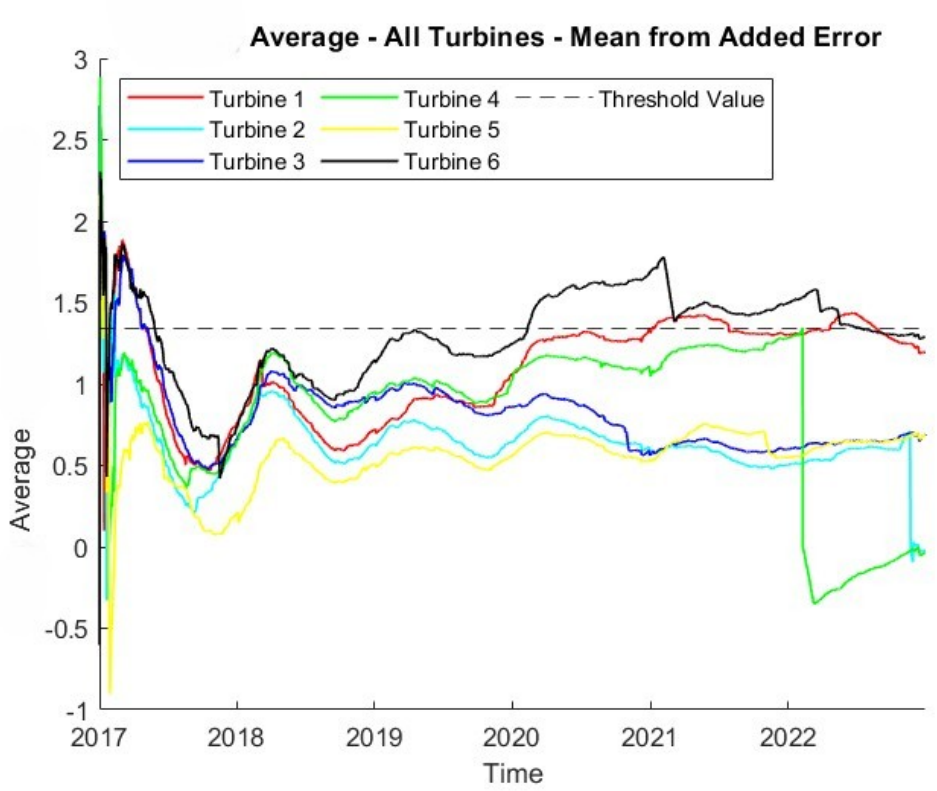

Figure 8.41: All Turbines - Cumulative Average Using Continuous Probability Distribution Method

The revised threshold value using this method is 1.34, this is an 11.7% increase from the value obtained when a random error was not included, in Chapter 7. In this scenario, all turbines cross this threshold at some point. This may be due to the fact that data from 2016 has not been included this time, as the 2016 data was used purely to determine any errors that were present within the model.

The probability distribution related to the temperature differences for Turbine 4 just prior to failure and Turbine 3, which had no notable failures, were plotted to make a comparison and are shown in Figures 8.42 and 8.43.

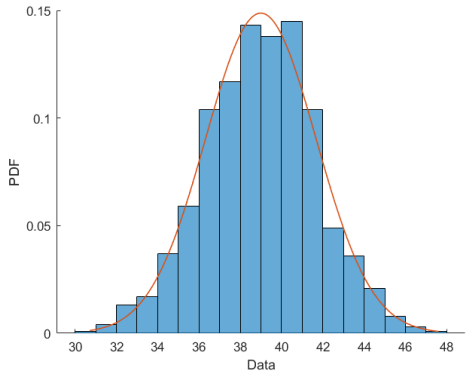

Figure 8.42: Turbine 4 - Probability Distribution Graph Two Days Prior to Failure

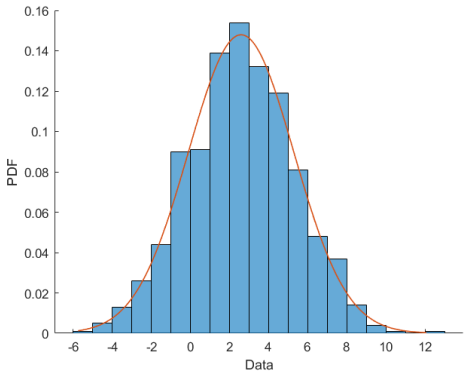

Figure 8.43: Turbine 3 - Probability Distribution Graph

Figure 8.42 shows a range of temperature difference values from 30°C to 48°C for Turbine 4, compared to a range of values from -8°C to 12°C for Turbine 3 (Figure 8.43), which is a noticeable difference between a turbine that failed and one that did not.

Repeating the process but this time including the 2016 data, produced the results shown in Figures 8.44 - 8.46.

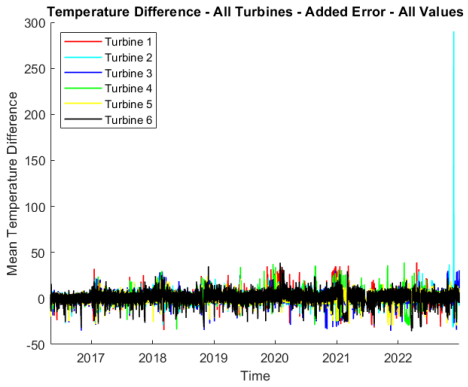

Figure 8.44: All Turbines - Temperature Difference - All Values - With Added Error

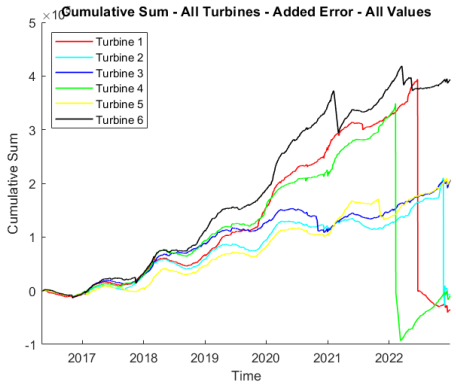

Figure 8.45: All Turbines - Cumulative Sum - All Values - With No Error

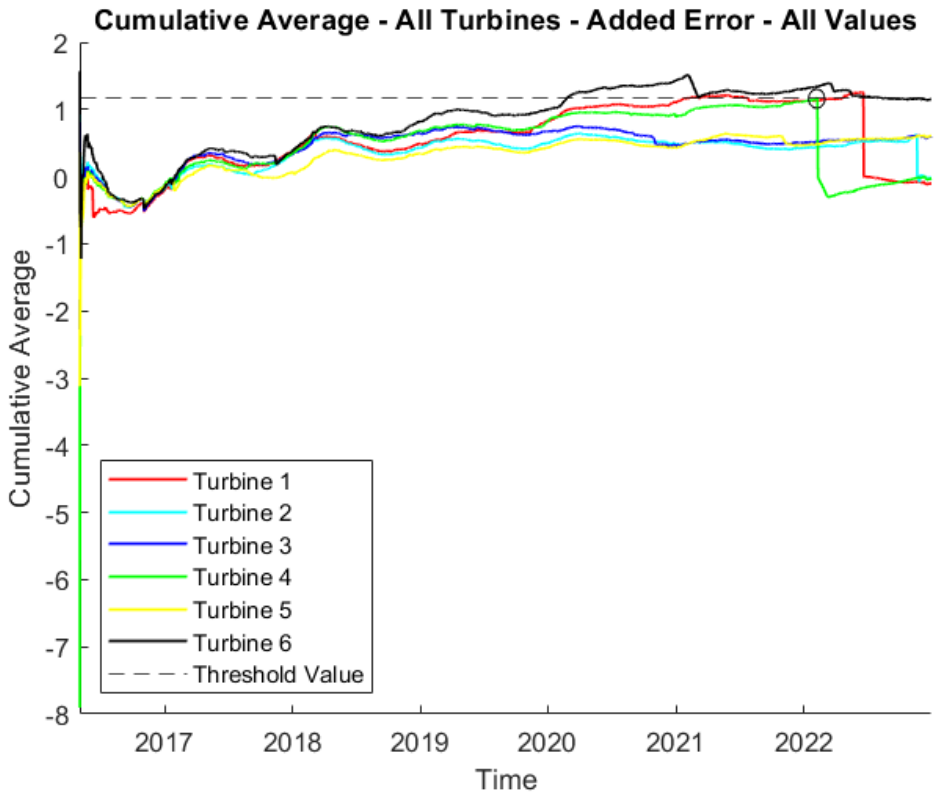

Figure 8.46: All Turbines - Cumulative Average (2016-2022) Using Continuous Probability Distribution Method

The revised threshold value in this scenario is 1.17, which is a 2.5% reduction from the original results. The same pattern is observed, with regards to the six turbines separating into two groups. The first group consisting of Turbines 1, 4 and 6, with the remaining three in the second group. As before, all turbines in the first group exceed the threshold value. Focusing on the points where the turbines cross the threshold, it can be seen that in the original results, Turbine 1 crosses the threshold initially, before dropping back below it and then crosses a second time simultaneously with Turbine 4 (Figure 8.47). However, when an error is taken into account, the second crossing of Turbine 1 occurs later than Turbine 4 (Figure 8.48), indicating a shorter interval

between the threshold crossing and the proactive replacement of the component, in this case.

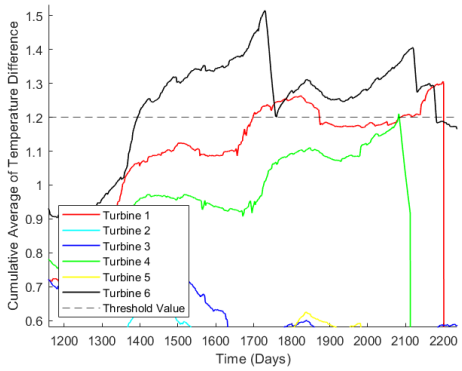

Figure 8.47: Zoomed in Graph where Turbines Cross the Threshold - Original

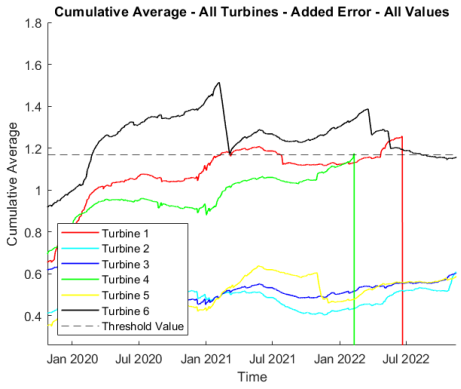

Figure 8.48: Zoomed in Graph where Turbines Cross the Threshold - Revised

Figures 8.49 and 8.50 show the cumulative average plots from repeating the process but this time including the 2016 data within the testing data, converting each 10-minute data value to the daily mean, as well as recording the predicted temperature values both with and without the added 'error', respectively.

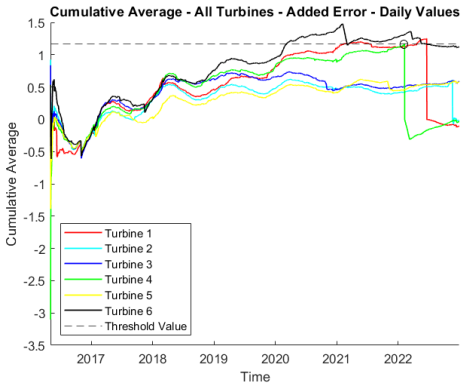

Figure 8.49: All Turbines - Cumulative Average - Daily Values - With Added Error

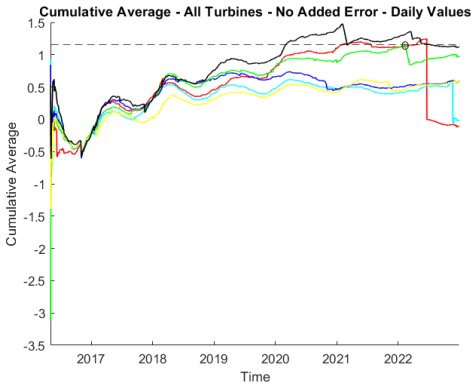

Figure 8.50: All Turbines - Cumulative Average - Daily Values - With No Error

Figure 8.49 shows a threshold value of 1.17, whereas Figure 8.50 shows a threshold value of 1.165. Therefore, by adding an 'error' to the predicted temperature values

to compensate for the model error, the threshold value increases slightly. However, this value is again lower than the original results documented in Chapter 7.

Figures 8.51 - 8.56 show the results obtained by determining the 95% confidence interval from the normal probability distribution for each 10-minute interval.

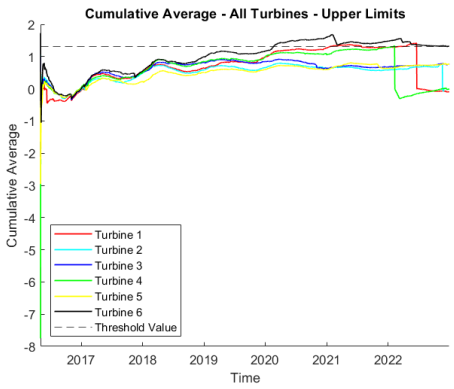

Figure 8.51: All Turbines - Cumulative Average - All Values - Upper Limits

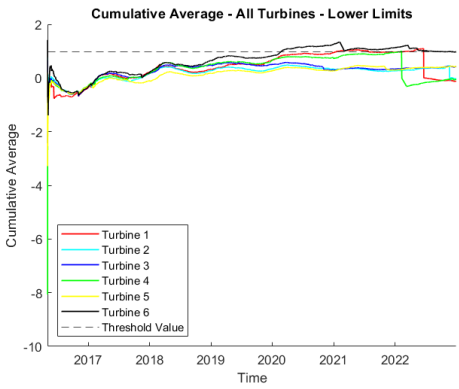

Figure 8.52: All Turbines - Cumulative Average - All Values - Lower Limits

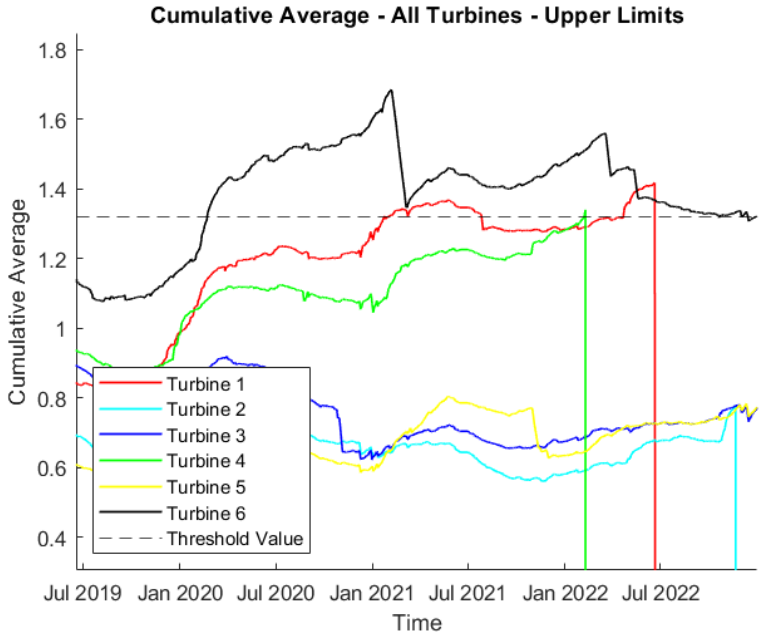

Figure 8.53: All Turbines - Cumulative Average - All Values - Upper Limits -Zoomed In

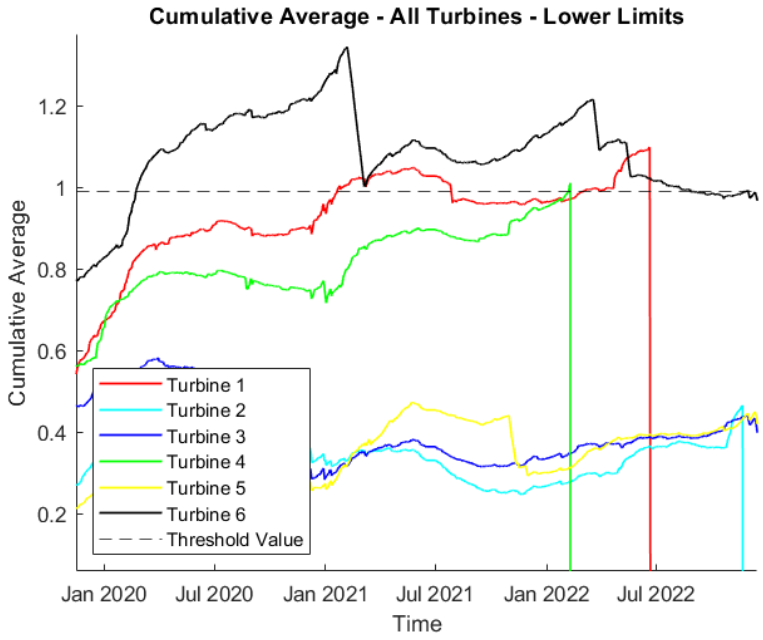

Figure 8.54: All Turbines - Cumulative Average - All Values - Lower Limits -Zoomed In

It can be seen from Figure 8.56, that the upper and lower limits of the threshold value are 1.32 and 0.99 respectively.

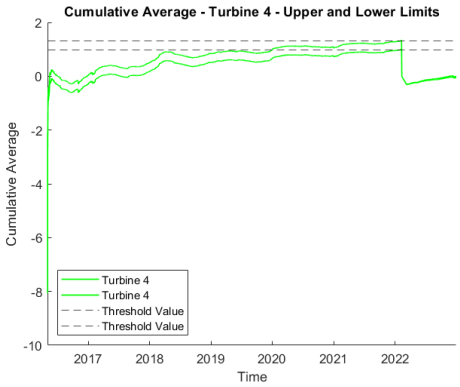

Figure 8.55: Turbine 4 - Cumulative Average - All Values - Upper and Lower Limits

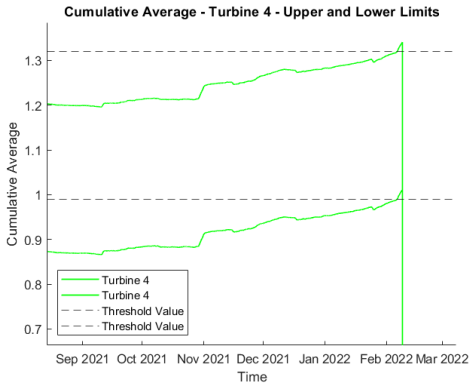

Figure 8.56: Turbine 4 - Cumulative Average - All Values - Upper and Lower Limits - Zoomed In

A graph combining the upper and lower limits, along with the threshold values, is shown in Figures 8.57 and 8.58.

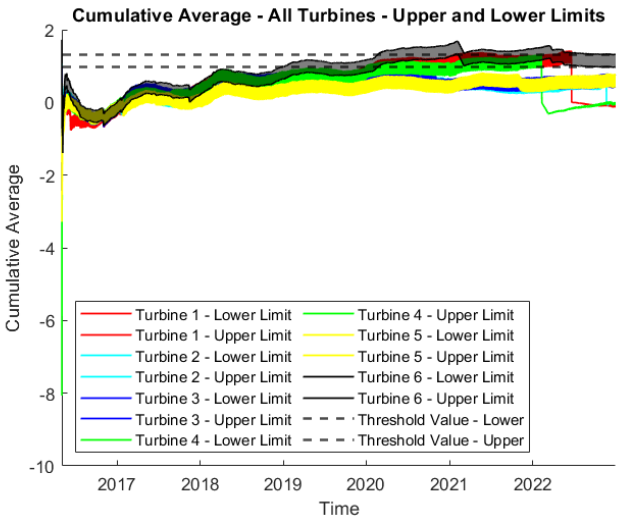

Figure 8.57: All Turbines - Cumulative Average - Upper and Lower Limits

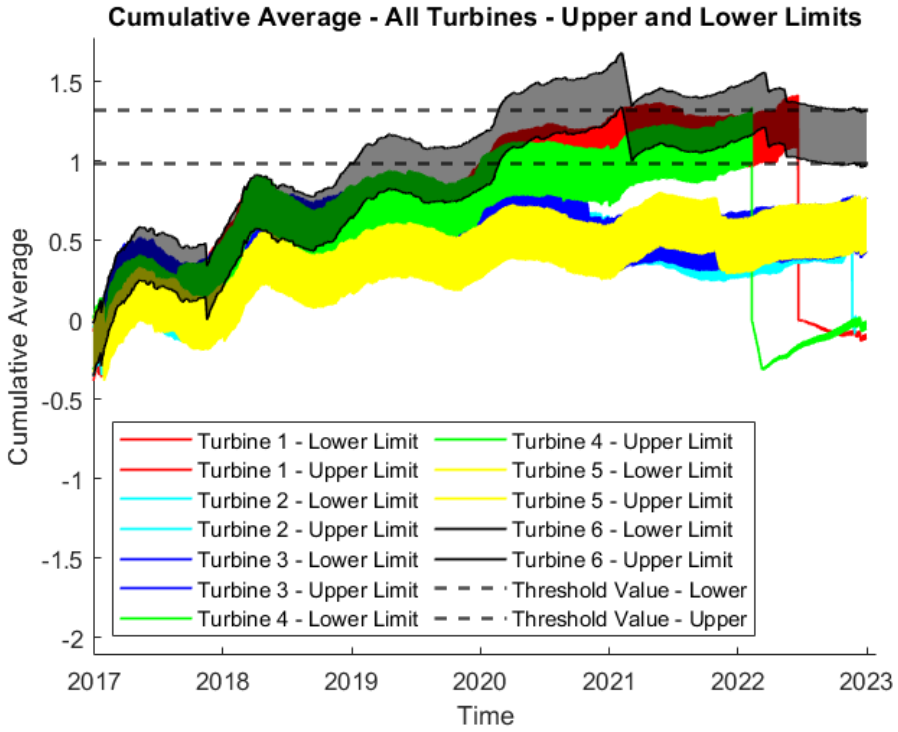

Figure 8.58: All Turbines - Cumulative Average - Upper and Lower Limits - Zoomed In

8.3 Summary

It has been mentioned numerous times throughout this thesis, how important obtaining an accurate and reliable prediction is, so this chapter looked at investigating the model errors and accounting for them.

Two approaches were investigated in this chapter, using the Monte Carlo method/simulation - the discrete confidence interval-based approach and a continuous probability distribution-based approach. Both approaches started the same, the ”healthy" data or data collected during the first year of the turbine operating, was split into 70% training and 30% test data. The temperature differences between the actual and predicted component temperatures of the test data were determined and fit with a normal probability distribution. From this, the mean and standard deviation were obtained and these values were then used to generate a random ’error’. The model was then applied to a new dataset, which consisted of data from years 2016 to 2022 and this random ’error’ was added to the predicted component temperatures. The number of runs was set to a thousand.

These results were then used to carry out the discrete confidence interval-based approach first, where both the 95% and 99% confidence intervals were established from the predicted temperature values. Then any actual temperature values that fell outside these intervals were noted and documented, as temperature differences. The same post-processing method was carried out, including calculating the cumulative sum of the temperature differences, cumulative average and moving average of the temperature differences.

The second approach carried out was based on the continuous probability distribution-based approach. For this approach, the temperature difference for each 10-minute interval and run, was calculated. The normal probability distribution was then fit for each 10-minute interval, across all runs. The mean, as well as the 95% confidence interval were then obtained. The same post-processing method was then carried out. A revised threshold value of 1.17 was obtained and whilst the values are very similar, the time the turbines exceeded this value varied.

8.4 References

[1] John D Sørensen and Henrik S Toft. Probabilistic design of wind turbines. *Energies*, 3(2):241–257, 2010.

[2] Amir Rasekhi Nejad, Zhen Gao, and Torgeir Moan. On long-term fatigue damage and reliability analysis of gears under wind loads in offshore wind turbine drivetrains. *International Journal of Fatigue*, 61:116–128, 2014.

[3] Wenbin Dong, Amir Rasekhi Nejad, Torgeir Moan, and Zhen Gao. Structural reliability analysis of contact fatigue design of gears in wind turbine drivetrains. *Journal of Loss Prevention in the Process Industries*, 65:104115, 2020.

[4] Arnab Chakrabarty, Sam Mannan, and Tahir Cagin. *Multiscale modeling for process safety applications*. Butterworth-Heinemann, 2015.

[5] M Waqar Ahmed. Understanding mean absolute error (mae) in regression: A practical guide, 2023. https://medium.com/@m.waqar.ahmed/understanding-mean-absolute-error-mae-in-regression-a-practical-guide-26e80ebb97df.

[6] Timothy O Hodson. Root mean square error (rmse) or mean absolute error (mae): When to use them or not. *Geoscientific Model Development Discussions*, 2022: 1–10, 2022.

[7] Amber Roberts. Mean absolute percentage error (mape): What you need to know,

2023. https://arize.com/blog-course/mean-absolute-percentage-error-mape-what-you-need-to-know/.

Chapter 9

Conclusion

9.1 Conclusion

As discussed in the Introduction, the main aim of this work, was to develop a methodology that could be used to determine whether lifetime extension of a wind turbines' drivetrain was a possibility. Lifetime extension is one of the three options that owner/operators have when their turbines are reaching the end of their operational life. The main benefit to lifetime extension, is that the turbine is able to operate safely for an additional X number of years with minimum cost. The method is specifically focused on the drivetrain because the drivetrain is where the kinetic energy from the wind is converted to electrical energy, which is supplied to the grid, so if the drivetrain fails, then the wind turbine is not operational. It is the “heart" of the wind turbine.

The first stage, which is documented in Chapter 2, was to study the wind turbine, the various equipment/components that make-up the drivetrain, the typical topologies and the loads/forces that they are subjected too. The main components include: the

main bearing, gearbox, generator and power converter, with the latter three having notably higher failure rates, making them the primary focus during lifetime extension assessments. This is due to the fact that lifetime extension is dependent upon the remaining useful life of the components, so the component with the shortest remaining useful life, dictates whether lifetime extension is a possibility and if so, the duration.

The next stage was to explore current methodologies for evaluating lifetime extension, both within the wind industry and in other industries. The wind industry was investigated to identify the current state-of-the-art processes and any potential gaps, whilst other industries, such as: oil and gas, vessels, nuclear, mechanical components, etc. were explored because they have been around much longer than the wind industry, so may have tried, tested and established methods. Chapter 4 highlights the key points and techniques that may be transferable to the wind industry.

Taking into account all the current state-of-the-art processes for determining lifetime extension reviewed in Chapter 4, a methodology was proposed in Chapter 5. The proposed methodology was broken down into a number of stages. The first stage was data collection, in which in theory it was determined that the more data collected, the more accurate and reliable the results but in reality there may be some situations where different data types could give conflicting recommendations. The second stage involved breaking down the drivetrain into equipment/components, so that they can be prioritised according to their failure rates, from highest to lowest, or remaining useful life, from lowest to highest. The next stages involved the assessments: practical, analytical or both. Ideally both should be carried out, in order to get an accurate prediction but in theory practical assessments may not be possible due to a variety of reasons, so

analytical assessments must be relied upon. Analytical assessments can be physics-based, data-driven or hybrid. Once the assessments have been carried out, typically the outcome is the components remaining useful life, which then determines whether lifetime extension is a possibility. In addition, establishing any errors or uncertainties within the method/model/process is an important stage to consider, due to the fact that accurate, reliable results are required, in order to make an important decision regarding lifetime extension, which may have safety and financial implications. Finally, any changes to support the final decision are noted, regarding operations, maintenance etc.

Chapter 6 investigated the selection of critical components, which is required in order to rank the components, so that analysis of these components are prioritised because as mentioned previously, their remaining useful life determines whether lifetime extension is a possibility. Previous work has been carried out on determining the critical components in mechanical equipment, via vulnerability mapping but to date a vulnerability map of electrical equipment had not been produced. Therefore, in this chapter, some failure data specifically related to power converters, was acquired for a number of turbines in a variety of countries. The power converter's topology was firstly assumed, then the failure data was used to determine which components had the highest failure rates and the vulnerability map produced. The converter control units, grid-side power modules, and generator-side power modules were the three components with the highest failure rates. This backs-up research done by other researchers. The work carried out in the chapter confirmed that a vulnerability map is a simple but effective tool for selecting and highlighting critical components.

SCADA data for an onshore wind farm was obtained and used in Chapter 7, to implement the method proposed in Chapter 5. The method had to be adapted to the amount of data available. Since SCADA data is the minimum amount of data that can be obtained from a wind turbine, it was assumed that documenting and implementing a method to use this data, to see if useful results could be obtained, would be highly beneficial. Firstly, selection of a suitable model predictor was required and after testing a number of regression models, it was determined that the regression tree ensemble model, using three SCADA input parameters: power, rotor speed and nacelle temperature, along with component temperature, was the most suitable predictor. Next, the most vulnerable component was determined, which was found to be the rear generator bearing and this was confirmed within the status reports. Once the model was run on all the data, the predicted component temperatures were compared to the actual component temperatures. The temperature differences, cumulative sum and cumulative averages were all determined. A threshold value of 1.2 was determined from the cumulative averages. Three turbines exceeded this threshold value, leading to failure or maintenance/downtime. However, the time between surpassing the threshold and the subsequent failure varied, making it impossible to provide an accurate prediction for lifetime extension. Therefore, it can be concluded, that consistent with previous research on SCADA data [1, 2], the results suggest that relying solely on SCADA temperature data, may not be a reliable indicator for estimating remaining useful life far in advance. However, the method presented could be used to help operators identify problematic components from historical data, or those needing replacement, enabling extended drivetrain usage over time.

The penultimate chapter, Chapter 8, explored two approaches for addressing errors, using a Monte Carlo method/simulation, in order to improve the accuracy of the method proposed in Chapter 7. Both approaches used the mean and standard deviation values, acquired from the probability distribution of the temperature differences from the “healthy" data to generate a random ’error’, which was added to a new dataset. The first approach employed a discrete confidence interval-based approach, while the second approach utilised a continuous probability distribution-based approach. With the discrete confidence interval-based approach, confidence intervals were established, where only actual component temperatures that exceeded these intervals were flagged and acknowledged. Whilst the approach based on continuous probability distribution, calculated the mean, standard deviation and 95% confidence intervals for each 10-minute interval, after the normal probability distribution was applied to the row. The post-processing for both included: cumulative sum and cumulative average. From the second approach, a threshold value of 1.17 was obtained. The threshold values were closely aligned, with values of 1.2 (original value), 1.17 (mean value with error accounted for) and a range from 0.99 to 1.32 (when an error was accounted for and confidence intervals used), but the time the turbines exceeded the threshold values varied. This means that whilst an accurate lifetime extension prediction can not still be made using solely SCADA temperature data, there has been a slight improvement when accounting for model errors.

The primary impact of this work was the development of a methodology that is applicable to various components within a drivetrain. To test and validate the methodology, a dataset with a decent amount of data over a number of years was required,

which also included the logs of the repair and failure of the components. Due to commercial sensitivity, obtaining many datasets with the mentioned layers of information is not so straightforward, but fortunately the authors were able to find a multi-year data set. This available dataset, which was used to validate the methodology, includes the failure data indicating that the rear generator bearing is the most vulnerable component, specific to that type of drivetrain used in the farm. However, within various drivetrain configurations, different turbines and farms depending on the specific loading patterns and varied components manufacturers and the operating regime of the turbines, some other components may be more vulnerable, where the developed methodology will still be applicable. An additional application of this methodology is with regards to predictive maintenance, by providing information to assist with scheduling repairs.

9.2 Contributions

The main contributions of this work include:

1. Development of a systematic methodology for determining the feasibility of lifetime extension, focusing on wind turbine drivetrains (Chapter 5).

2. Extending the concept of vulnerability maps to power converters, using a data-driven approach (Chapter 6).

3. Implementation of the data-driven methodology, utilising real-life SCADA data from a wind farm containing six (6) wind turbines, spanning seven (7) years (Chapter 7). This includes:

   (a) Determining which well-established machine learning regression model was the most suitable model to predict component operating temperatures.

   (b) Identifying tracking/monitoring metrics, that highlight trends and detect components that deviate from their normal operating temperatures, which may indicate that a component is reaching the end of it's operational life.

4. Development of probabilistic approaches, using Monte Carlo simulations along with confidence intervals, to incorporate model errors and uncertainties, with the aim of improving the accuracy and robustness of the previous deterministic approach. The approaches include:

   (a) Discrete confidence interval-based approach.

   (b) Continuous probability distribution-based approach.

   The threshold values were then updated accordingly (Chapter 8).

9.3 Revisiting the Research Questions

Research question 1 was:

1. *Lifetime extension has been implemented on structural components such as the tower, but how can it be applied on the drivetrain? What can be learnt from other industries?*

Addressing the second part of the question first, valuable insights can be drawn from practices in other industries. A common approach observed across various industries involves three key stages: data collection, system breakdown and assess-

ment. The assessment stage typically combines both a practical and analytical approach, with the analytical approach utilising either physics-based, data-driven, or hybrid techniques. Further details are provided in Chapter 4.

Returning to the first part of the question, a methodology was proposed in Chapter 5, incorporating key principles and best practices identified from these other industries.

Research question 2 was:

2. *What approach should be taken to evaluate potential lifetime extension of wind turbine drivetrains, when:*
    a. *Only Supervisory Control and Data Acquisition (SCADA) data is available?*
    b. *SCADA and vibration data are available?*

In response to this question, an approach was presented in Chapter 7 for scenarios where only supervisory control and data acquisition (SCADA) data is available. The results revealed that while an accurate lifetime extension prediction could not be achieved, it was possible to establish a threshold value derived from the cumulative average of temperature differences. Crossing this threshold could indicate that a component is approaching the end of its operational life, providing owner/operators with an early warning of potential issues with critical components. Furthermore, the approach proposed in Chapter 8, which investigated and accounted for model errors, demonstrated a slight improvement in the model's accuracy.

Unfortunately, implementing an approach that combines both SCADA and vibration data was not possible due to the unavailability of vibration data. However, based on

the findings obtained from using SCADA data alone, it is anticipated that integrating vibration data would yield a more accurate prediction of the remaining useful life of wind turbine components within the drivetrain.

9.4 Future Work

Future work will look at implementing the proposed methodology, using a combination of SCADA and condition monitoring (e.g. vibration) data, to see if a more accurate prediction can be achieved, when determining whether lifetime extension of the drivetrain is a possibility.

Implementation of the proposed methodology on electrical equipment (e.g. power converters) will also be investigated, to see if the same methodology is applicable for both mechanical and electrical equipment.

With regards to the power converter, more research will be carried out on the selection of critical components (vulnerability maps) for different power converter topologies, as well as for fully rated and partially rated power converters. This will be useful because fully rated and partially rated power converters are subjected to different loadings, so the ranking of critical components may vary accordingly.

Identification of more monitoring/tracking metrics will also be studied, in order to see if different metrics produce more useful methods of monitoring trends and anomalies.

Creating a health indicator will also be explored. Determining an indicator that will represent the current health of a component will be useful. A health indicator could

integrate a number of data sources, so should be more effective, than relying solely on temperature data.

9.5 References

[1] Dongdong Zhang and Zheng Qian. Probability warning for wind turbine gearbox incipient faults based on scada data. In *2017 Chinese Automation Congress (CAC)*, pages 3684–3688. IEEE, 2017.

[2] Long Wang, Zijun Zhang, Huan Long, Jia Xu, and Ruihua Liu. Wind turbine gearbox failure identification with deep neural networks. *IEEE Transactions on Industrial Informatics*, 13(3):1360–1368, 2016.

APPENDICES

Appendix A

Summary of Manufacturers

Drivetrain Layouts

A.1 Siemens Gamesa

Table A.1: Summary of Manufacturers Drivetrain Layouts (Siemens Gamesa).

Model	Power	Geared	Direct-Drive	Generator / Converter
SG 2.1-114	2.1 MW	3-stage		DFIG
SG 2.1-122	2.1 MW	3-stage		DFIG
SG 2.2-122	2.2 MW	3-stage		DFIG
SG 2.6-114	2.625 MW	3-stage		DFIG
SG 2.6-126	2.6 MW	3-stage		DFIG
SG 2.7-129	2.7 MW	3-stage		Full Scale Converter
SG 2.9-129	2.9 MW	3-stage		Full Scale Converter
SG 3.4-132	3.465 MW	3-stage		DFIG
SG 3.4-145	3.465 MW	3-stage		DFIG
SG 4.2-145	4.2 MW	3-stage		DFIG
SG 4.5-145	4.5 MW	3-stage		DFIG
SG 4.7-155	4.7 MW	3-stage		DFIG
SG 5.0-132	5.0 MW	3-stage		DFIG
SG 5.0-145	5.0 MW	3-stage		DFIG
SG 5.8-155	5.8 MW	3-stage		DFIG
SG 5.8-170	5.8 MW	3-stage		DFIG
SG 6.6-155	6.6 MW	Geared		
SG 6.6-170	6.6 MW	Geared		
SG 7.0-170	7.0 MW	Geared		
SG 11.0-200	11 MW		DD	
SWT-DD-120	4.3 MW		DD	Sync PM
SWT-DD-130	4.3 MW		DD	Sync PM
SWT-DD-142	4.1 MW		DD	Sync PM
SWT-6.0-154	6.0 MW		DD	Sync PM
SWT-6.6-155	6.6 MW	Geared		DFIG
SWT-6.6-170	6.6 MW	Geared		DFIG
SWT-7.0-154	7.0 MW		DD	Sync PM
SWT-7.0-170	7.0 MW	Geared		DFIG
SG 8.0-167 DD	8.0 MW		DD	Sync PM
SG 8.0-167 DD Flex	8.6 MW		DD	
SG 10.0-193 DD	10.0 MW		DD	Sync
SG 11.0-193 DD Flex	11.0 MW		DD	
SG 11.0-200 DD	11.0 MW		DD	
SG 14-222 DD	14.0 MW		DD	
SG 14-236 DD	14.0 MW		DD	

A.2 GE

Table A.2: Summary of Manufacturers Drivetrain Layouts (GE)

Model	Power	Geared	Direct-Drive	Generator / Converter
1.5s	1.5 MW	3-stage		DFIG
1.5se	1.5 MW	3-stage		DFIG
1.5sl	1.5 MW	3-stage		DFIG
1.5sle	1.5 MW	3-stage		DFIG
1.5xle	1.5 MW	3-stage		DFIG
1.6sle	1.5 MW	3-stage		DFIG
1.6-100	1.6 MW	3-stage		Async DF
1.6-82.5	1.6 MW	3-stage		DFIG
1.6xle	1.6 MW	Geared		
1.62-87	1.62 MW	Geared		
1.7-100	1.7 MW	Geared		DFIG
1.7-103	1.7 MW	Geared		DFIG
1.85-82.5	1.85 MW	Geared		Async DF
1.85-87	1.85 MW	Geared		Async DF
2.0-116	2.0 MW	Geared		DFIG
2.0-127	2.0 MW	Geared		DFIG
2.2-107	2.2 MW	Geared		DFIG
2.3	2.3 MW	Geared		
2.3-107	2.3 MW	Geared		DFIG
2.3-116	2.3 MW	Geared		DFIG
2.3-127	2.3 MW	Geared		DFIG
2.4-107	2.4 MW	Geared		DFIG
2.5-100	2.5 MW	3-stage		DFIG
2.5-103	2.5 MW	Geared		Sync PM
2.5-116	2.5 MW	Geared		DFIG
2.5-120	2.5 MW	Geared		DFIG
2.5-127	2.5 MW	Geared		DFIG
2.5-132	2.5 MW	Geared		DFIG
2.5-88	2.5 MW	3-stage		Async DF
2.5xl	2.5 MW	3-stage		DFIG
2.75-100	2.75 MW	Geared		Async DF
2.75-103	2.75 MW	Geared		Async DF
2.75-120	2.75 MW	Geared		DFIG
2.8-127	2.8 MW	Geared		DFIG
2.8-132	2.8 MW	Geared		DFIG
2.85-100	2.85 MW	Geared		Async DF
2.85-103	2.85 MW	Geared		Async DF
3.0s	3.0 MW	3-stage		DFIG
3.0sl	3.0 MW	3-stage		DFIG
GE 3000	3.0 MW	Geared		
3.2-103	3.2 MW	Geared		DFIG

Table A.3: Summary of Manufacturers Drivetrain Layouts (GE) Contd.

Model	**Power**	**Geared**	**Direct-Drive**	**Generator / Converter**
3.2-130	3.2 MW	Geared		DFIG
3.2-137	3.2 MW	Geared		Async DF
3.4-130	3.4 MW	Geared		DFIG
3.4-137	3.4 MW	Geared		DFIG
3.6-130	3.6 MW	Geared		Async DF
3.6-137	3.6 MW	Geared		DFIG
3.6s	3.6 MW	3-stage		Async DF
3.6sl	3.6 MW	3-stage		Async
3.8-117	3.8 MW	Geared		Async DF
3.8-130	3.8 MW	Geared		DFIG
3.8-137	3.8 MW	Geared		Async DF
4.0-110	4.0 MW		DD	Sync PM
4.1-113	4.1 MW		DD	Sync PM
4.2-117	4.2 MW	Geared		Async DF
4.8-158	4.8 MW	Geared		DFIG
4.9-158	4.9 MW	Geared		DFIG
5.3-158	5.3 MW	Geared		DFIG
5.5-158	5.5 MW	Geared		DFIG
5.8-158	5.8 MW	Geared		DFIG
6.0-164	6.0 MW	Geared		DFIG
Haliade 150	6.0 MW		DD	Sync PM
6.1-158	6.1 MW	Geared		DFIG
Haliade-X 12 MW	12.0 MW		DD	Sync PM
Haliade-X 13 MW	13.0 MW		DD	Sync PM
Haliade-X 14 MW	14.0 MW		DD	Sync PM
Haliade-X 250	15.5 MW		DD	Sync PM

A.3 Goldwind

Table A.4: Summary of Manufacturers Drivetrain Layouts (Goldwind).

Model	Power	Geared	Direct-Drive	Generator / Converter
S43/600	0.6 MW	3-stage		Induction
S43/750	0.75 MW	3-stage		Induction
S48/750	0.75 MW	2-stage		Induction
S50/750	0.75 MW	3-stage		DFIG
GW62/1200	1.2 MW		DD	Sync PM
GW70/1500	1.5 MW		DD	Sync PM
GW77/1500	1.5 MW		DD	Sync PM
GW82/1500	1.5 MW		DD	Sync PM
GW87/1500	1.5 MW		DD	Sync PM
GW93/1500	1.5 MW		DD	Sync PM
GW108/2000	2.0 MW		DD	Sync PM
GW115/2000	2.0 MW		DD	Sync PM
GW131/2000	2.0 MW		DD	Sync PM
GW100/2500	2.5 MW		DD	Sync PM
GW103/2500	2.5 MW		DD	Sync PM
GW106/2500	2.5 MW		DD	Sync PM
GW109/2500	2.5 MW		DD	Sync PM
GW121/2500	2.5 MW		DD	Sync PM
GW130/2500	2.5 MW	5-stage		
GW90/2500	2.5 MW		DD	Sync PM
GW136/3000	3.0 MW		DD	Sync PM
GW140/3000	3.0 MW		DD	Sync PM
GW140/3300	3.3 MW		DD	Sync PM
GW155/3300	3.3 MW		DD	Sync PM
GW140/3400	3.4 MW		DD	Sync PM
GW140/3570	3.57 MW		DD	Sync PM
GW136/4000	4.0 MW		DD	Sync PM
GWH171-4.X	4.0 MW	Geared		
GWH191-4.X	4.0 MW	Geared		
GW136/4200	4.2 MW		DD	Sync PM
GW155/4500	4.5 MW		DD	Sync PM
GW136/4800	4.8 MW		DD	Sync PM
GW165/5200	5.2 MW		DD	
GWH171-5.3	5.3 MW			
GW165/5600	5.6 MW		DD	
GWH171-5.6	5.6 MW			

Table A.5: Summary of Manufacturers Drivetrain Layouts (Goldwind) Contd.

Model	**Power**	**Geared**	**Direct-Drive**	**Generator / Converter**
GW165/6000	6.0 MW		DD	
GWH171-6.0	6.0 MW			
GWH191-6.X	6.0 MW			
GWH171-6.25	6.25 MW			
GW164/6450	6.45 MW		DD	Sync PM
GW168/6450	6.45 MW			
GW171/6450	6.45 MW		DD	Sync PM
GW154/6700	6.7 MW		DD	Sync PM
GWH182-7.X	7.0 MW			
GW175/8000	8.0 MW			
GW184/8000	8.0 M			
GW252/16000	16.0 MW			

A.4 Vestas

Table A.6: Summary of Manufacturers Drivetrain Layouts (Vestas)

Model	Power	Geared	Direct-Drive	Generator / Converter
V20/100	0.1 MW	1-Stage		Async
V23/150	0.15 MW			
V23/200	0.2 MW			
V25/200	0.2 MW	2-Stage		Async
V27/225	0.225 MW	2-Stage		Async
V29/225	0.225 MW	2-Stage		Async
V27/270	0.27 MW			
V34/400	0.4 MW			
V39/500	0.5 MW	3-Stage		Async
V42/500	0.5 MW			
V39/600	0.6 MW			
V42/600	0.6 MW	3-Stage		Async
V44/600	0.6 MW	2-Stage		Async
V47/660	0.66 MW	3-Stage		Async
V52/850	0.85 MW	3-Stage		Async
V60/850	0.85 MW			Async
V63/1500	1.5 MW	3-Stage		Async
V82/1500	1.5 MW	2-Stage		Sync
V66/1650	1.65 MW	3-Stage		Async
V70/1650	1.65 MW			
V82/1650	1.65 MW	2-Stage		Async
V66/1750	1.75 MW	3-Stage		Induction
V100/1800	1.8 MW	3-Stage		Async DF
V80/1800	1.8 MW			Induction
V90/1800	1.8 MW	3-Stage		Async
V100/2000	2.0 MW	3-Stage		DFIG
V110/2000	2.0 MW	3-Stage		DFIG
V116/2000	2.0 MW	3-Stage		
V120/2000	2.0 MW			DFIG
V66/2000	2.0 MW			Induction
V80/2000	2.0 MW	3-Stage		Async
V90/2000	2.0 MW	3-Stage		Async
V116/2100	2.1 MW	3-Stage		
V100/2200	2.2 MW	3-Stage		DF
V110/2200	2.2 MW	3-Stage		DF
V120/2200	2.2 MW	3-Stage		DFIG

Table A.7: Summary of Manufacturers Drivetrain Layouts (Vestas) Contd.

Model	Power	Geared	Direct-Drive	Generator / Converter
V100/2600	2.6 MW	3-Stage		Async DF
V100/2750	2.75 MW	3-Stage		Async
V112/3000	3.0 MW	4-Stage		Sync PM
V112/3000 Offshore	3.0 MW	4-Stage		Sync PM
V126/3000	3.0 MW	4-Stage		Async
V138/3.0 MW	3.0 MW	2-Stage		
V90/3000	3.0 MW	3-Stage		Async
V90/3000 Offshore	3.0 MW	3-Stage		Async
V112/3075	3.075 MW	4-Stage		Sync PM
V105/3300	3.3 MW	3-Stage		
V112/3300	3.3 MW	3-Stage		
V117/3300	3.3 MW	3-Stage		
V126/3300	3.3 MW	3-Stage		
V155/3300	3.3 MW			
V105/3450	3.45 MW	3-Stage		
V112/3450	3.45 MW	3-Stage		
V117/3450	3.45 MW	3-Stage		
V126/3450	3.45 MW	3-Stage		
V136/3450	3.45 MW	3-Stage		
V105/3600	3.6 MW			
V112/3600	3.6 MW			
V117/3600	3.6 MW	3-Stage		
V155/3.6MW	3.6 MW	3-Stage		
V117/4000-4200	4.0 MW	3-Stage		
V136/4000-4200	4.0 MW	3-Stage		
V150/4000-4200	4.0 MW	3-Stage		
V136/4.5MW	4.5 MW	3-Stage		
V150/4.5MW	4.5 MW	3-Stage		
V163/4.5MW	4.5 MW	3-Stage		
V150/5.6MW	5.6 MW	2-Stage		
V162/5.6MW	5.6 MW	2-Stage		
V150/6.0MW	6.0 MW	2-Stage		
V162/6.0MW	6.0 MW	2-Stage		
V162/6.2MW	6.2 MW	2-Stage		
V162/6.8MW	6.8 MW	2-Stage		
V164/7000	7.0 MW			PM
V162/7.2MW	7.2 MW	2-Stage		
V172/7.2MW	7.2 MW	2-Stage		
V164/8000	8.0 MW			PM
V164/9500	9.5 MW			PM
V174/9.5MW	9.5 MW	Geared		PM
V164/10MW	10.0 MW			PM
V236/15.0 MW	15.0 MW	3-Stage		

Appendix B

Summary of Lifetime Extension Processes in All Industries

TITLE	DESCRIPTION	INDUSTRY			
		OIL & GAS	MARINE VESSELS	NUCLEAR POWER PLANTS	WIND INDUSTRY
LTE OBJECTIVE	Maintain equipment reliability, integrity and operational safety.	✖	✖	✖	✖
	Be economically beneficial.	✖	✖	✖	✖
	Considers changes to the surrounding environment.			✖	
	Meet the planned power requirements made by the countries leadership.			✖	
RUL APPROACHES	**Analytical**	✖	✖	✖	✖
	- Physic-Based Approach.	✖			✖
	- Data-Driven Approach.	✖			✖
	- Fusion Approach.	✖			
	- Engineering Activities.		✖		
	- Modelling.				
	Practical	✖	✖	✖	✖
	- Survey Activities.		✖		
METHODOLOGY	**Investigation Phase**				
	Collection of data and information.	✖	✖		✖
	System Breakdown.	✖			
	Engineering Assessment (Strength, Fatigue and/or Stability Analysis).		✖		
	Baseline Survey.		✖		
	Analysis of Failures and Challenges.	✖			
	Determination Phase				
	Reassessment.		✖		
	Conditions for Life Extension Provision.		✖		
	Development of a Lifetime Extension Management Plan.	✖	✖		
	Implementation Phase		✖		

Figure B.1: Summary of Lifetime Extension Process in All Industries.

TITLE	DESCRIPTION	INDUSTRY			
		OIL & GAS	MARINE VESSELS	NUCLEAR POWER PLANTS	WIND INDUSTRY
METHODOLOGY	**Risk Assessment**				
	Identification and Evaluation of Risk Reducing Measures / Risk Assessment.	✖	✖		
	Assessment of the Overall Risk Picture.	✖	✖		
	System Breakdown.	✖			
	Criticality Screening.	✖			
	Analysis of Failures and Challenges.	✖			
	Development of a Lifetime Extension Management Plan.	✖			
	Application for extending the operating license.			✖	
	Conduct safety reviews.			✖	
	Conduct environmental impact assessments.			✖	
	Conduct technical reviews.			✖	
	Carry out research, modelling and simulations of degradation scenarios.			✖	
	Collect data of previous incidents and accidents.			✖	
	Utilise reactor ageing management programs.			✖	
	Use SCADA data and aeroelastic design basis to estimate the shaft torsional load, using the collage method and Tikhonov method. Once the shaft torsional load has been determined the damage equivalent loads (DEL) can then be calculated on all major structural components. DEL values are then used to estimate fatigue life.				✖
	Model impacts of electrical transients, wind turbulence and shear on wind turbine drivetrains. (FAST CAE Tool and Simscape).				✖
	Consider transient torque reversals.				✖
	Use the measured strain data to link measured oceanographic data to fatigue damage as well as using the Bayesian approach.				✖
	Determine the actual loads and stresses that the wind turbine has been exposed to and by computer simulations. The simulations must reproduce the design conditions after type testing and the actual operating conditions.				✖
	Data analysis, inspections, aero-elastic simulations and data from SHM systems can all be used to determine the LTE of the turbine.				✖
	Use a joint aeroelastic-finite element analysis, taking into consideration the wind direction, operational history and stress magnification present around the door of the tower.				✖
	Use the Submatrices Damage Method to establish damage indicators in terms of stiffness degradation.				✖
	Data evaluation using SCADA data, maintenance reports, survey reports, wind history and CMS. Inspections of the drivetrain, NDI of any connections that are bolted and welded, corrosion areas, blades and electrical components.				✖
	Perform fatigue assessments on a select number of wind turbines in a wind farm, using site specific environmental data during the design phase and then comparing them with fatigue reassessments carried out on the turbines at the end of the designed service life when the environmental conditions were known.				✖
	Conduct load simulations along with technical assessments.				✖

Figure B.2: Summary of Lifetime Extension Process in All Industries